

AUXILIARY FIELD MONTE-CARLO FOR QUANTUM MANY-BODY SYSTEMS

thesis by
Gayle Sugiyama

In Partial Fulfillment of the Requirements
For the Degree of
Doctor of Philosophy

California Institute of Technology
Pasadena, California
1984

(Submitted July 6, 1984)

Acknowledgements

This thesis is dedicated to my parents, Hiroshi and Yuri Sugiyama, for encouragement and support through the years. Special thanks is due to Steve Koonin, my advisor, who introduced me to nuclear theory research and has provided valuable insights and advice. For help and friendship during my stay, I would like to express my gratitude to the rest of the members of Kellogg and to my roommates during my stay - R. Gupta, J. Osborne, L. and M. Finger. Thanks are also due B. Alder and D.Ceperley for providing me with computer time at Lawrence Livermore Laboratory.

Abstract

An algorithm is developed for determining the exact ground state properties of quantum many-body systems which is equally applicable to bosons and fermions. The Schroedinger eigenvalue equation for the ground state energy is recast into the form of a many-dimensional integral through the use of the Hubbard-Stratonovitch representation of the imaginary time many-body evolution operator. The resulting functional integral is then evaluated stochastically. The algorithm is tested for an exactly soluble boson system and is then extended to include fermions and repulsive potentials. Importance sampling is crucial to the success of the method, particularly for more complex systems. Improved computational efficiency is attained by performing the calculations in momentum space.

Table of Contents

§1.	Introduction	1
§2.	Hubbard Stratonovitch representation of the propagator	11
§3.	Time-dependent mean-field approximation	18
§4.	Numerical techniques - discretization of the integral	26
§5.	Metropolis algorithm	33
§6.	Numerical techniques - Metropolis calculation of the integral	37
§7.	Model calculation - the delta function potential	43
§8.	Fermions	56
§9.	Momentum space algorithm	67
§10.	Treatment of repulsive potentials	74
§11.	Conclusion	84
	References	92

Tables

Table 1.	Goldstone diagram energy contributions	98
Table 2.	Parameters for the delta function interaction	99
Table 3.	Parameters for fermions - attractive interaction	100
Table 4.	Variational energies for fermions	101
Table 5.	Parameters for bosons - attractive interaction	102
Table 6.	Parameters for fermions - momentum space	104
Table 7.	Parameters for fermions - attractive and repulsive interaction	106

Figures

Figure 1.	Goldstone diagram expansion for the energy	108
Figure 2.	$E(T)$ for 6 bosons, delta function interaction	109
Figure 3.	$E(T)$ for 10 bosons, delta function interaction	110
Figure 4.	$E(T)$ for 20 bosons, delta function interaction	111
Figure 5.	Autocorrelation function for 10 bosons, delta function interaction	112
Figure 6.	Energy gap plot for 10 bosons, delta function interaction	113
Figure 7.	Wavefunction for 10 bosons, delta function interaction	114
Figure 8.	Sigma field for 10 bosons, delta function interaction	116
Figure 9.	$E(T)$ for 4 fermions, exponential potential interaction	118
Figure 10.	$E(T)$ for 4 fermions, exponential potential interaction	119
Figure 11.	$E(T)$ for 8 fermions, exponential potential interaction	120
Figure 12.	$E(T)$ for 12 fermions, exponential potential interaction	121
Figure 13.	Autocorrelation function for 12 fermions, exponential potential interaction	122
Figure 14.	Wavefunctions for 12 fermions, exponential potential interaction	123
Figure 15.	Comparison of spatial and momentum space importance sampling for 10 bosons, exponential potential interaction	127

Figure 16.	Comparison of spatial and momentum space importance sampling for 12 fermions, exponential potential interaction	128
Figure 17.	Autocorrelation function using momentum space importance sampling for 12 fermions, exponential potential interaction	129
Figure 18.	Wavefunctions using momentum space importance sampling for 12 fermions, exponential potential interaction	130
Figure 19.	Sigma field using momentum space importance sampling for 12 fermions, exponential potential interaction	134
Figure 20.	One-body potential using momentum space importance sampling for 12 fermions, exponential potential interaction	136
Figure 21.	Static nuclear potential	138
Figure 22.	$E(T)$ for 4 fermions, attractive exponential interaction with repulsive core	140
Figure 23.	Autocorrelation function for 4 fermions, attractive exponential interaction with repulsive core	141
Figure 24.	Wavefunctions for 4 fermions, attractive exponential interaction with repulsive core	142
Figure 25.	One-body potential for 4 fermions, attractive exponential interaction with repulsive core	147

§1. Introduction

In this thesis, an algorithm is developed for determining the exact ground state properties of quantum many-body systems. The Schroedinger eigenvalue equation for the ground state energy is recast into the form of a many-dimensional integral through the use of the Hubbard-Stratonovitch representation of the imaginary time many-body evolution operator. The resulting functional integral is then evaluated stochastically. The advantage of this algorithm is that fermions and bosons are incorporated equally into the formalism.

Background. Exact solutions of the many-body Schroedinger equation are of interest as benchmarks against which to test approximation methods and as tests of given Hamiltonians by comparison with experimental observables. Several methods have been used to obtain such solutions. The Green's Function Monte-Carlo (GFMC) and the related path integral or diffusion Monte-Carlo (DMC) algorithms [Ka74,Ce79,Wh83] are the most commonly used approaches. In both, properties of many-body systems are calculated by filtering a trial wavefunction Φ to the exact ground state. The GFMC involves filtering by means of the operator $1/(E+H)$, while the DMC uses the propagator filter, e^{-HT} , in the form of a diffusion equation. The many-body wavefunction is described statistically by an evolving ensemble of configurations, each of which is specified by the coordinates of the particles. These methods have been applied to the many-boson problems of liquid He [Ka74,Ce79,Ka81], liquid and solid hydrogen [Ce81] and three- and four-nucleon systems with state-independent central potentials [Za81].

Unfortunately, the GFMC and DMC algorithms provide only a restricted description of fermion systems. The proper inclusion of the

Pauli principle is a major difficulty and has in fact precluded their unrestricted application to nuclear systems with $A > 4$ or with state-dependent potentials. The difficulty arises because antisymmetrization enforces a spatially non-local constraint between configurations differing by the exchange of a pair of particles - a condition difficult to apply with the simple local algorithms used to evolve the ensembles.

Consider the DMC in which the Schroedinger equation in imaginary-time is written as

$$-\frac{\partial \Psi(R, T)}{\partial T} = (H - E_T) \Psi(R, T) = \left[-\frac{\hbar^2}{2m} \nabla^2 + V(R) - E_T \right] \Psi(R, T), \quad (1.1)$$

where R is a $3A$ dimensional vector specifying the coordinates of A particles and E_T is a constant shift in the zero energy. This is a diffusion equation for Ψ with the ∇^2 term representing random diffusion due to zero-point motion and $[V(R) - E_T]$ describing a branching process in which the number of diffusers changes in proportion to the density. The branching decreases/increases the probability density in regions where $V(R)$ is large/small. Starting from the initial condition, $\Psi(R, 0) = \Phi(R)$, the solution to Eq. (1.1),

$$\Psi(R, T) = e^{\int_0^T E_T dt} e^{-HT} \Phi(R),$$

can be calculated by a Monte-Carlo method. The ground state energy is then given by

$$E_o = \lim_{T \rightarrow \infty} \frac{\langle \Phi | H | \Psi \rangle}{\langle \Phi | \Psi \rangle}. \quad (1.2)$$

For the diffusion interpretation to be valid, however, Ψ must always be positive (or always negative) since it is a population density. This is true for bosons. However, fermion wavefunctions have nodes - places where the wavefunction vanishes and changes sign. Theoretically, if e^{-HT} could be applied exactly, beginning with an antisymmetric trial

wavefunction Φ would provide a good fermion energy. However, Monte-Carlo evaluations are not exact and the diffusion process itself (Eq. (1.1)) incorporates nothing about wavefunction symmetries. Thus, "symmetric noise" grows with T as configurations cross the nodes, and antisymmetry is destroyed. In fact, as $T \rightarrow \infty$, the denominator and numerator in Eq. (1.2) vanish. One can say that the fermion "excited" state relaxes to the symmetric boson "ground" state.

A number of solutions to this problem have been proposed, but each restricts the application of the DMC to many systems of physical interest. The GFMC has the same limitation, since it also relies on an interpretation of the wavefunction as a density. The obvious solution involves brute force; i.e., starting with a good guess for Φ , keeping the total time T short and using a great many configurations to ensure good statistics.

A more acceptable solution used in the GFMC and DMC algorithms is the fixed node approximation. Inside a connected nodal region, the wavefunction is of one sign and vanishes at the boundaries. If each such region can be treated separately, the problem becomes equivalent to that for bosons. This is accomplished by considering the nodal surfaces as fixed absorbing barriers in the diffusion process. A new probability density function $f(R, T) = \Psi(R, T)\Phi(R)$ is introduced in Eq. (1.1), yielding

$$\frac{\partial f}{\partial T} = \frac{\hbar^2}{2m} \nabla^2 f - \frac{\hbar^2}{m} \nabla \cdot \left[\frac{1}{\Phi} (\nabla \Phi) f \right] - \left[\frac{H\Phi}{\Phi} - E_T \right] f . \quad (1.3)$$

The random diffusion remains the same, but the branching term now depends on the trial wavefunction Φ . By making a proper choice for Φ , branching can be reduced, improving the efficiency of the diffusion algorithm - a process known as importance sampling [Ka74,Ce79,Ce80]. The remaining term in Eq. (1.3) is a drift directed by the force $\nabla\Phi/\Phi$. In regions of low probability (small Φ), this force is large, "repelling"

configurations. Thus, the trial wavefunction prevents diffusion across nodes by fixing their location throughout the calculation.

The energy obtained using this method is an upper bound on E_0 , within statistical errors. The closer the nodes of Φ are to the actual ground state nodes, the better the value achieved. In one-dimension, antisymmetrization alone is sufficient to specify the locations of the nodes. In two or three-dimensions, however, antisymmetrization is not a sufficient condition and nodal surfaces must be determined by the dynamics. In this case, the nodes are not specified uniquely and only variational estimates result. This has given reasonable results in such problems as the electron gas [Ce80], molecules [An75,Re82,Ce83] and nuclear systems [Se83].

A third way of treating fermion systems is to write the wavefunction as the difference of two non-negative functions - $\Psi = \Psi^+ - \Psi^-$. A GFMC can then be performed using pairs of points, one from each of the two distinct populations. This has been applied to few-body problems [Ar82]. Unfortunately, the precise algorithm requires a sufficient density of points in configuration space in order to filter out a significant portion of the symmetric components in Ψ^+ and Ψ^- . For systems containing more than 3-4 particles, this population requirement appears to make computations unfeasible.

Auxiliary field Monte-Carlo (AFMC). Considering the difficulties just described, the development of an alternative algorithm for many-body ground states, useful for fermions as well as bosons, is of interest as a general approach to many-body physics. Two alternative algorithms, the method of coherent states [Ko82a,Av83] and the AFMC [Ko82b,Su84], have been investigated. They appear to be related though this has not been

rigorously proved. Both are based on the possibility of using a different basis to specify the many-body system - one that allows the exact enforcement of the Pauli principle. Rather than working with configurations of particle coordinates, the wavefunction is used directly, so that antisymmetrization can be built in at each step.

In the coherent state method, use is made of the resolution of unity operator for an overcomplete set of states [Bl80,Ko82a]. The result is a path integral for the system wavefunction (rather than for coordinates) with the evolution expressed as a functional integral over all wavefunction paths [Av83]. An alternative formulation using a real Slater determinant resolution of unity has also been discussed [Tr83b].

The auxiliary field algorithm involves a path integral representation of the many-body propagator. The "path" is defined not by the state of the system directly, but indirectly in terms of the history of an external one-body field coupled linearly to the density (or the pairing density). The many-body wavefunction is represented by a set of single-particle wavefunctions evolving in this random one body potential - a symmetrized product of single-particle orbitals for bosons or a Slater determinant for fermions.

This algorithm is motivated by a method utilized in nuclear problems - the mean-field approximation [Ne82b and references cited therein]. The mean free path of nucleons in nuclear matter is quite long for excitations up to the Fermi energy (10 Mev/nucleon). Thus to a good approximation, each nucleon feels only an average one-body field generated by the others. This "mean-field" picture is crucial to the nuclear shell model. It also provides the basis for understanding many systems in condensed matter [Bi79] and solid state physics [Mu78].

In dynamical problems, the mean-field is time-dependent and can be determined self-consistently by all of the nucleons. This idea is employed in time-dependent-Hartree-Fock (TDHF) theory. The total wavefunction of the system is taken to be a Slater determinant with the time evolution of the single-particle wavefunctions defined by a time-dependent least action principle - the deviation between the many-body determinant and the Schroedinger equation solution is minimized [Ke76,Ri80]. The TDHF method has been used extensively in such problems as slab geometries [Bo76], induced fission [Ne78], light and heavy ion systems [Ko77] and analytically solvable models [Yo77].

In the time-dependent mean-field approximation (TDMFA), attention is shifted from the wavefunction to the evolution operator, $U(t) = e^{-\frac{i}{\hbar}Ht}$, where H is the many-body Hamiltonian. $U(T)$ has several useful properties. If the Hamiltonian has eigenstates $|n\rangle$ with corresponding energies E_n , $U(t)$ can be expanded as

$$U(t) = \sum_n |n\rangle e^{-iE_n t} \langle n|. \quad (1.4)$$

The trace, formed by summing the diagonal matrix elements of U over a complete set of states, is then given by

$$\text{tr}U(t) = \sum_n e^{-iE_n t}, \quad (1.5a)$$

with Fourier transform

$$\int_0^\infty dt e^{iEt} \text{tr} U(t) = \sum_n \frac{i}{E - E_n}. \quad (1.5b)$$

Thus, the energy eigenvalues can be determined by locating the poles of the transform of the propagator.

Another useful expression emerges in the imaginary-time limit, $t = -iT$. In this case, the propagator expansion becomes

$$U(T) = \sum_n |n\rangle e^{-E_n T} \langle n| . \quad (1.6)$$

As $T \rightarrow \infty$, only the ground state survives in the sum and $U(T)$ acts like a ground state filter - the large T limit of the trace (which is just the partition function for a system with temperature $1/T$) decays exponentially as $e^{-E_0 T}$, and the ground state energy can be read off directly.

A different representation for the propagator is derived via the Hubbard-Stratonovitch transformation - an operator identity which allows linearization of the exponent of the square of an operator through the introduction of an auxiliary field (σ). $U(t)$ is expressed exactly by a coherent sum of one-body evolution operators, $U_\sigma(t)$, each propagating the system in a time-dependent one-body potential specified by σ . The sum is over all possible configurations of the potential [Le80a]. This is a functional integral [Fe65] with the "paths" defined by the auxiliary field. The process may be conceived of as the extraction of an effective boson field responsible for the fermion-fermion interaction. A similar approach is used in the semi-classical analysis of relativistic field theories [Ra75, Da75].

In the TDMFA, the stationary phase approximation is used to evaluate matrix elements of the Hubbard-Stratonovitch representation of the propagator, $\langle f | U(T) | i \rangle$, between any given states $|f\rangle$ and $|i\rangle$. Only the configuration - the one-body potential - expected to give the most significant contribution to the functional integral is retained. Note that this potential depends on the precise matrix element being calculated - it is an artificial theoretical construct which cannot be defined uniquely, let alone measured. Nevertheless, it does provide a convenient physical insight. The TDMFA has been used to extract information about bound states [Re79, Le80, Re80, Ne82b], spontaneous and induced fission

[Le80c,Ke81,Ne82b], the nuclear partition function [Le80b], and scattering in many-nucleon problems [Al81a,Al81b,Ne82b,Tr83].

The auxiliary field Monte-Carlo (AFMC) algorithm developed here, is also based on the calculation of matrix elements of the Hubbard-Stratonovitch (HS) representation of the evolution operator. As in the GFMC and DMC, the imaginary-time propagator $U(T) = e^{-HT}$ is used to filter a trial wavefunction, Φ , to the exact ground state Ψ ; i.e., the ground-state energy, E_0 , for a system of A particles is written as

$$E_0 = \lim_{T \rightarrow \infty} \frac{\langle \Phi | H e^{-HT} | \Phi \rangle}{\langle \Phi | e^{-HT} | \Phi \rangle}, \quad (1.7)$$

where Φ is, in principle, any trial wavefunction not orthogonal to Ψ . When the functional integral expression for $U(T)$ is substituted in the matrix elements of Eq. (1.7), the resulting equation is amenable to exact evaluation via the standard Metropolis Monte-Carlo technique [Me53]. This involves a random walk over trajectories defined by the HS one-body potential. The principle advantage of the HS expression for the energy is that it allows the evolving many-body wavefunction, $e^{-HT} |\Phi\rangle$, to be expressed as a combination of single-particle orbitals. For fermions, antisymmetrization of the orbitals can be enforced exactly throughout the time evolution.

The use of an auxiliary field to eliminate fermion-fermion interactions, has been applied to the restricted problem of particles on a one-dimensional lattice [Hi83]. The system is described by a Hamiltonian $H = H_0 + H_I$, where H_0 is bilinear in the fermion operators and

$$H_I = C n_\uparrow n_\downarrow$$

is the two-body interaction. The n are occupation numbers at a lattice site for electrons with spin up or down. The Hubbard-Stratonovitch transformation applied to the partition function

$$Z \equiv \text{tr} e^{-\beta H} = e^{-\beta(H_0 + H_I)}$$

allows the exponent of the interaction term to be expressed in a form bilinear in fermion operators. The linearization is performed by introducing either an integral over a continuous auxiliary variable or a trace over a discrete Ising variable which takes on only the values ± 1 . Expectation values, written in terms of the partition function, can then be evaluated stochastically [Hi82].

This thesis describes the AFMC algorithm. Section 2 derives the Hubbard-Stratonovitch representation of the many-body evolution operator. Approximate solutions of transition amplitudes using this formulation are given in Section 3 and the relationship of this method to other standard nuclear physics techniques is briefly discussed. The approximations provide an indication of the proper initial conditions to be used in the exact AFMC solution.

The Metropolis Monte-Carlo method and its utilization in the auxiliary field formalism are discussed in Sections 4-6. Section 7 describes the application to a simple test case - the exactly soluble delta function potential for a system of bosons. The various contributions to the energy resolved by the AFMC are discussed in some detail.

Section 8 extends the method to fermions interacting via finite range potentials. The formalism remains the same as for bosons, but in practical terms a procedure to maintain antisymmetrization is introduced. Section 9, discusses improvements in the efficiency of the method by working in momentum space, rather than defining the wavefunction on a space mesh. These are important if the method is to be extended to more realistic systems. In Section 10 the difficulties involved in applications to repulsive potentials are treated. Two possible algorithms are then investi-

gated for incorporating systems with strong repulsive cores. Finally, Section 11 summarizes the results and discusses limitations of the method. Possible future applications are indicated.

§2. Hubbard-Stratonovitch representation of the propagator

The imaginary-time evolution operator filters a trial wavefunction Φ to the exact ground state Ψ . That is, the ground state energy E_0 for a system of A particles is given by

$$E_0 = \lim_{T \rightarrow \infty} \frac{\langle H\Phi | e^{-HT} | \Phi \rangle}{\langle \Phi | e^{-HT} | \Phi \rangle}, \quad (2.1)$$

where Φ is any trial wavefunction not orthogonal to Ψ . This is clear from the spectral expansion of the propagator:

$$e^{-HT} = \sum_{\mathbf{n}} | \mathbf{n} \rangle e^{-E_{\mathbf{n}} T} \langle \mathbf{n} | .$$

As $T \rightarrow \infty$ only the smallest $E_{\mathbf{n}}$ (namely, E_0) survives in the sum, and only the ground state value remains in the expression for the energy.

Eq. (2.1) allows a more efficient evaluation of the resulting path integral for the energy than does use of the unselective trace of Eq. (1.5), since the statistical errors associated with the use of a finite ensemble of trajectories are reduced. (Note that if Φ is the exact ground state, Eq. (2.1) will give $E = E_0$ independent of the errors in the numerator and denominator.) As in the GFMC and DMC methods, the efficiency of calculations is enhanced when Φ closely approximates Ψ .

We now wish to recast the expression for the energy into the form of a multi-dimensional integral. This is done using the auxiliary field or Hubbard Stratonovitch representation of the imaginary-time propagator $U(T) = e^{-HT}$. To derive the necessary transformation, consider the general Hamiltonian

$$\begin{aligned} H &= \sum_{\alpha\beta} T_{\alpha\beta} a_{\alpha}^{\dagger} a_{\beta} + \frac{1}{2} \sum_{\alpha\beta\gamma\delta} v_{\alpha\beta\gamma\delta} a_{\alpha}^{\dagger} a_{\beta}^{\dagger} a_{\delta} a_{\gamma} \\ &= \sum_{\alpha\beta} K_{\alpha\beta} \rho_{\beta\alpha} + \frac{1}{2} \sum_{\alpha\beta\gamma\delta} v_{\alpha\beta\gamma\delta} \rho_{\gamma\alpha} \rho_{\delta\beta} \end{aligned} \quad (2.2)$$

where

$$\rho_{\beta\alpha} \equiv a_{\alpha}^{\dagger} a_{\beta}$$

is the density operator and

$$K_{\alpha\beta} = T_{\alpha\beta} - \frac{1}{2} \sum_{\gamma} v_{\alpha\gamma\gamma\beta}$$

contains the kinetic energy plus a self-interaction term which will be removed later. The subscripts α, β, γ , and δ represent internal degrees of freedom - spin, isospin, etc. - as well as spatial coordinates.

It is convenient to work in the interaction representation. The Hamiltonian is divided into an "unperturbed" part $K \equiv K_{\alpha\beta} \rho_{\beta\alpha}$ and a "perturbed" part $v \equiv v_{\alpha\beta\gamma\delta} \rho_{\gamma\alpha} \rho_{\delta\beta}$. Operators are then time-dependent and include evolution under K - for example, the density operator becomes

$$\rho_{\beta\alpha}(t) = e^{Kt} \rho_{\beta\alpha} e^{-Kt} .$$

The interaction many-body propagator describes evolution under the "perturbed" part of the Hamiltonian, $v_I(t) = e^{Kt} v e^{-Kt}$ [Fe71]. Writing this out in full,

$$\begin{aligned} U_I(t_f, t_i) &= T_t e^{(-\int_{t_i}^{t_f} v_I(t) dt)} \\ &= T_t e^{-\frac{1}{2} \int_{t_i}^{t_f} dt \sum_{\alpha\beta\gamma\delta} \rho_{\gamma\alpha}(t) v_{\alpha\beta\gamma\delta} \rho_{\delta\beta}(t)} \\ &\equiv T_t e^{-\frac{1}{2} \int_{t_i}^{t_f} (\rho(t), v\rho(t))} , \end{aligned} \tag{2.3}$$

where T_t indicates the time ordering operator. The Schroedinger many-body evolution operator is related to U_I by $U(t) = e^{-Kt} U_I(t)$.

The Hubbard-Stratonovitch (HS) transformation introduces an auxiliary field in order to reduce the exponential of a two-body operator (e.g., v_I in Eq. (2.3)) to a functional integral over an infinite set of exponentials of one-body operators. The traces of such exponentials can be evaluated easily and also can be approximated using the stationary phase approxi-

mation (SPA). The transformation was originally developed to calculate the many-body partition function for systems containing two-body interactions [Hu59,St57]. It is based on the integration of an exponential of a quadratic form:

$$\int \prod_m \frac{d\sigma_m}{\sqrt{2\pi}} e^{\frac{1}{2} \sum_{mn} \sigma_m B_{mn} \sigma_n} = (\det B)^{-\frac{1}{2}}, \quad (2.4)$$

where B_{mn} is any real symmetric matrix. This can be seen to be correct by diagonalizing B_{mn} via an orthogonal transformation, noting that the required Jacobian is unity, and then performing standard Gaussian integrations to get a product of inverses of square roots of the eigenvalues of B. Shifting σ_m by a constant ρ_m (i.e. undiagonalizing the exponent), results in the desired expression

$$e^{-\frac{1}{2} \sum_{mn} \rho_m B_{mn} \rho_n} = \sqrt{\det \bar{B}} \int \prod_m \frac{d\sigma_m}{\sqrt{2\pi}} e^{\frac{1}{2} \sum_{mn} \sigma_m B_{mn} \sigma_n} e^{-\sum_{mn} \sigma_m B_{mn} \rho_n}. \quad (2.5)$$

Here, the σ_n have been introduced to linearize an exponent quadratic in ρ . Eq. (2.5) also holds when ρ_n are a set of commuting bounded operators, as may be seen by considering the action on a complete set of eigenstates. This commutation requirement will turn out to be superfluous.

Eq. (2.5) can be applied to the propagator in Eq. (2.3) by discretizing the time integral into intervals Δt such that $t_k = k \Delta t$ and letting the labels m and n in (2.5) represent α, β , and t_k so that

$$\begin{aligned} \rho_n &\rightarrow \rho_{\beta\alpha}(t_k) \\ \sigma_n &\rightarrow \sigma_{\beta\alpha}(t_k) \\ B_{mn} &\rightarrow B_{\alpha\beta,\alpha'\beta'}(t_k, t_{k'}) \Delta t^2. \end{aligned}$$

Confining interest to instantaneous potentials,

$$B_{\alpha\beta,\alpha'\beta'}(t, t') = v_{\alpha\alpha'\beta\beta'} \delta(t - t'),$$

we obtain an expression for the propagator for a single time step Δt

$$U_I(\Delta t) = e^{-\frac{1}{2}(\rho(t), v\rho(t)) \Delta t} = \int D[\sigma] e^{\frac{1}{2}(\sigma(t), v\sigma(t)) \Delta t} e^{-(\sigma(t), v\rho(t)) \Delta t}. \quad (2.6)$$

A shorthand notation has been used here -

$$(\rho(t), \nu\rho(t)) \equiv \sum_{\alpha\beta\alpha'\beta'} \rho_{\beta\alpha}(t) \nu_{\alpha\alpha'\beta\beta'} \rho_{\beta'\alpha'}(t)$$

- and similarly for the $(\sigma(t), \nu\sigma(t))$ and $(\sigma(t), \nu\rho(t))$ integrals. The measure of integration is

$$D[\sigma] = \det[\nu\delta] \prod_{\alpha\beta k} \frac{\Delta t \, d\sigma_{\beta\alpha}(t_k)}{\sqrt{2\pi}}. \quad (2.7)$$

Passing to the limit $\Delta t \rightarrow 0$ and from sums over k to integrals over t , we obtain the complete expression for the propagator from time t_i to t_f -

$$\begin{aligned} U_I(t_f, t_i) &= T_i e^{-\frac{1}{2} \int_{t_i}^{t_f} dt (\rho(t), \nu\rho(t))} \\ &= \int D[\sigma] e^{\frac{1}{2} \int_{t_i}^{t_f} dt (\sigma(t), \nu\sigma(t))} U_I^\sigma(t_f, t_i) \end{aligned} \quad (2.8)$$

where

$$U_I^\sigma = T_i e^{-\int_{t_i}^{t_f} dt (\sigma(t), \nu\rho(t))}.$$

This is a path integral expression for the propagator in which a time-dependent auxiliary field, $\sigma(t)$, which is coupled linearly to the density, has been introduced. At this point, it should be noted that the noncommutative nature of the ρ does not invalidate the derivation. The time ordering T_i implies the appropriate products of exponentials at different times and as $\Delta t \rightarrow 0$, equal time commutators vanish.

For actual evaluations, it is convenient to return to the Schroedinger picture. The HS representation of the many-body propagator is then given by

$$U(t_f, t_i) = \int D[\sigma] e^{\frac{1}{2} \int_{t_i}^{t_f} dt (\sigma, \nu\sigma)} U_\sigma(t_f, t_i), \quad (2.9a)$$

where

$$U_\sigma \equiv T_t e^{-\int_{t_i}^{t_f} dt h_\sigma(t)} \quad (2.9b)$$

describes the evolution with respect to

$$\begin{aligned} h_\sigma(t) &= \sum_{\alpha\beta} [K_{\alpha\beta} + \sum_{\alpha'\beta'} \sigma_{\beta'\alpha'}(t) v_{\alpha'\alpha\beta'\beta}] \rho_{\beta\alpha}(t) \\ &= \sum_{\alpha\beta} [K_{\alpha\beta} + W_{\alpha\beta}(t)] \rho_{\beta\alpha}(t) . \end{aligned} \quad (2.9c)$$

Amidst all the notation, it is important to note the significance of Eq. (2.9). The A -body operator U_σ describes the propagation due to a one-body time-dependent hamiltonian which is a linear functional of the auxiliary field. The total evolution operator, U , is then a coherent sum of an infinite number of these one-body propagators (each involving a different one-body potential parametrized by a different σ field) with a "gaussian weighting factor" $e^{\frac{1}{2}(\sigma, v\sigma)}$.

To see more clearly what this means physically, consider a Hamiltonian involving only an instantaneous local two-body potential, $v_{\alpha\beta\gamma\delta} = \delta_{\alpha\gamma} \delta_{\beta\delta} v(x_\alpha - x_\delta)$. For simplicity, spin and isospin variables are suppressed so that the labels α and β can be replaced by a single spatial coordinate and only the diagonal density operator $\rho(x) = a^\dagger(x) a(x)$ contributes in Eq. (2.9c). In first quantization, the Hamiltonian is

$$H = \sum_{i=1}^A \frac{p_i^2}{2m} + \frac{1}{2} \sum_{i \neq j=1}^A v(x_i - x_j)$$

and the corresponding propagator is given by

$$U(T) = \int D[\sigma(x,t)] e^{\frac{1}{2} \int_0^T dt dx dx' \sigma(x,t) v(x-x') \sigma(x',t)} U_\sigma(T) . \quad (2.10)$$

Here, $\sigma(x,t)$ is a real field integration variable whose measure is defined in Eq. (2.7) and

$$\begin{aligned} U_\sigma(T) &\equiv T_t e^{-\int_0^T dt [K + \int dx dx' \sigma(x,t) v(x-x') \rho(x')]} \\ &= T_t e^{-\int_0^T dt \sum_{i=1}^A h_\sigma(x_i,t)} \end{aligned} \quad (2.11)$$

with

$$h_{\sigma}(x, t) = -\frac{\hbar^2}{2m} \partial^2 / \partial x^2 \pm \frac{1}{2} v(0) + \int dx' v(x-x') \sigma(x', t) .$$

The -(+) refers to fermions (bosons). U_{σ} describes a simultaneous evolution of A particles from $t=0$ to $t=T$ in a time-dependent potential, $W_{\sigma}(x, t) = \int v(x-x') \sigma(x', t) dx'$. All particle interactions are now mediated through the σ field. Thus, the HS transformation has mapped an interacting particle problem to a system of non-interacting particles coupled to a fluctuating external field.

The expansion for the propagator (Eq. (2.9)) can be substituted into the expression for the ground state energy (Eq. (2.1)) to give the form chosen for Monte-Carlo evaluation:

$$E_0 = \lim_{T \rightarrow \infty} \frac{\int D[\sigma(x, t)] e^{\frac{1}{2} \int_0^T (\sigma, v \sigma) dt} \langle \Phi | U_{\sigma} | \Phi \rangle \frac{\langle H \Phi | U_{\sigma} | \Phi \rangle}{\langle \Phi | U_{\sigma} | \Phi \rangle}}{\int D[\sigma(x, t)] e^{\frac{1}{2} \int_0^T (\sigma, v \sigma) dt} \langle \Phi | U_{\sigma} | \Phi \rangle} . \quad (2.12)$$

Before describing the numerical techniques required, it is important to understand the various energy contributions being resolved in the exact calculation of this integral. Therefore, some approximate solutions to Eq. (2.12) are considered in the next section. These also provide an indication of the proper trial wavefunctions and initial conditions on the σ field for use in the Monte-Carlo process.

The AFMC method is in some respects similar to a formulation used in Monte-Carlo simulations of relativistic field theories [Fu80, Bl81, Sc81]. In these problems, the fermion degrees of freedom are "integrated out", leaving only a boson theory with an effective action (analogous to the our HS representation). The principal problem in such calculations is the evaluation of the enormous determinant (of dimension equal to the

number of lattice sites) appearing in the effective action. This is essentially due to the presence of the filled Dirac sea. For non-relativistic systems, the dimensionality of the determinant required to compute $\langle \Phi | U_{\sigma} | \Phi \rangle$ is relatively small and its direct evaluation is possible. This also emphasizes the advantage of the AFMC algorithm over the GFMC or DMC methods - positive and negative contributions to the norm are canceled exactly rather than statistically.

§3. Time-dependent mean-field approximation (TDMFA)

The auxiliary field formulation for the transition amplitude between initial and final states $|i\rangle$ and $|f\rangle$,

$$\begin{aligned} \langle f | U | i \rangle &= \int D[\sigma] e^{\frac{i}{\hbar} \int (\sigma, v\sigma)} \langle f | U_\sigma | i \rangle \\ &\equiv \int D[\sigma] e^{S[\sigma]} \end{aligned} \quad (3.1)$$

can be evaluated semiclassically using the stationary phase approximation (SPA). This amounts to solving $\delta S[\sigma] = 0$ by picking out the configuration(s) - the field(s) σ_0 - which provide(s) the most significant contribution(s) to the integral. It seems likely that if all the particles are affected by the interaction, small changes of the σ field will produce large changes in S , so that this approximation is valid - at least for a sufficiently large number of particles. An exact criterion for applicability is difficult to formulate, however.

For clarity, only the simplified case of an instantaneous local potential is treated, though everything in this section can be done for the general Hamiltonian, Eq. (2.2). Setting the variation

$$\begin{aligned} \frac{\delta S}{\delta \sigma(x,t)} &= \int dx' v(x-x') \sigma(x',t) - \frac{\langle f | T_t \int dx' v(x-x') \rho(x',t) e^{-\int h_\sigma} | i \rangle}{\langle f | T_t e^{-\int h_\sigma} | i \rangle} \\ &= \int dx' v(x-x') \left[\sigma(x',t) - \frac{\langle f | U_\sigma(t_f,t) \rho(x',t) U_\sigma(t,t_i) | i \rangle}{\langle f | U_\sigma(t_f,t_i) | i \rangle} \right] \end{aligned}$$

to zero, results in a self-consistent equation for σ_0 . The solution is the time-dependent mean-field approximation

$$\sigma_0(x,t) = \frac{\langle f | U_{\sigma_0}(t_f,t) \rho(x,t) U_{\sigma_0}(t,t_i) | i \rangle}{\langle f | U_{\sigma_0}(t_f,t_i) | i \rangle} \quad (3.2)$$

corresponding to a transition amplitude $e^{S[\sigma_0]}$. To ensure that a real mean-field is obtained, the integral (3.1) can be written instead as

$$\int D[\sigma] |\langle f | U_\sigma | i \rangle| e^{S_{eff}[\sigma]} \quad (3.3)$$

where

$$S_{eff}[\sigma] \equiv \frac{1}{2} [(\sigma, v\sigma) + i \ln \langle f | U_\sigma | i \rangle - i \ln \langle f | U_\sigma | i \rangle^*] .$$

The resulting SPA solution is just the real part of Eq. (3.2) and the transition amplitude is $|\langle f | U_{\sigma_0} | i \rangle| e^{S_{eff}[\sigma_0]}$. The difference between this result and (3.2) arises from the use of different parts of the integrand to define the SPA. Note that the precise form of σ_0 is also dependent on the final and initial states; i.e., the exact matrix element being evaluated. This points out the unphysical nature of the mean-field. It is not a fundamental entity and is not uniquely defined or measurable.

We now consider an important case in which the initial and final states are A -particle Slater determinants:

$$|i\rangle = (A!)^{-\frac{1}{2}} \sum_P \prod_{j=1}^A \psi_{Pj}^i \quad (3.4)$$

$$|f\rangle = (A!)^{-\frac{1}{2}} \sum_P \prod_{j=1}^A \varphi_{Pj}^f ,$$

where the sum over P stands for all possible permutations. Bosons can be treated by replacing the permutations with simple products. The transition amplitude for the Slater determinant wavefunctions is

$$\begin{aligned} \langle f | U | i \rangle &= \int D[\sigma] e^{\frac{1}{2} \int (\sigma, v\sigma)} \det \langle \varphi^i | U_\sigma | \psi^f \rangle \\ &= \sum_P (-1)^P \int D[\sigma] e^{\frac{1}{2} \int (\sigma, v\sigma)} \prod_{j=1}^A \langle \varphi_j | U_\sigma^j | \psi_{Pj} \rangle . \end{aligned} \quad (3.5)$$

In writing this, we have used the fact that U_σ is just a product of commuting one-body operators (see Eq. (2.11))

$$U_\sigma = \prod_{j=1}^A U_\sigma^j \quad (3.6)$$

and is therefore symmetric in particle coordinates. The SPA mean-field solution to (3.5) is

$$\sigma_o(x, t) = \text{Re} \frac{\sum_P (-1)^P \sum_{j=1}^A \varphi_j^*(x, t) \psi_{Pj}(x, t)}{\det \langle \varphi(x, t) | \psi(x, t) \rangle} \quad (3.7a)$$

where

$$\begin{aligned} |\psi_j(x, t)\rangle &= U_{\sigma_o}^j(t, t_i) |\psi_j^i\rangle \\ |\varphi_j(x, t)\rangle &= U_{\sigma_o}^j(t_f, t)^\dagger |\psi_j^f\rangle . \end{aligned} \quad (3.7b)$$

Expressed in different language, the functions φ_j and ψ_j satisfy the differential equations

$$\begin{aligned} \frac{\partial \psi_j(x, t)}{\partial t} &= -(K + W_{\sigma_o}) \psi_j(x, t) \\ \frac{\partial \varphi_j(x, t)}{\partial t} &= -(K + W_{\sigma_o}) \varphi_j(x, t) \end{aligned} \quad (3.7c)$$

where

$$K = p^2/2m - \frac{1}{2}v(0)$$

is the kinetic plus self-energy term and

$$W_{\sigma_o}(x, t) = \int v(x - x') \text{Re} \frac{\sum_P (-1)^P \sum_{j=1}^A \varphi_j^*(x', t) \psi_{Pj}(x', t)}{\det \langle \varphi_j(x', t) | \psi_{Pj}(x', t) \rangle} dx'$$

is the one-body potential determined by the mean-field, σ_o . The mean-field can be calculated self-consistently using Eqs. (3.7). An initial guess is made for σ_o which is then used to generate the wavefunctions $\psi_j(x, t)$ and $\varphi_j(x, t)$ via Eqs. (3.7c). Substituting the results in (3.7a) gives a new value for σ_o , for which the process is then repeated.

In special cases, the mean-field solution can be related to other standard approaches in many-body physics. In particular, if $|f\rangle \equiv U_{\sigma_o}(t_f, t_i) |i\rangle$, the differential Eqs. (3.7c) reduce to

$$\frac{\partial \psi_j}{\partial t} = -\left[\frac{p^2}{2m} - \frac{1}{2}v(0) + \int v(x-x') \sum_{j=1}^A |\psi_j(x', t)|^2 dx' \right] \psi_j . \quad (3.8)$$

This is similar to the time-dependent Hartree-Fock (TDHF) equation but without the exchange term in the potential - it is actually just the

Hartree approximation.

Another important special case occurs when the final state is required to be identical to the initial state and an eigenfunction of the Hamiltonian; i.e., $\langle i | U(t_f, t_i) | i \rangle \equiv e^{-iE(t_f - t_i)}$. The single-particle wavefunctions are taken to be

$$\begin{aligned}\psi_j(x, t) &= e^{-i\varepsilon_j(t-t_i)} \psi_j \\ \varphi_j(x, t) &= e^{-i\varepsilon_j(t-t_f)} \psi_j ,\end{aligned}$$

where ψ_j is a normalized, time-independent single-particle wavefunction and ε_j acts as a single-particle energy. The differential Eqs. (3.7c) then reduce to

$$\left(\frac{p^2}{2m} - \frac{1}{2}v(0) + W_{\sigma_0} \right) \psi_j(x, t) = \varepsilon_j \psi_j(x, t) \quad (3.9a)$$

with

$$W_{\sigma_0}(x) = \int v(x-x') \sigma_0(x') dx' \quad (3.9b)$$

and

$$\sigma_0(x) = \sum_{j=1}^A |\psi_j(x)|^2 . \quad (3.9c)$$

As expected, the mean-field σ_0 is independent of time and just equal to the single-particle density. The energy E is determined by writing out the SPA transition amplitude

$$\begin{aligned}e^{-E(t_f - t_i)} &\equiv \langle i | U(t_f, t_i) | i \rangle \\ &= e^{\frac{1}{2}(\sigma_0, v\sigma_0)(t_f - t_i)} \det \langle \varphi_j(x, t) | \psi_j(x, t) \rangle \\ &= e^{\frac{1}{2} \int (\sigma_0, v\sigma_0)} \prod_{j=1}^A e^{-\varepsilon_j(t_f - t_i)} \langle \psi_j | \psi_j \rangle .\end{aligned} \quad (3.10a)$$

and equating the exponents to obtain

$$\begin{aligned}E &= \sum_{j=1}^A \varepsilon_j - \frac{1}{2}(\sigma_0, v\sigma_0) \\ &= \sum_{j=1}^A \langle j | \frac{p^2}{2m} - \frac{1}{2}v(0) | j \rangle + \frac{1}{2} \sum_{i,j=1}^A \langle ij | v | ij \rangle .\end{aligned} \quad (3.10b)$$

Thus, the energy of the static system in the mean-field approximation is

the standard Hartree energy plus the self-energy term.

It is crucial to note that the *character* (*not* the value) of the mean-field is unaffected by the form of the initial and final states. Despite the fact that antisymmetrized wavefunctions (3.4) were used, only a direct matrix term appeared in the differential Eqs. (3.8) and (3.9) and the energy Eq. (3.10); i.e., the SPA solutions correspond to the Hartree and not the Hartree-Fock approximation. This could pose a problem, particularly in nuclear systems where exchange matrix elements are comparable to direct matrix elements.

There is a connection between the artificial σ field and nuclear field theory [Le80b]. The mean-field corresponds to the meson field generated by the self-consistent distribution of fermions. The scalar meson coupling produces the direct and the vector meson coupling the exchange matrix elements. In particular, the one-pion-exchange-potential contributes to the HF energy of nuclear matter only through the exchange term.

Quadratic corrections. A study of the higher order corrections to the SPA clarifies the issue of the exchange matrix elements and provides several interesting features. Quadratic contributions to the transition amplitude are obtained from an expansion of $S[\sigma]$ to second order in $\zeta \equiv \sigma - \sigma_0$, the variation of σ from the mean-field solution:

$$\int D[\sigma] e^{S[\sigma]} \approx \int D[\sigma] \exp \{S[\sigma_0] + \int dx dx' dt dt' \frac{\delta^2 S}{\delta \sigma(x,t) \delta \sigma(x',t')} \zeta(x,t) \zeta(x',t')\} \quad (3.11a)$$

$$= \left[\frac{\det[v(x-x') \delta(t-t')]}{\det\left[\frac{\delta^2 S}{\delta \sigma(x,t) \delta \sigma(x',t')}\right]} \right]_{\sigma_0}^{\frac{1}{2}} e^{S[\sigma_0]} \quad (3.11b)$$

where the subscript indicates that the quantity in brackets is to be

evaluated at σ_0 . The second equality is derived from Eq. (2.4). Using the fact that the measure $D[\sigma]$ is defined relative to $\det(\nu \delta)$ (Eq. (2.7)) and making the change of variables from σ to ζ , we obtain

$$\int D[\zeta] e^{\frac{1}{2} \sum_{mn} \zeta_m B_{mn} \zeta_n} = \left[\frac{\det(\nu \delta)}{\det B} \right]^{\frac{1}{2}}.$$

Letting m and n stand for space-time coordinates, $\delta^2 S / \delta^2 \sigma$ correspond to B and going to the continuum limit, the result (3.11b) follows.

The second functional derivative of S is

$$\begin{aligned} \frac{\delta^2 S}{\delta \sigma(x, t) \delta \sigma(x', t)} &= \delta(t-t') v(x-x') \\ &\quad - \int \int dx'' dx''' v(x-x'') v(x'-x''') C_0(x''t''; x'''t''') \\ &= \int \int dx'' dt'' \delta(t-t'') v(x-x'') [\delta(t''-t) \delta(x''-x) \\ &\quad + \int \int dx''' dt''' C_0(x''t''; x'''t''') v(x'''-x') \delta(t'''-t')] \\ &\equiv [\nu \delta][1 - C_0 \nu \delta] \end{aligned} \quad (3.12)$$

where C_0 is defined by

$$\begin{aligned} C_0(xt; x't') &\equiv \frac{\langle f | T_t \rho(xt) \rho(x't') e^{-\int h_{\sigma_0}(t)} | i \rangle}{\langle f | T_t e^{-\int h_{\sigma_0}(t)} | i \rangle} \\ &\quad - \frac{\langle f | T_t \rho(xt) e^{-\int h_{\sigma_0}(t)} | i \rangle \langle f | T_t \rho(x't') e^{-\int h_{\sigma_0}(t)} | i \rangle}{\langle f | T_t e^{-\int h_{\sigma_0}(t)} | i \rangle \langle f | T_t e^{-\int h_{\sigma_0}(t)} | i \rangle}. \end{aligned} \quad (3.13)$$

Note that C_0 is just a time-dependent generalization of the familiar density-density correlation function. Substituting (3.12) in the quadratic term in (3.11b), cancelling the ratio in $\det(\nu \delta)$, and using the identity $\det B = \exp(\text{tr} \ln B)$, yields

$$\det[1 - C_0(\nu \delta)]^{-\frac{1}{2}} = \exp(-\frac{1}{2} \text{tr} \ln[1 - C_0(\nu \delta)]) = \exp \frac{1}{2} \sum_{n=1}^{\infty} \text{tr} \frac{1}{n} [C_0(\nu \delta)]^n$$

so that to second order

$$\int D[\sigma] e^{S[\sigma]} \approx e^{S[\sigma_0]} \exp \frac{1}{2} \sum_{n=1}^{\infty} \text{tr} \frac{1}{n} [C_0(v \delta)]^n . \quad (3.14)$$

In the stationary limit, in which $|i\rangle = |f\rangle$ is considered to be an eigenstate of h_σ and σ is time-independent, C_0 reduces to

$$\begin{aligned} C_0^{static} &= \langle i | \psi^\dagger(x) \psi(x) \psi^\dagger(x') \psi(x') | i \rangle - \langle i | \psi^\dagger(x) \psi(x) | i \rangle \langle i | \psi^\dagger(x') \psi(x') | i \rangle \\ &= \rho(x) \delta(x-x') - \rho(x, x') \rho(x', x) \end{aligned}$$

where

$$\rho(x, x') \equiv \sum_{j=1}^A \psi_j^*(x) \psi_j(x')$$

is the one-body density matrix. Substituting this expression into the first contribution to the sum over n in Eq. (3.14), the leading order correction to the SPA is obtained:

$$\begin{aligned} \frac{1}{2} \text{tr} C_0^{static}(v \delta) &= \frac{1}{2} \int dx dx' dt C_0^{static}(x t, x' t') v(x-x') \quad (3.15) \\ &= -\frac{1}{2} \int dx dx' dt [\rho(x) \delta(x-x') - \rho(x, x') \rho(x', x)] \\ &\quad \times v(x-x') \\ &= -[\frac{1}{2} A v(0) - \frac{1}{2} \sum_{jk} \langle jk | v | kj \rangle] (t_f - t_i) . \end{aligned}$$

The first term exactly cancels the unpleasant self-energy term $v(0)$ in (3.10b) while the second adds the proper Fock exchange matrix elements.

To understand the physical meaning of the remaining terms in the sum over n in (3.14) write C_0 as

$$\begin{aligned} C_0^{static} &= \frac{\langle i | T_t [e^{h_\sigma t} \rho(x) e^{-h_\sigma t}] [e^{h_\sigma t'} \rho(x') e^{-h_\sigma t'}] | i \rangle}{\langle i | i \rangle} \quad (3.15) \\ &\quad - \frac{\langle i | [e^{h_\sigma t} \rho(x) e^{-h_\sigma t}] | i \rangle \langle i | [e^{h_\sigma t'} \rho(x') e^{-h_\sigma t'}] | i \rangle}{\langle i | i \rangle \langle i | i \rangle} . \end{aligned}$$

Expressed in terms of field operators, this result is just a product of two Green's functions, starting at t and t' and ending at t' and t respectively; i.e., it is just a particle-hole excitation bubble. $[C_0(v \delta)]^n$ is therefore made up of a chain of n such bubbles connected by matrix elements of the instantaneous interaction potential v . The trace connects the chain

back on itself to form the random phase approximation (RPA) ring, with the factor of $\frac{1}{n}$ stemming from a counting argument about different ways of choosing the top of the ring.

Combining all the quadratic corrections yields an expression for the transition amplitude

$$\langle i | U(t_f, t_i) | i \rangle \approx e^{-\left[\sum_j \langle j | \frac{p^2}{2m} | j \rangle + \frac{1}{2} \sum_{jk} \langle jk | v | jk - kj \rangle + E_{RPA} \right] (t_f - t_i)}$$

The energy of the system now contains the proper Hartree-Fock plus the RPA contributions, without the self-energy term. For a time-dependent h_σ , the details are more complex, but the structure of the $\frac{1}{2} \text{tr} C_\sigma(v\delta)$ terms is identical, generating the self-energy and exchange pieces.

The recovery of the exchange terms can be accomplished in another way. Different pairings of creation operators a_α^\dagger and a_β in Eq. (2.2) will lead to different means of introducing the σ field. Such alternative formulations are useful for suggesting different approximations - ie. one results in the Fock terms in the SPA solution with the Hartree contributions arising from the quadratic corrections.

In the AFMC algorithm, use is made of the original pairing of creation operators, Eq. (2.2). This results in the appearance of density, rather than pairing density, operators. Typically, initial conditions are taken from the static mean-field solution (3.9). Thus, in exact Monte-Carlo evaluation, we are actually resolving the exchange, RPA, and other higher order corrections. This will be discussed in detail in Section 7 where the AFMC is applied to an exactly soluble system.

§4. Numerical techniques - discretization of the integral

In the next three sections, techniques for the numerical evaluation of the auxiliary field energy integral (Eq. (2.12)) are discussed. A tractable many-body wavefunction is constructed from sets of single-particle functions. The fields are then discretized on a space-time mesh and an appropriate approximation for the single-particle evolution operator U_σ is derived. The center-of-mass motion is treated by the addition of a harmonic oscillator potential which confines the system to the mesh. In Section 5, the Metropolis algorithm is described and techniques for performing the AFMC random walk are discussed in Section 6.

Many-body wavefunction. Although, in principle, the ground state energy

$$E_0 = \lim_{T \rightarrow \infty} \frac{\langle \Phi | He^{-HT} | \Phi \rangle}{\langle \Phi | e^{-HT} | \Phi \rangle}$$

can be found by using any trial wavefunction, Φ , not orthogonal to the true ground state, the AFMC method is tractable only if Φ is made up of single-particle orbitals. In particular, symmetrized product states are used for bosons and Slater determinants for fermions. U_σ is written as a product of propagators, each of which separately evolves one of the single-particle states, Eq. (3.6), so that many-body matrix elements reduce to one- or two-body integrals, which can be evaluated directly (see Eqs. (3.4)-(3.5) for the appropriate matrix elements and wavefunctions). The limitations created by this restriction on the form of Φ are discussed later.

Space-time discretization. We consider only one space dimension and bound space-time to a region $0 \leq t \leq T$, $|\mathbf{x}| \leq L/2$ by defining an $(N+1) \times M$ mesh.

$$x_j = (j - \frac{1}{2}M - \frac{1}{2}) \Delta x, \quad j=1, \dots, M \quad \Delta x = L / M$$

$$t_i = (i-1)\Delta t, \quad i=1, \dots, N+1 \quad \Delta t = T / N$$

M is taken to be even to avoid points at the spatial origin - in case of potentials with singularities. Of course, we suppose that Δx and Δt are sufficiently small. For Δx , this is determined by the accuracy of spatial integrations, while Δt must be small compared to all time scales in the problem and must yield sufficient accuracy for the discrete evolution operator (see below).

The wavefunctions are defined on the mesh, while the σ fields are taken to be on the half-time points, i.e. $\sigma_j^i = \sigma(t_i - \frac{1}{2}\Delta t, x_j)$. The equation for the energy (2.12) is discretized as

$$E_0(T=N\Delta t) = \frac{\int D[\sigma_j^i] e^{\frac{1}{2} \sum_{i=1}^N (\sigma, v \sigma)_i \Delta t} \langle \Phi | U_\sigma | \Phi \rangle \frac{\langle H \Phi | U_\sigma | \Phi \rangle}{\langle \Phi | U_\sigma | \Phi \rangle}}{\int D[\sigma_j^i] e^{\frac{1}{2} \sum_{i=1}^N (\sigma, v \sigma)_i \Delta t} \langle \Phi | U_\sigma | \Phi \rangle}, \quad (4.1)$$

where the measure is just $D[\sigma_j^i] = \prod_{i=1}^N \prod_{j=1}^M d\sigma_j^i$ (since any overall constants cancel in the ratio) and the inner product is given by the sum

$$(\sigma, v \sigma)_i = \sum_{j=1}^M \sum_{k=1}^M \sigma_j^i v_{jk} \sigma_k^i (\Delta x)^2 \quad v_{jk} \equiv v(x_j - x_k) .$$

The discretized evolution operator is expressed as a product $U_\sigma = \prod_{i=1}^N U_\sigma^i$ with $U_\sigma^i(\Delta t)$ effecting the evolution of single-particle wavefunctions from t_i to t_{i+1} under the one-body hamiltonian $h_\sigma^i(x_j) = -D^2/2m + \sum_{k=1}^M v_{jk} \sigma_k^i(\Delta x)$. (D^2 is the usual 3-point discretization of the second-derivative).

Discretization of the propagator - Crank-Nicholson approximation.

From the standard derivation of the Hubbard-Stratonovich transforma-

tion using a discretization of the time, it can be shown that any form used for U_σ^i must meet certain accuracy requirements. Consider the auxiliary field representation for a single time step, Eq. (2.6). Expanding the exponents schematically and performing the resulting Gaussian integrals results in

$$\begin{aligned} e^{\frac{\Delta t}{2}(\rho, v\rho)} &= \int D[\sigma] e^{\frac{1}{2}\Delta t(\sigma, v\sigma)} e^{-\Delta t(\sigma, v\rho)} \\ &\sim C \int d\sigma e^{\frac{1}{2}\Delta t(\sigma, v\sigma)} (1 + \Delta t(\sigma, v\rho) + \frac{1}{2}\Delta t^2(\sigma, v\rho)^2 \dots) \\ &\sim C \left(\frac{\sqrt{\pi}}{\sqrt{\frac{1}{2}v\Delta t}} + 0 + \frac{\frac{1}{2}\Delta t^2 \rho^2 v^2 \sqrt{\pi}}{2\sqrt{\frac{1}{2}v\Delta t}^3} \dots \right) \end{aligned}$$

Writing out the term on the left hand side as $1 + \frac{1}{2}\Delta t(\rho, v\rho) \dots$ and equating coefficients of ΔT , we see that the constant C must be $\sqrt{v\Delta t}/\sqrt{2\pi}$. Furthermore, the contribution from the order Δt^2 term in the expansion for U_σ evidently corresponds to the order Δt term in the expansion for U . The implication is that any discrete approximation for the propagator $U_\sigma = \prod_i U_\sigma^i(\Delta t)$ had better be correct through second order to ensure that the Hubbard-Stratonovitch transformation works.

The Crank-Nicholson formula for U_σ , familiar from time-dependent Hartree-Fock calculations [Bo76,Ke76,Ko77] is of the required accuracy. It is also computationally efficient for the AFMC, since its effect on a single-particle wavefunction can be quickly evaluated. To derive this formula for the propagator, we begin with the discretized Schroedinger equation ($\hbar = 1$)

$$i \left(\frac{\varphi_j^{i+1} - \varphi_j^i}{\Delta t} \right) = \sum_k h_{jk}^{i+\frac{1}{2}} \varphi_k^{i+\frac{1}{2}} . \quad (4.2a)$$

Here, the superscript i labels the time discretization and the subscripts j and k the space mesh points. h is the discretized form of the Hamiltonian,

$$h_{jk}^{i+\frac{1}{2}} = -\frac{1}{2m \Delta t^2} (\delta_{j,k+1} + \delta_{j,k-1} - 2\delta_{j,k}) + W_j^{i+\frac{1}{2}} \delta_{j,k} \quad (4.2b)$$

where $W_j^{i+\frac{1}{2}}$ is the auxiliary field (or the Hartree-Fock) potential at the half-time points on the mesh.

The naive approximation is to set $\varphi^{i+\frac{1}{2}} \approx \varphi^i$. If any time-dependence of h is ignored, this results in a formula for the evolution operator

$$\varphi^{i+1} \approx (1 - i \Delta t h) \varphi^i ,$$

where the spatial variables have been suppressed for simplicity. Note that if the Hamiltonian is hermitian, the expression $(1 - i \Delta t h)$ is not unitary. Therefore, this discretization of the propagator results in numerical instabilities - in particular, problems with those components of φ having the largest modulus eigenvalues.

A better approximation is given by

$$\varphi^{i+\frac{1}{2}} \approx (\varphi^i + \varphi^{i+1})/2 ,$$

so that

$$\varphi^{i+1} \sim \left(\frac{1 - i h \Delta t/2}{1 + i h \Delta t/2} \right) \varphi^i , \quad (4.3)$$

as can be seen by direct substitution. This is the Crank-Nicholson formula. It possesses two advantages over the previous expression. First, in real time, it is manifestly unitary, while in the imaginary-time limit, the existence of h in both numerator and denominator prevents exponential amplification of that component of φ associated the eigenvalue of largest modulus. Secondly, the expression is good through order Δt^2 as can be seen by a simple expansion

$$\begin{aligned} \left(\frac{1 - i h \Delta t/2}{1 + i h \Delta t/2} \right) &= \left(1 - \frac{i \Delta t}{2} h \right) \left(1 - \frac{i \Delta t}{2} h - \frac{\Delta t^2}{4} h^2 \dots \right) \\ &= 1 - i \Delta t h - \frac{\Delta t^2}{2} h^2 \dots , \end{aligned}$$

which is just $U_\sigma(\Delta t) = e^{-ih\Delta t}$ to second order.

The discrete U_σ involves operations using only sparse matrices - in fact, tridiagonal matrices, as long as a three-point expression for the second derivative is used in the formula for the Hamiltonian h (4.2b). Rewriting Eq. (4.3) in imaginary time as

$$(1 + h_\sigma \tau / 2)(\varphi^{i+1} + \varphi^i) = 2\varphi^i \quad (4.4)$$

it is clear that the operation of finding $\varphi^{i+1} + \varphi^i$ (and hence φ^{i+1}) is equivalent to inverting a tridiagonal matrix $(1 + h_\sigma \tau / 2)$. A method known as Gaussian elimination and backwards substitution provides an efficient algorithm for doing this [Va62]. Explicitly, consider solving $Az=k$ for z , where A is an $M \times M$ tridiagonal matrix with elements labeled as

$$A = \begin{bmatrix} b_1 & c_1 & 0 & 0 & 0 \\ a_2 & b_2 & c_2 & 0 & 0 \\ 0 & a_3 & b_3 & \cdots & 0 \\ 0 & 0 & \cdots & \cdots & \cdots \\ 0 & 0 & 0 & \cdots & \cdots \end{bmatrix}$$

and k is an M component column vector. The components of z are given by the recursion relation

$$z_{n+1} = w_n z_n + g_n \quad 1 \leq n \leq M-1 \quad (4.5a)$$

with

$$w_{n-1} = \frac{-a_n}{b_n + c_n w_n} \quad 2 \leq n \leq M \quad (4.5b)$$

$$g_{n-1} = \frac{k_n - c_n g_n}{b_n + c_n w_n}$$

These equations are derived by substituting (4.5a) for z_{n-1} and z_{n+1} in the matrix component equation $a_n z_{n-1} + b_n z_n + c_n z_{n+1} = k_n$ and equating the coefficients of z_n and 1. The initial values used in the recursion equations are determined by the boundary conditions on z . Since the wavefunction vanishes at the edges of the coordinate mesh, i.e. $\varphi_M = \varphi_1 = 0$, it follows that $w_{M-1} = g_{M-1} = 0$. Two sweeps through the

space mesh of M points are then required to invert the matrix A using (4.5) - the first to calculate the w_i and g_i , the second to determine the z components.

In the case of a time-dependent Hamiltonian the approximation

$$\varphi^{i+1} = \left[\frac{2}{1 + h^{i+\frac{1}{2}} \tau / 2} - 1 \right] \varphi^i \quad (4.6)$$

can be used by first calculating an approximate $h^{i+\frac{1}{2}}$ and then performing the wavefunction evolution. This requires two inversions for each time step.

Self-interaction term. The auxiliary field representation of the propagator contains a self-energy term which was ignored in formulating the Hamiltonian of Eq. (4.2b). To see that this is permissible, consider a Hamiltonian involving instantaneous two-body interactions

$$H = \sum_{i=1}^A \frac{p_i^2}{2m} - \frac{1}{2} \sum_{i \neq j} V(x_i - x_j) . \quad (4.7)$$

The corresponding propagator, U_σ , describes single particle evolution under

$$h_\sigma = \int [K(x) + W(x,t)] \rho(x,t) dx \quad (4.8)$$

where

$$K = \frac{p^2}{2m} + \frac{1}{2} V(0)$$

and

$$W(x,t) = \int dx' V(x-x') \sigma(x',t) .$$

It is evident that the self-interaction term contributes only a constant shift of the energy scale $\frac{1}{2} A V(0)$ in the time evolution. Since this does not affect the results, the term can be eliminated in actual computations. In fact, to maintain a convenient normalization of the wavefunctions, an arbitrary constant term is added to h_σ , without affecting the energy

values obtained.

Center-of-mass motion. In nuclear systems, all particles are of approximately the same mass. Therefore, the center-of-mass of the system cannot be fixed. To get around this problem, an harmonic oscillator potential is included which confines the system within the space mesh. The Hamiltonian for A particles then has an additional term

$$\begin{aligned} H_{\Omega} &= \frac{1}{2} mA\Omega^2 \left(\sum_i x_i / A \right)^2, \\ &= \frac{m\Omega^2}{2A} \sum_i x_i^2 + \frac{m\Omega^2}{2A} \sum_{i \neq j} x_i x_j \end{aligned}$$

containing both one- and two-body pieces. When this is incorporated into the auxiliary field equation, Eq. (4.8), the additional terms

$$-\frac{1}{2} \frac{m\Omega^2}{A} x^2 + \frac{m\Omega^2}{A} x \left[\int dx' x' \sigma(x', t) \right]$$

are added to the one-body Hamiltonian h_{σ} and the exponent in $(\sigma, v\sigma)$ has an extra piece

$$\frac{m\Omega^2}{A} \left[\int \sigma(x') dx' \right]^2.$$

These changes are easily incorporated into the calculation. The resulting ground state energy is merely shifted by the zero-point energy of the oscillator, namely $\frac{1}{2}\hbar\Omega$.

§5. Metropolis algorithm

The expression for the ground state energy in Eq. (2.12) is a form amenable to Monte-Carlo evaluation. This is evident when the equation is written as

$$E_0 = \lim_{T \rightarrow \infty} \frac{\int D[\sigma] W[\sigma] \frac{\langle H\Phi | U_\sigma | \Phi \rangle}{\langle \Phi | U_\sigma | \Phi \rangle}}{\int D[\sigma] W[\sigma]} \quad (5.1a)$$

where

$$W[\sigma] = e^{\frac{1}{2} \int (\sigma, v \sigma) dt} \langle \Phi | U_\sigma | \Phi \rangle . \quad (5.1b)$$

$W[\sigma]$ plays the role of a probability distribution for an evaluation of the energy term $\langle H\Phi | U_\sigma | \Phi \rangle / \langle \Phi | U_\sigma | \Phi \rangle$.

The integral (5.1) can be evaluated using a Monte-Carlo technique developed by Metropolis et al. [Me53,Bi79]. The Metropolis algorithm is a Markov process - that is, instead of choosing a set of configurations σ randomly and weighting them according to some factor, W , it constructs a random walk through configuration space according to W and weighs the resulting configurations equally. Applied to the auxiliary field representation, an uncorrelated sequence of σ fields is generated, distributed according to the weight functional $W[\sigma]$. The energy is then simply the average of the estimator term, $\langle H\Phi | U_\sigma | \Phi \rangle / \langle \Phi | U_\sigma | \Phi \rangle$, over the various configurations.

The precise algorithm is stated as follows:

Metropolis algorithm. Let $W[\sigma_I]$ be the weight of the initial configuration I . If changing σ_I to σ_{II} results in a configuration II with weight $W[\sigma_{II}]$, then the change is accepted if

$$\frac{W[\sigma_{II}]}{W[\sigma_I]} > 1$$

or if

$$\frac{W[\sigma_{II}]}{W[\sigma_I]} > \text{a uniform random number on } [0,1] .$$

Otherwise the change is rejected and configuration I is kept as the new configuration in taking the energy average.

The Metropolis algorithm can be proved rigorously using the central limit theorem. However a more intuitive argument shows that a Markov chain, established according to the above rule, asymptotically approaches the distribution of states determined by the weight W . Consider a change from configuration I to configuration II , where the weight $W[\sigma_{II}] > W[\sigma_I]$. Such a move has an *a priori* probability $T_{I \rightarrow II} = T_{II \rightarrow I}$, since this is just determined by the probability of a random walk in any direction. Using the Metropolis algorithm, the total transition probabilities for changes between configurations I and II are just

$$T(I \rightarrow II) = T_{I \rightarrow II} \frac{W[\sigma_{II}]}{W[\sigma_I]}$$

$$T(II \rightarrow I) = T_{II \rightarrow I} = T_{I \rightarrow II} .$$

The total number of transitions between states I and II , $N_{I \leftrightarrow II}$, is given by the transition probabilities times the populations, N_I and N_{II} , of those states

$$N_{I \rightarrow II} = N_I T(I \rightarrow II) = N_I T_{I \rightarrow II} \frac{W[\sigma_{II}]}{W[\sigma_I]}$$

$$N_{II \rightarrow I} = N_{II} T(II \rightarrow I) = N_{II} T_{I \rightarrow II} .$$

Then the net change in population between the two states is

$$\Delta N_{I \rightarrow II} = N_I T_{I \rightarrow II} \left[\frac{W[\sigma_{II}]}{W[\sigma_I]} - \frac{N_{II}}{N_I} \right]$$

Note that as long as the population ratio N_{II}/N_I is smaller than that determined by the relative $W[\sigma]$, N_{II} increases. Contrarily, if the N ratio

is the larger, N_{II} decreases. Therefore, asymptotically - after many moves - the Metropolis algorithm results in a distribution which is the same as that of the weights $W[\sigma]$. A similar discussion holds when $W[\sigma_{II}] < W[\sigma_I]$, of course.

Many transitions $\sigma_I \rightarrow \sigma_{II}$ result in large changes in the weights. Hence the probability of acceptance of a given change is small and convergence is slow. To remove this difficulty, one can introduce a parameter Δ and require that $|\sigma_{II} - \sigma_I| < \Delta$ in some sense. The parameter Δ is adjusted so that the acceptance ratio - the percentage of changes accepted - is appropriately large. However, the size of the changes in σ must not be limited too stringently or the new configuration will be highly correlated with the previous one. This will slow the approach to the asymptotic region, creating difficulties in the energy calculations (see the discussion of error analysis in Section 6).

The Metropolis algorithm requires that $W[\sigma]$ be positive definite. This condition is always satisfied by symmetrized product boson states and spin and/or isospin symmetric fermion Slater determinant wavefunctions in a state-independent potential. More general systems, in particular those with partially filled levels [Hi83], are not guaranteed to meet the requirement. If $W[\sigma]$ is not positive definite, $|W|$ can be used as the weight and the sign $W/|W|$ appended to the energy contribution from each configuration. However, even here W must be predominantly of one sign for the denominator in (5.1a) to remain large and good statistical accuracy be achieved. While we have no guarantee that W is well-behaved in the general case, results for fermion systems treated by other methods offer some encouragement on this point [Bl81].

As is also clear from the form of the weight factor, the integrals over

σ in (5.1) will not converge unless $(\sigma, \nu \sigma)$ is negative definite; i. e., the eigenvalues of the potential ν are all less than zero. For attractive potentials this creates no difficulties. In the repulsive case, one can enforce this condition by adding an appropriate two-body interaction term to H which shifts E_0 in a trivial way (Section 10).

§6. Numerical techniques - Metropolis calculation of the integral

The Metropolis algorithm is applied to the discretized auxiliary field integral, Eq. (4.1), by making random changes in the value of the σ field at points on the space-time mesh (σ_j^i). Each such change results in a new field configuration for which the Monte-Carlo weighting test can be applied and an energy estimator calculated. A sweep or trajectory is defined as completed when changes have been attempted for all points on the space-time mesh.

In practice, the σ field is updated for all space points at a single time value before the acceptance/rejection test is applied. Energy contributions are calculated only after this has been done for all times, i.e. at the end of a trajectory. In fact, energies are actually estimated even less often, due to the necessity of using statistically independent values in averaging (see error analysis, below).

Computation of the Metropolis weights. There are two computational simplifications that result from this method of performing the Metropolis random walk. The weight function in discretized form is

$$W[\sigma] = e^{-\frac{1}{2}\Delta\tau \int \sum_{i=1}^N (\sigma, v\sigma)_i} \langle \Phi | U_N U_{N-1} \dots U_i \dots U_2 U_1 | \Phi \rangle \quad (6.1)$$

where $U_i \equiv e^{-h_\sigma(t_i)\Delta t}$ is the evolution operator from t_i to t_{i+1} . Considering the exponential factor, it is evident that changes in the σ field at a fixed time point t_i , affect only one piece in the sum, giving a net contribution to $W[\sigma_{II}]/W[\sigma_I]$ of

$$e^{-\frac{1}{2}\Delta\tau \left[\int dx dx' (\sigma_I(x, t_i) v(x-x') \sigma_I(x', t_i) - \int dx dx' \sigma_{II}(x, t_i) v(x-x') \sigma_{II}(x', t_i) \right]}$$

The σ fields at other time slices can be ignored.

A further gain in computational time is achieved by evolving the trial

wavefunction $\langle \Phi |$ from the left once before the Monte-Carlo sweep begins and storing the resulting $\langle \Phi | U_N U_{N-1} \dots U_i$ for all i . During the sweep, the "changed" fields σ' are used to evolve the wavefunction forward, so that at any time i , the wavefunction $U'_{i-1} U'_{i-2} \dots U'_1 | \Phi \rangle$ is known (U'_i describes evolution under the "new" potential determined by σ'). To perform one step in the Metropolis walk, only a single evolution, U'_i , and the calculation of two overlaps of already known wavefunctions

$$\frac{\langle \Phi | U_N \dots U_{i+1} U'_i U'_{i-1} \dots U'_1 | \Phi \rangle}{\langle \Phi | U_N \dots U_{i+1} U_i U'_{i-1} \dots U'_1 | \Phi \rangle} ,$$

are necessary to determine the matrix element contribution to the weight ratio.

Initial conditions. The efficiency of AFMC calculations is enhanced if the trial wavefunction Φ closely approximates the true ground state Ψ . In actual calculations we have used either the stationary phase approximation (SPA) states (Hartree solutions) or a basis with variationally set parameters (Section 8).

The initial condition on the σ field is also taken to be the SPA solution in the Hartree limit - namely σ_o from Eq. (3.9c) - at all time slices:

$$\sigma_{init}(x_j, t_i) = \sigma_o(x_j) = \sum_{l=1}^A |\psi_l(x_j)|^2 \quad \text{for all } t_i . \quad (6.2)$$

This is just the particle density; i.e., the mean-field generated by all of the particles in the stationary limit.

Importance sampling. To improve the efficiency of the Metropolis random walk, the AFMC algorithm incorporates a form of importance sampling - a biasing of the trajectories beyond that determined by the weight factor W . In general, if the same size random change is made for σ_j^i at every space-time point, a great many configurations will be

rejected. For example, the tails of both the trial and ground state wavefunctions are likely to be very similar while their peaks may be considerably different. Thus the size of a step which would be accepted for a point in the tail region would be far too small to allow points in the peak to approach their asymptotic values in a reasonable amount of computer time.

The importance sampling technique used to improve convergence is one in which changes in the σ field are scaled according to some field $\eta(\mathbf{x}, t)$. That is, the new sigma field σ' is randomly generated from the old field by

$$\sigma'_j{}^i = \sigma_j{}^i + \delta \eta_j{}^i \Delta\sigma \quad (6.3)$$

where j and i indicate points on the space-time mesh, δ is a random number between -1 and 1, and $\Delta\sigma$ is a constant factor used to increase or decrease the overall size of the random steps. Typically, the scaling field η is only a function of spatial coordinates; i.e., it is the same at every time slice. A reasonable choice for η has been found to be the initial sigma field, σ_0 , so that fractional changes are being made in the field.

It turns out to be practical to choose $\Delta\sigma$ - a measure of the size of changes in σ - so that 30-70% of the moves are accepted according to the Metropolis test; i.e., the acceptance ratio is between 0.3 and 0.7. This enables the σ field distribution to converge to the asymptotic limit in a reasonable amount of computer time. Of course the precise value for $\Delta\sigma$ is highly dependent on the choice of the weighting scheme as discussed above. In a general way, a value of $\Delta\sigma$ on the order of one indicates a reasonable choice of the importance sampling field η .

Error analysis. There are absolute constraints on the accuracy of results obtained using the AFMC, imposed by the numerical techniques,

especially the use of a finite time step Δt . The algorithm is, of course, exact as $\Delta t \rightarrow 0$ but this limit is impossible to reach in actual calculations. A lower bound on the time step is set by the rate at which the trial functions evolve. Too small a Δt and the evolution operator will not filter the system to the asymptotic limit in a reasonable number of steps. On the other hand, an upper limit on Δt is imposed by the accuracy with which $\prod_{i=1}^N U_{\sigma}^i$ for the discretized propagator (the Crank-Nicholson version), approximates $U_{\sigma}(T)$. In practice, Δt is set approximately according to time scales in the problem and then varied until consistent results are obtained for different step sizes.

Statistical error analysis is performed as for standard Gaussian statistics [Bi79]. The estimate for the energy is given by $\bar{E} \pm \delta E$, where

$$\bar{E} = \frac{1}{m} \sum_{i=m_0}^{m+m_0} E(\nu) \quad \nu = i \tau_{corr} \quad (6.4)$$

is an average calculated only once every τ_{corr} sweeps, over a total of $(m+m_0)\tau_{corr}$ trajectories, and

$$(\delta E)^2 = \frac{1}{m(m-1)} \sum_{i=m_0}^{m+m_0} [E(\nu) - \bar{E}]^2 \quad (6.5)$$

is the standard deviation. $E(\nu)$ is the energy estimator $\langle H \Phi | U_{\sigma} | \Phi \rangle / \langle \Phi | U_{\sigma} | \Phi \rangle$ after ν Metropolis sweeps.

The energies $E(\nu)$ must not be affected by the initial conditions on the wavefunctions and σ field. In order to ensure this, $\nu_0 = m_0 \tau_{corr}$ trajectories are performed before contributions to the energy average are taken. For ν larger than ν_0 , $E(\nu)$ should differ from \bar{E} by no more than expected statistical deviations - the asymptotic limit. The value for the relaxation time is checked by performing a special long run and ensuring

that the resulting energy average does not differ from those found in the production runs. The use of different initial conditions provides another test of the relaxation.

Once the initial relaxation has occurred, the precision of the energy estimate is increased by averaging at many subsequent times. Any desired precision can, in principle, be achieved simply by increasing the sample size m . In practice the $m^{-1/2}$ dependence of the statistical errors renders it impractical to compute observables to a precision greater than 1%.

For the averages to be meaningful and for the calculation of variance to be valid, statistically independent values must be used. Since each configuration is generated from the previous one, some correlations are to be expected. This can be taken into account by allowing a sufficient number of trajectories, τ_{corr} , to occur between each contribution to the energy estimator (see Eqs. (6.4)-(6.5)). To determine the correct value for this quantity, a correlation test on the energies is performed. The autocorrelation function C is given by

$$C = \frac{\langle E(t) E(t+\tau) \rangle - \langle E(t) \rangle \langle E(t+\tau) \rangle}{\sqrt{(\langle E^2(t) \rangle - \langle E(t) \rangle^2) (\langle E^2(t+\tau) \rangle - \langle E(t+\tau) \rangle^2)}} \quad (6.6)$$

where the time variables t and τ now refer to computational time; i.e., to the number of trajectories. Note that if the energies at different times are completely uncorrelated, the autocorrelation C vanishes. In actual calculations, the energies are considered sufficiently uncorrelated when C is less than 0.1. The correlation length, τ_{corr} , is then defined as the number of trajectories satisfying this condition.

The relaxation times and correlation lengths are strongly affected by the choice of the importance sampling field η . A poor choice of the

weighting for the random walk will result in a need for a great many trajectories in order to compute statistically independent values. For a particularly poor case, the system will fail to approach the asymptotic region within a reasonable amount of computational time.

§7. Model calculation - the delta function potential

For a first investigation, the AFMC method is applied to a system which is exactly soluble and has been studied in some detail. This allows appropriate initial conditions to be set up so that convergence to the known answers can be investigated. It also permits a detailed consideration of the various energy contributions beyond the mean-field values being resolved by the AFMC.

The model system consists of A bosons of mass m in one-dimension, interacting with each other through an attractive zero-range potential of strength V_0 - the delta function potential. The Hamiltonian is given by

$$H = \sum_{i=1}^A \frac{p_i^2}{2m} - \frac{1}{2} V_0 \sum_{i \neq j} \delta(x_i - x_j) + \frac{1}{2} mA\Omega^2 \left(\sum_i x_i / A \right)^2, \quad (7.1)$$

where an harmonic oscillator of frequency Ω has been added to the system to confine the center-of-mass motion. By measuring lengths in terms of $\frac{\hbar^2}{m}$ and energies in terms of $\frac{2V_0^2}{\hbar^2}$, the interaction strength V_0 can be removed from the problem so that the only meaningful parameter is A (and Ω , but this is not intrinsic to the system). For notational convenience, in the following discussion, $\frac{\hbar^2}{m}$ is set equal to 1.

The Hamiltonian (7.1) with $\Omega = 0$, (i.e., without the harmonic oscillator), has solutions of the form $\Psi = \prod_{i,j=1}^A f(x_i - x_j)$. Note that if the wavefunction is antisymmetric in any two variables, one of the delta function interactions in the Hamiltonian will not contribute, and the system will then be unstable with respect to breakup into two subsystems. Therefore, only systems with complete spatial symmetry form bound states - i.e. bosons or fermions having a "color" degree of freedom with degeneracy A , which provides the correct antisymmetrization. The analytical

solution [Mc64,Mc65,Ca75,Yo76] shows that a boson systems has exactly one bound state with eigenvalue

$$E_A = -A(A-1)(A+1)V_o^2/24 \quad (7.2)$$

and eigenfunction

$$\Psi_A(x_1, \dots, x_A) = C_A e^{-\frac{V_o}{4} \sum_{i < j}^A |x_i - x_j|}$$

$C_A = A! [(A-1)! V_o^{A-1}]^{1/2}$ is the normalization factor.

Mean-field approximation and higher order corrections. The Hartree mean-field approximation solution [Ca75] uses a product trial wavefunction

$$\Phi_H(x_1, \dots, x_A) = \prod_{i=1}^A \varphi_b(x_i) \quad (7.3)$$

and minimizes

$$\langle \Phi_H | H_{\Omega=0} | \Phi_H \rangle = A \left[\int \frac{1}{2} |\nabla \varphi_b(x)|^2 - \frac{1}{2} V_o (A-1) \int |\varphi_b|^4 \right]$$

with respect to the normalized single particle wavefunction $\varphi_b(x)$. This results in an equation for φ_b

$$\left[-\frac{1}{2} \nabla^2 - V_o (A-1) |\varphi_b(x)|^2 - \varepsilon \right] \varphi_b(x) = 0 \quad (7.4a)$$

with one bound state solution

$$\varphi_b(x) = \frac{\sqrt{V_o(A-1)}}{2 \cosh(\frac{1}{2} V_o (A-1) x)} \quad (7.4b)$$

and single particle energy

$$\varepsilon = -V_o^2(A-1)^2/8 \quad (7.4c)$$

The Hartree energy of the bound state

$$E_H \equiv \langle H_{\Omega=0} \rangle = A \left[\varepsilon + \frac{1}{2} V_o (A-1) \int |\varphi_b|^4 \right] \quad (7.5)$$

$$= -\frac{A}{24} V_o^2 (A-1)^2$$

agrees with the exact solution to leading order in A .

Recalling that the particle number is the only parameter in the model after appropriate scaling, an examination of the Hartree values suggests an expansion in $\frac{1}{A}$. Perturbation theory provides the correct series and gives systematic corrections to the mean-field approximation. The Hamiltonian is divided into an unperturbed part involving the Hartree definition of the single particle potential

$$H_o = \sum_i \left[\frac{1}{2} p_i^2 - (A-1) V_o |\varphi_b(x_i)|^2 \right] \quad (7.6a)$$

(note the similarity to equation (7.4a)) and a perturbed part which reproduces the correct interaction

$$V = -V_o \sum_{i \neq j} \delta(x_i - x_j) + (A-1) V_o \sum_i |\varphi_b(x_i)|^2 .$$

The single particle solutions to (7.6a) are just the bound state φ_b and the excited continuum states

$$\varphi_k(x) = \left[\frac{2 V_o (A-1)}{4\pi} \right]^2 e^{ik \frac{1}{2} V_o (A-1) x} \left[\frac{\tanh(\frac{1}{2} (A-1) V_o x) - ik}{1 + ik} \right] \quad (7.6b)$$

with energies

$$\varepsilon_k = (A-1)^2 V_o^2 k^2 / 8 . \quad (7.6c)$$

The lowest order correction term in the perturbation series is then

$$\Delta E^2 = \sum_l' \frac{\langle \Phi_H | V | \Phi_l \rangle \langle \Phi_l | V | \Phi_H \rangle}{(E_H - E_l)}$$

where Φ_l are a complete set of excited states of the Hartree equation constructed from symmetrized products of the eigenfunctions φ_b and φ_k [De74]. The prime indicates that the sum excludes Φ_H . Explicitly,

$$\Delta E^2 = \frac{1}{2} A(A-1) V_o^2 \frac{\int dk dk' \left| \int dx \varphi_b(x)^2 \varphi_k(x) \varphi_{k'}(x) \right|^2}{(2\varepsilon_b - \varepsilon_k - \varepsilon_{k'})} \quad (7.7)$$

$$\approx 0.9956 A(A-1) V_o^2 / 24$$

which is of order A^2 .

The terms in the perturbation series can be shown diagrammatically by use of the Goldstone expansion [Fe71]. While this expansion is derived for fermions, it can be applied to a boson system by introducing a fictitious "color" degeneracy and disregarding the unphysical color singlet (see Figure 1 and Table 1). The A dependence of the various diagrams is easily determined. Any linked diagram has I interactions and C closed loops. The contribution of each interaction yields a factor of $(A-1)^2$ from the normalization of the eigenfunctions (7.4b,7.6b) and a factor of $(A-1)^{-1}$ from the integration over spatial variables. (All wavefunctions depend on $(A-1)\mathbf{x}$ and the potential has zero-range allowing the removal of the A dependence by a change of variables.) A diagram containing I interactions, also has $I-1$ energy denominators, each yielding a factor of $(A-1)^{-2}$ (7.4c,7.6c). Closed loops contribute as A from the sum over "color" degeneracies. Thus the overall dependence of the energy goes as A^{C+2-I} . Self-energy insertions in the propagators have $C=1$ and $I=1$ and hence are independent of A .

In Figure 1, the term labeled SPA is that part of the Hartree energy which has order A^3 . The A^2 energy contributions come from the exchange diagram labeled $n=1$ and the random phase approximation (RPA) diagrams. The $n=1$ term provides the remaining contribution to the Hartree energy, being incorporated with the SPA diagram into equation (7.5). The $n=2$ diagram, the first term in the RPA series, yields the ΔE^2 energy explicitly derived in Eq. (7.7). The rest of the order A^2 corrections arise from the remainder of the RPA chain. In passing, it should be noted that this expansion, which allows the A^3 contribution to be restricted to a single diagram, depends crucially upon the choice of basis in Eq. (7.6).

The spurious center-of-mass motion leads to corrections of order A^{-1} relative to the leading term. If the mean-field solution is obtained for the Hamiltonian without the center of mass energy $H_{c.m.} = -\frac{1}{2A}(\sum_{i=1}^A p_i)^2$; i.e., for $H_{\Omega=0} - H_{c.m.}$, the Hartree energy obtained is $-\frac{A^2(A-1)V_0}{24}$ so that $E_{c.m.} = \frac{A(A-1)V_0}{24}$, an order A^2 correction.

In summary, the exact energy is made up of the following contributions:

$$E_A = E_H + E_{c.m.} + \Delta E^2 + O(2 \times 10^{-4} A^2 V_0^2) \quad (7.8)$$

with

$$E_H = -A(A-1)^2 V_0 m / 24\hbar^2 = \left(\frac{A-1}{A+1}\right) E_A$$

the Hartree energy,

$$E_{c.m.} = \left(\frac{1}{A+1}\right) E_A$$

the center-of-mass term, and

$$\Delta E^2 = .9956 \left(\frac{1}{A+1}\right) E_A$$

the leading order (RPA) correction. The center-of-mass term makes up exactly half of the difference between the Hartree and exact ground state energies, with all but .5% of the remaining gap accounted for by the leading term in the RPA chain. Choosing the Hartree wavefunction as the trial state means that essentially, the order A^2 center-of-mass and RPA energies must be resolved by the AFMC.

AFMC model calculation. AFMC calculations of the ground state energy $E(T) = \lim_{T \rightarrow \infty} \frac{\langle H\Phi | e^{-HT} | \Phi \rangle}{\langle \Phi | e^{-HT} | \Phi \rangle}$ for the delta function interaction have been performed for several different numbers of particles. For this potential, the propagator reduces to a very simple form:

$$U = \int D[\sigma(x,t)] e^{\frac{i}{\hbar} \int dt -V_0 \sigma^2(x,t)} U_\sigma \quad (7.9a)$$

with

$$U_\sigma = T_t e^{-\int dt [\sum_{i=1}^A (\frac{\hbar^2 \nabla^2}{2m} - V_0 \sigma(x,t)) \delta(x-x_i)]} . \quad (7.9b)$$

Since the wavefunction consists of A identical one-body functions and the evolution operator U_σ is exactly the same for each, the problem is equivalent to that for a one-particle system; i.e. only one single-particle wavefunction and one σ field must be used in the calculation. Of course, in determining many-body matrix elements, appropriate powers of A are necessary.

For simplicity, physical units appropriate to nuclear systems are used - $\hbar^2/m = 41.47 \text{ MeV-fm}^2$ and $V_0 = 41.47 \text{ MeV-fm}$. Parameters for the $A=6, 10,$ and 20 particle systems are given in Table 2. A mesh is used consisting of 30 spatial points and up to 160 time points. The results are checked not to have any significant dependence on the size of the discretizations in space and time, Δt and Δx , when these parameters are small enough. Typical values of Δt are on the order of $10^{-26} - 10^{-25}$ s, while the spatial mesh interval is about 0.1 fm.

The strength of the center-of-mass harmonic oscillator can be chosen freely within certain limits. The oscillator length, $r_{c.m.} = \sqrt{\hbar/m\bar{A}\bar{\Omega}}$, is required to be smaller than the mesh size, $L/2$, so that the system is confined and zero boundary conditions can be imposed on the single-particle wavefunctions at $x = \pm L/2$. The edges of the mesh will then have no affect on the solution. This condition provides a lower bound on the frequency Ω .

As remarked earlier, for the Metropolis algorithm to be usable, the exponent in the weight factor ($\sigma, v\sigma$) must be negative definite (Section

5). This is identical to requiring the potential v to have only negative eigenvalues. Since v now includes both the delta function potential and the two-body piece from the harmonic oscillator, the negativity condition enforces another bound on Ω . Consider the eigenvalue equation

$$Vf(x) = -V_0 f(x) + \frac{m\Omega^2}{A} x \int_{-L/2}^{L/2} dx' f(x') x' = \lambda f(x). \quad (7.10)$$

Expanding $f(x)$ in a Legendre series, it is immediately clear that the only solutions are

$$\lambda = -V_0$$

with $f(x)$ any function orthogonal to x and

$$f(x) = cx \quad \lambda = -V_0 + \frac{2m\Omega^2}{A} \frac{2}{3} \frac{L^3}{8} < 0$$

The nontrivial eigenvalue provides an upper limit for Ω .

Thus, the oscillator frequency can be taken to be anywhere in the range

$$\frac{4\hbar}{mAL^2} < \Omega < \sqrt{6A\bar{V}_0/m\bar{L}^3}. \quad (7.11)$$

For the given systems, a convenient choice for the center-of-mass oscillator is $\hbar\Omega = 25$ MeV. This corresponds to a oscillator length of $r_{c.m.} = \sqrt{1.65/\bar{A}}$ fm - several times the space discretization. The precise values for $r_{c.m.}$, as well as the potential eigenvalues λ , are given in Table 2. Use of the harmonic oscillator, shifts the exact ground state energy, E_0 , by the zero-point energy, $\frac{1}{2}\hbar\Omega = 12.5$ MeV. To check that the system is being properly confined by the potential, different choices of Ω are tested for total times T in the asymptotic limit. The resulting values for the ground state energy $E(T)$ vary in the expected way.

In the Hartree mean-field limit, the oscillator term can be treated non-self-consistently since it gives only a very small contribution to the

energy for the parameters used -

$$\begin{aligned} \Delta E_{c.m.} &= \frac{1}{2}m\Omega^2 \frac{1}{A^2} \left[A \int |\varphi_b(x)|^2 x^2 + \frac{1}{2}A(A-1) \left(\int |\varphi_b(x)|^2 x \right)^2 \right] \\ &= \frac{1}{2}m\Omega^2 \int |\varphi_b(x)|^2 x^2 . \end{aligned}$$

The total Hartree energy for the confined delta function potential system (7.1) is

$$E_H = \pi^2 m \Omega^2 b^2 / 24A - A(A-1)^2 V_0^2 m / 24 \hbar^2 .$$

Parameters for the Metropolis random walk. The trial function Φ is taken to be the Hartree single-particle product wavefunction of Eqs. (7.3)-(7.4). Following the discussion of Section 3, an appropriate choice for the initial σ field is the SPA solution for the Hartree case, Eq. (3.9) - $\sigma_{initial} = A \varphi_b^2(x)$. Importance sampling is implemented by weighing changes in the σ field according to the initial field; i.e., the weighting field η in Eq. (6.3) is just $\sigma_{initial}$. Table 2 gives the Monte-Carlo sampling parameters. The size of changes in σ , weighted according to the initial field, range from $\Delta\sigma = 2.0-5.0$, giving an acceptance ratio between 0.50 and 0.60.

To obtain correct energy values, the number of trajectories required for relaxation from the initial conditions and for decorrelation of energies must be determined. These values are, of course, highly dependent on the choice of the importance sampling field and the size of $\Delta\sigma$. For the parameters chosen, a "thermalization" interval of some 1000 sweeps is taken before the calculation of the energies begins. To test that this initial relaxation period is sufficient, a couple of long runs of up to 20000 trajectories are made, with no change in the resulting energy values. A variety of choices for $\Delta\sigma$ are also used to check the thermalization; all yielded the same results.

To assure that only statistically independent energies are averaged, the autocorrelation test of Eq. (6.6) is performed. A typically example for the ten particle system is shown in Figure 2 as a plot of the autocorrelation function $C(\tau)$ versus trajectory number. The correlation length, τ_{corr} , is taken to be the number of trajectories at which C falls to less than 0.1. For the systems chosen, $\tau_{corr} = 20-25$ trajectories (Table 2). Contributions to the energy are then computed only once every τ_{corr} trajectories. The energies are calculated over the 1000^{th} to 6000^{th} trajectories, so that some 200 to 250 field configurations are used in the averages. Note that the initial relaxation period is some 40-50 times τ_{corr} .

Results. Results are shown in Figures 3-5, in the form of plots of $E(T)$. The dashed and dotted lines indicate the Hartree and exact energies respectively, including the harmonic oscillator contribution. Two energy estimators are used: the standard $\langle \Phi | H U_\sigma | \Phi \rangle / \langle \Phi | U_\sigma | \Phi \rangle$ and the equivalent form with the Hamiltonian on the right, $\langle \Phi | U_\sigma | H \Phi \rangle / \langle \Phi | U_\sigma | \Phi \rangle$. For reference, the case of a time step $\Delta t = 1.0 \times 10^{-25} s$ where the discretization is slightly too large for proper evolution is displayed in Figure 4. The data points in the asymptotic region are consistently slightly below the exact energy value and that given by the next smaller time discretization. Thus the correct size for Δt can be determined by performing the AFMC with various size time steps and checking that the results converge to the same value.

$E(T)$ shows an initial relaxation and then asymptotically approaches a value which fluctuates around the expected result for each A . The convergence becomes more rapid with increasing numbers of particles. This is due to the nature of the spectrum of excited states of the model, in which the energy gap to be resolved increases with increasing A . Consider

Figure 6, where the logarithm of the difference between $E(T)$ and its asymptotic value are plotted for $A=10$. Two different relaxation scales are clearly seen.

The rapid initial relaxation is related to the energy gap between the intrinsic ground state and the excited states. Suppose the trial wavefunction Φ can be written approximately as

$$\Phi \sim \Phi_0 + \alpha\Phi_1 \quad \alpha \ll 1 ,$$

a linear combination of the ground (E_0) and first excited states. The latter consists of $A-1$ bound particles plus one particle in the excited continuum at zero energy ($E_1 = \frac{A-2}{A+1}E_0$). Then, the expression for $E(T)$ is

$$\begin{aligned} E(T) &= \frac{\langle H\Phi | e^{-HT} | \Phi \rangle}{\langle \Phi | e^{-HT} | \Phi \rangle} & (7.12) \\ &= \frac{\langle E_0\Phi_0 + \alpha E_1\Phi_1 | e^{-E_0T}\Phi_0 + \alpha e^{-E_1T}\Phi_1 \rangle}{\langle \Phi_0 + \alpha\Phi_1 | e^{-E_0T}(\Phi_0 + \alpha e^{(E_0-E_1)T}\Phi_1) \rangle} \\ &= \frac{[E_0 + \alpha^2 E_1 e^{-\Delta E T}]}{[1 + \alpha^2 e^{-\Delta E T}]} \\ &\approx E_0 [1 - \alpha^2 e^{-\Delta E T}] \end{aligned}$$

where $\Delta E = E_1 - E_0$ is the energy gap. In this approximation, a plot of $\ln\left[\frac{(E(T)-E_0)}{E_H-E_0}\right]$ versus time T will have slope $-\Delta E$. In Figure 6, this slope is indicated by the dotted line. It is a lower bound on the relaxation, since other excited states also contribute in Eq. (7.12). The dashed line is associated with the relaxation of the center-of-mass motion in the harmonic oscillator potential. While the asymptotic region is not reached for times T used in the calculation, T is long enough for the oscillator energy to be resolved within statistics.

Figure 7 shows plots of the wavefunction for the 10 particle system, averaged every 20 trajectories, over the range from 1000-2000 sweeps. The wavefunctions are obtained for calculations with N , the number of time steps, set at 0, 20, 40, 60, 80 and 100. For the parameters used, the asymptotic limit of the ground state energy is reached after approximately 80 time steps. After that, the wavefunctions are identical within error bars except for normalizations.

The wavefunction normalizations are arbitrary since various constant factors have been altered in the propagator exponent - the self-energy term is removed (see Section 5) and a constant equal to the Hartree single-particle energy (7.4c) is introduced to h_σ precisely in order to maintain the wavefunction norm. These factors do not affect the energy values obtained. In the asymptotic limit, the wavefunction normalization is expected to rise exponentially as $e^{-E_0 T}$.

The wavefunction error bars are primarily due to the statistics generated by the random walk in the thermalized region. However, the center-of-mass oscillation has not been removed and so some of the variation particularly at the peak is due to zero point motion. This is fairly small since the oscillator length is only a few mesh spacings.

A plot of the σ field for the 10 particle system is shown in Figure 8. Once again, each field value is the result of averaging every 20 trajectories, over the range from 1000 to 2000 sweeps. The σ field is extremely erratic in nature and a question arises as to how such a random one-body potential, $W(x) = -V_\sigma \sigma(x)$, is generating the correct results. However, the wavefunction responds very little to wild fluctuations in the σ field. The evolution of Φ produces physically reasonable functions (Figure 7), allowing accurate calculations of expectation values. The lack of

smoothness in the σ field is, of course, caused by the method chosen for the Metropolis walk, where single points in space-time are randomly changed. The possibility of a better, more physical, algorithm is discussed in Section 9.

These results provide an encouraging demonstration that the AFMC method can be applied to describe the ground state energy of a simple many-boson system. A typical calculation of some 60 time steps took 4 hours of CPU time on a VAX 11/750 without floating point accelerator (about 5 minutes on a CDC 7600). It is particularly noteworthy that the computational effort for the system does not increase with the number of particles.

A question of time scales arises. The total time necessary to resolve the trial wavefunction to the ground state is expected to be on the order of $T \approx \hbar/\Delta E$, where ΔE is a measure of the energy gap involved. Since the delta function potential has only a single bound state, T is quite short since the energy gap ΔE is large. For systems with several bound states, the time needed may be much greater. On the other hand, it should be noted that although the total time T involved is greater for the smaller systems, the number of discrete time steps required in the calculation - and therefore the amount of computer time - are on the same order (Table 1).

Unfortunately, the delta function potential used in this initial investigation is a very special case. The Hartree potential becomes deeper and narrower with increasing A ; i.e., the system does not saturate. This is a major limitation of the test model, since saturation is an important feature of nuclear matter. Further, the accuracy of the Hartree approximation does not generalize to other potentials. The same feature that

prevents saturation is crucial to obtaining the $1/A$ expansion of the energy contributions - the lack of a length scale in the delta function interaction. For a more general finite range potential, making the transformation $v_{\alpha\beta\gamma\delta} \rightarrow A v_{\alpha\beta\gamma\delta}$ changes the Hamiltonian so that the coupling constant cannot be removed from the problem.

§8. Fermions

One of the primary motives for developing the AFMC method is the proper treatment of fermions. Several considerations are important in dealing with such systems. First, the formalism is very similar to that obtained for bosons, especially in the case of state-independent potentials. The enforcement of antisymmetric statistics, however, requires a few additional numerical techniques. Second, the method must be extended to finite range potentials. The delta function interaction is a poor choice for studying fermions, since only those particles with the same spatial wavefunction (and different "colors") interact. Finally, since a general many-body system does not have an obvious expansion of the energy in powers of A^{-1} , the choice of a trial wavefunction requires a little investigation.

Except for the admission of variables describing internal degrees of freedom, the propagator formalism is identical to that used for the boson delta function interaction system. Consider a Hamiltonian with an instantaneous local two-body potential which possesses spin and isospin as well as spatial dependence:

$$H = K + \frac{1}{2} \int \sum_{\alpha, \beta} dx dx' \rho_{\alpha}(x) v_{\alpha\beta}(x, x') \rho_{\beta}(x') \quad (8.1)$$

where α and β run over the combined spin sums and the density operator is defined as

$$\rho_{\alpha}(x) = a_{\alpha}^{\dagger}(x) a_{\alpha}(x) .$$

K is the kinetic plus self-energy piece

$$K = \sum_{\alpha} \int a_{\alpha}^{\dagger}(x) \left[-\frac{\hbar^2}{2m} \nabla^2 - \frac{1}{2} v(0) \right] a_{\alpha}(x) .$$

The time variable has been suppressed for notational simplicity. Specializing to the above Hamiltonian, Eq. (2.9) yields the auxiliary field represen-

tation of the many-body propagator

$$U = \int D[\sigma_\alpha(x, t)] e^{\frac{1}{2} \sum_{\alpha\beta} \int dt (\sigma_\alpha, v_{\alpha\beta} \sigma_\beta)} U_\sigma \quad (8.2a)$$

where the inner product is

$$(\sigma_\alpha, v_{\alpha\beta} \sigma_\beta) \equiv \int dx dx' \sigma_\alpha(x) v_{\alpha\beta}(x-x') \sigma_\beta(x') , \quad (8.2b)$$

and

$$U_\sigma = e^{-h_\sigma T} = T_t e^{-\int dt [K + \int dx dx' \sum_{\alpha\beta} \sigma_\alpha(x) v_{\alpha\beta}(x-x') \rho_\beta(x')]} \quad (8.2c)$$

is the one-body propagator. It should be noted that although the above discussion was in terms of specific spin degrees of freedom, it obviously holds for any internal "color" variables.

If the potential is "color"-independent, $v_{\alpha\beta} = v$, a combined sigma field and density can be defined of the form

$$\bar{\sigma}(x) \equiv \sum_{\alpha} \sigma_{\alpha}(x) \quad (8.3a)$$

$$\bar{\rho}(x) \equiv \sum_{\alpha} \rho_{\alpha}(x) \quad (8.3b)$$

where the sums are over the non-spatial degrees of freedom. In this case, the propagator written in terms of the redefined fields

$$U = \int D[\bar{\sigma}(x, t)] e^{\frac{1}{2} \int \bar{\sigma}(x) v(x-x') \bar{\sigma}(x')} U_\sigma \quad (8.4)$$

$$U_\sigma = e^{-h_\sigma T} = T_t e^{-\int dt [K + \int dx dx' \bar{\sigma}(x) v(x-x') \bar{\rho}(x')]} \quad (8.4)$$

becomes formally identical in appearance to the case without internal variables, see Eqs. (2.10)-(2.11). As in the boson case, only one sigma field is necessary - i.e. all the individual σ_α are subsumed in $\bar{\sigma}$, which determines the evolution of the trial wavefunction. For a more general interaction, all the fields σ_α must be kept separately, each being used to evolve the corresponding single-particle wavefunctions independently - the problem then involves simultaneous solving of α systems of the form considered here, one for each of the non-spatial degrees of freedom.

Slater determinant fermion wavefunctions. The numerical application of Eq. (8.4) to a fermion system requires an antisymmetric form for the wavefunction, while the Crank-Nicholson algorithm used to evolve the many-body system works only for single particle wavefunctions. These two requirements mean that the AFMC is tractable in practice only if the wavefunction is taken to be a Slater determinant:

$$|\Phi\rangle = (A!)^{-1/2} \sum_P \prod_{\mu=1}^A \varphi_{P\mu}(x_\mu)$$

where P is a sum over the permutations of the A particles and the φ_μ are linearly independent.

The use of Slater determinants adds a few numerical complexities to the computation of the ground state energy. Both the Metropolis weights and the energy estimators for fermions now involve matrix elements between determinants [Br66]. These are given for the overlap and general one-body ($T = \sum_{\mu=1}^A t_\mu$) and two-body ($V = \sum_{\mu\nu} v_{\mu\nu}$) operators below:

$$\langle\Phi|\Psi\rangle = \sum_P (-1)^P \prod_{\mu=1}^A \langle\varphi_\mu|\psi_{P\mu}\rangle \equiv \det B_{\mu\nu} \quad (8.5a)$$

where $B_{\mu\nu}$ is the matrix made up of the elements $\langle\varphi_\mu|\psi_\nu\rangle$ as $\mu, \nu = 1, \dots, A$;

$$\langle\Phi|T|\Psi\rangle = \langle\Phi|\Psi\rangle \sum_{\mu,\nu} \langle\varphi_\mu|t|\psi_\nu\rangle (B^{-1})_{\nu\mu} ; \quad (8.5b)$$

and

$$\langle\Phi|V|\Psi\rangle = \frac{1}{2} \langle\Phi|\Psi\rangle \sum_{\mu\nu\gamma\delta} \langle\varphi_\mu\varphi_\nu|v|\psi_\gamma\psi_\delta\rangle \times [(B^{-1})_{\gamma\mu}(B^{-1})_{\delta\nu} - (B^{-1})_{\gamma\nu}(B^{-1})_{\delta\mu}] . \quad (8.5c)$$

The above equations are derived by noting that they are merely expansions of the overlap determinant in the cofactors, $c(\alpha\beta)$ and $c(\alpha\beta, \gamma\delta)$, defined by

$$\det B = \sum_{\beta} b_{\alpha\beta} c_{\alpha\beta}$$

and

$$\det B = \sum_{\gamma\delta} b_{\alpha\gamma} b_{\beta\delta} c(\alpha\beta, \gamma\delta) .$$

For a spin-isospin degenerate system, (i.e., a state-independent potential), A particles exist in $N = A/4$ different orbital states. The matrix elements then split into four identical $N \times N$ blocks each of which is an orbital overlap matrix. Letting the particle numbers (μ, ν) stand for orbital (i, j) and internal (α, β) quantum numbers,

$$B_{\mu\nu} = \langle \varphi_{i\alpha} | \psi_{j\beta} \rangle = \langle \varphi_i | \psi_j \rangle \delta_{\alpha\beta} = B_{ij} \delta_{\alpha\beta} ,$$

and the matrix elements become

$$\langle \Phi | \Psi \rangle = (\det B_{ij})^4 \tag{8.6a}$$

$$\langle \Phi | T | \Psi \rangle = \langle \Phi | \Psi \rangle \sum_{ij\mu\nu} \langle \varphi_{i\mu}, t \psi_{j\nu} \rangle ((B^{-1}))_{j\nu, i\mu} \tag{8.6b}$$

$$= 4 \langle \Phi | \Psi \rangle \sum_{ij} \langle \varphi_i, t \psi_j \rangle ((B^{-1}))_{ji}$$

$$\langle \Phi | V | \Psi \rangle = \frac{1}{2} \langle \Phi | \Psi \rangle \sum \langle \varphi_{i\alpha} \varphi_{j\beta} | v | \psi_{k\alpha} \psi_{l\beta'} \rangle \tag{8.6c}$$

$$\times [(B^{-1})_{ki} (B^{-1})_{lj} \delta_{\alpha\alpha'} \delta_{\beta\beta'} - (B^{-1})_{kj} (B^{-1})_{li} \delta_{\alpha\beta'} \delta_{\beta\alpha'}]$$

$$= 8 \langle \Phi | \Psi \rangle \sum_{ijkl} \langle \varphi_i \varphi_j | v | \psi_k \psi_l \rangle$$

$$\times [(B^{-1})_{ki} (B^{-1})_{lj} - \frac{1}{2} (B^{-1})_{kj} (B^{-1})_{li}] .$$

Note that for the various matrix elements required in the AFMC random walk and energy average, it is necessary to calculate determinants and inverses of N by N matrices. The computational time needed for this can become prohibitive for very large systems involving few degeneracies.

The discretized Crank-Nicholson propagator, $U_\sigma(\Delta t)$, is composed of a product of one-body operators, each separately evolving a spatial one-body wavefunction in the Slater determinant. As has been noted earlier

(see Section 3), there is nothing intrinsic to the propagator formulation that guarantees that fermion statistics will be preserved. Therefore, in order to maintain the antisymmetry of the system, a Schmidt orthogonalization of the spatial states, $\varphi_1, \varphi_2, \dots, \varphi_N$, is performed after each step of the time evolution

$$\varphi_i^{new} = \varphi_i^{old} - \sum_{j=1}^{i-1} \langle \varphi_j^{new} | \varphi_i^{old} \rangle \varphi_j^{new} . \quad (8.7)$$

It is important to note that the single particle wavefunctions are *not* normalized in this process. The orthogonalization is just equivalent to a change of basis, $\varphi_i^{new} = \sum_j A_{ij} \varphi_j^{old}$. This results in a change in the Slater determinant wavefunction which is just a constant factor. Indeed, $\Phi^{new} = (\det A) \Phi^{old} = \Phi^{old}$, since A is a lower triangular matrix with diagonal elements equal to one.

Finite-range potential. For a test case of the fermion formalism, a more realistic finite range interaction is needed. An exponential potential (i.e., a one-dimensional Yukawa) is selected:

$$v(x) = \frac{V_0}{2a} e^{-|x|/a} \quad (8.8)$$

where V_0 is the strength and a the range of the potential. Note that in the limit $a \rightarrow 0$, this is identical to the delta function potential. The main computational complexity entailed by use of this interaction is the performance of the convolution integral $W(x) = \int v(x-x') \sigma(x') dx'$ for the one-body potential.

The convolution of v may be determined easily by noting that $W(x)$ satisfies a Helmholtz equation. The second derivative of W is given by

$$\begin{aligned} W''(x) &= \frac{d}{dx} \left[\frac{V_0}{2a^2} \int (2\Theta(x-x') - 1) e^{-|x-x'|/a} \sigma(x') dx' \right] \\ &= \frac{V_0}{a^2} \int \delta(x-x') e^{-|x-x'|/a} \sigma(x') dx' - \frac{V_0}{2a^3} \int e^{-|x-x'|/a} \sigma(x') dx' \end{aligned}$$

$$= \frac{V_0}{a^2} \sigma(x) + \frac{1}{a^2} W(x)$$

so that W satisfies the differential equation

$$W''(x) - \frac{1}{a^2} W(x) = \frac{V_0}{a^2} \sigma(x) . \quad (8.9)$$

In discretized form, this is a tridiagonal matrix equation (again assuming the three point formula for the second derivative) and can be solved by the method of Gaussian elimination and backwards substitution discussed for the evolution operator (Section 4). The only extra difficulty is that the initial condition for the method requires that $W(x)$ be zero at the edges of the spatial lattice. To satisfy this condition, the spatial mesh for the convoluted field must be extended on the order of a - the range of the potential - beyond the mesh points where the wavefunction boundary condition is zero.

It might be assumed that an even more simplified evaluation is possible for this interaction. The convolution for $W(x)$ is just a Laplace transform of the σ field with the inverse transformation given by $\sigma(x) = \frac{a^2 \nabla^2 - 1}{V_0} W(x)$. Since this acts like a change of variables, the AFMC can be constructed with $W(x,t)$ - the actual external potential - used as the random field instead of σ . Recall that this is actually done in the delta function interaction model, since the sigma field and the external potential are identical except for a constant factor. Unfortunately, calculations performed in this manner for the finite-range potential result in extremely long correlation lengths for the energy estimator and hence a failure to obtain good statistics in a reasonable amount of computer time. This occurs due to a poor biasing in the importance sampling scheme used to select the W fields - a point that will be seen to be particularly relevant later.

AFMC calculations. As a first check, the $a \rightarrow 0$ limit of the potential is taken by setting the range to be less than a tenth of the mesh spacing Δx . By appropriate choice of the strength $V_0 = 41.47a$, the problem is identical to the delta function problem of the previous section. The bosons are treated as fermions with A internal degrees of freedom and the combined field formulation (8.3-8.4) is used. The results are identical within statistics to those given earlier.

Spin-isospin degenerate systems are chosen for the application of the AFMC to a finite range exponential interaction. Such systems can be viewed as containing pairs of protons and neutrons with spin up and down. This choice has certain advantages. First, it allows a test of the combined field formalism of Eq. (8.4). Secondly, a larger number of particles are involved for the same amount of computer time, helping to ensure that the mean-field picture is valid - attempts to apply the AFMC to systems of two particles fail to yield convergence with good statistics. Finally, the weight factor for a system with four spin-isospin degrees of freedom, can immediately be seen to be positive definite. Recalling the discussion leading up to equation (8.6a), all matrix elements consist of determinants of spatial overlap integrals raised to the fourth power and are obviously non-negative. For non-degenerate fermions and unfilled levels this is not true *a priori*.

The constants for the potential (8.8) are taken to be $V_0 = 41.47$ Mev-fm and $a = 0.8$ fm - on the order of typical nuclear strengths and ranges. Systems of 4, 8, and 12 particles are treated - corresponding to 1 (bosons), 2 and 3 orbitals. Table 3 contains the sets of parameters used in the calculations. Mesh sizes vary from 40 to 60 points, with the spatial lattice becoming slightly more closely spaced for the multiple level systems

as well as extended in range ($\Delta x \approx 0.20-0.25$ fm). The increased length and fineness of the spacing are needed due to the qualitative nature of the higher orbital wavefunctions, which have greater curvature and elongated tails. Results are verified not to depend on the size of the spatial mesh if Δx is sufficiently small. Time lattices of up to 160 points are used, with at least two values of Δt tested for each system. Values of Δt range from 10^{-25} to 10^{-24} s.

As before, a center-of-mass oscillator is used to confine the system. The complete Hamiltonian is then

$$H = \sum_{i=1}^A \frac{p_i^2}{2m} + \frac{V_0}{2a} \sum_{i<j}^A e^{-|x_i - x_j|/a} + \frac{1}{2} mA\Omega^2 \left(\sum_i^A x_i/A \right)^2 . \quad (8.10)$$

For the combined exponential potential plus harmonic oscillator, an exact determination of the eigenfunctions of the total potential is difficult. However, the requirement that the exponent ($\sigma, \nu\sigma$) be negative definite can still be met if the strength of the harmonic oscillator is not too great. For the given systems, $\hbar\Omega$ is taken to be 10 MeV and the sign of the exponent is checked explicitly during the calculation. The center-of-mass zero point motion is on the order of $r_{c.m.} = 0.6-1.0$ fm, (several times the discretization) so that the systems are confined within the spatial mesh.

The choice of a trial wavefunction Φ is no longer obvious for fermions with finite range interactions. For the standard formulation of the auxiliary field used to derive the propagator expression Eq. (8.2), Slater determinant wavefunctions yield a first order SPA solution for the energy which contains only direct terms (Section 3). Therefore, Hartree-Fock wavefunctions do not necessarily provide the optimal Φ . In the present AFMC calculations, trial Slater determinants composed of basis states for

a harmonic oscillator are used instead - a common self-consistent potential for the shell model -

$$\varphi_n = H_n(\beta x) e^{-\frac{1}{2}\beta^2 x^2} ,$$

where H_n are the Hermite polynomials [Ab70,De74]. As a check on the initial condition and the energy convergence, the AFMC is also run for the 4 particle boson system using the trial wavefunction $1/\cosh(\beta x)$, the Hartree wavefunction for the delta function interaction. The parameters, β are set variationally to minimize the energy - the variation being performed without the center-of-mass oscillator potential. Table 4 shows the parameters and variational energies for the three systems. It should be noted that in all cases the sums of binding energies for the possible subsystems are smaller in magnitude than the energy for the complete system. The non-self-consistent contribution of the center-of-mass oscillator to the initial energy of the system is also given in Table 4.

Taking a hint from the delta function calculation, the initial σ field is assigned to be $\sum_{\mu=1}^A |\varphi_{\mu}(\mathbf{x})|^2 = 4 \sum_{i=1}^N |\varphi_i(\mathbf{x})|^2$, where the μ sum is over all single-particle states, and the i sum is over different spatial orbitals. This field is also taken to be the importance sampling function η in Eq. (6.3). It is not clear that this is the optimum choice in either case.

Results. Results are shown as plots of $E(T)$ in Figures 9-12 for the 4, 8, and 12 particle systems. Variational energies for the trial wavefunction, including the center-of-mass oscillator contribution, are indicated by the dotted lines E_v . As always, checks are made to insure independence of the mesh discretization and the strength of the harmonic oscillator. All plots show the same initial relaxation and asymptotic approach to a limiting energy around which the remaining points fluctuate as in the delta

function case. Figure 10 compares the results for the two different trial wavefunctions. Both provide a quick resolution to the same ground state energy. Note that in all cases the energies include a 5 MeV contribution from the center-of-mass oscillator.

Figure 13 shows a typical autocorrelation function for the 12 fermion system. Typical values of τ_{corr} are around 20-25 trajectories. These correlation lengths are the same as in the delta function case - a good sign, since it means that the spatial range of the potential does not translate into longer correlation lengths. The initial relaxation is taken to be 1000 sweeps, with energies taken over the next 2000. These values are checked by a few runs, some involving many more trajectories and others much larger total times.

Plots of the single-particle wavefunctions are shown in Figure 14 for the three level system after $N=0, 40, 80,$ and 120 time steps of size $\Delta t = 2.5 \times 10^{-25} \text{s}$. Note that the asymptotic limit in the energy is achieved at $N=120, T=300 \times 10^{-25} \text{s}$. The plots are averaged every 25 trajectories over sweeps 1000-2000, with the center-of-mass motion included. The normalizations are held roughly constant by removing the self-energy term and inserting an appropriate energy shift in the evolution routine. An examination of the plots shows that the spatial wavefunctions maintain their relative antisymmetry, remaining quite smooth within error bars. As in the delta function case, the σ field and one-body potential are irregular in nature and no meaningful physical interpretation is possible. Nevertheless, the wavefunctions appear quite reasonable.

The total time needed to resolve the ground state energy is on the order of $T = \hbar / E_0$ in all three cases - i.e.; T is shorter for the systems with more particles and larger binding energies. The number of discrete

time steps is on the same order as in the delta function potential case. Since the number of trajectories required by thermalization and statistical independence of the energies is also the same, the necessary CPU time is increased only by the additional time needed for the evaluation of the convolutions and a multiplicative factor depending on the number of orbital states involved. Typical computational times for the 3-level system (note that only half as many trajectories are used to calculate the energy than in the delta function case) are on the order of 6 hours of CPU time for the same Vax 11/750 with floating point accelerator.

§9. Momentum space algorithm

Several considerations suggest that a better algorithm for the auxiliary field Monte-Carlo is possible. The method used in the previous sections has the disadvantage of resulting in extremely irregular σ fields. This is caused not by insufficient resolution due to the space discretization, but by the Metropolis walk itself in which random changes are made at every mesh point. The integrability of such extremely erratic functions becomes rather questionable. Further, the physical interpretation of the convolution integral $W(x) = \int dx' v(x-x')\sigma(x')$ as a one-body external potential in which the particles move is made difficult by its corresponding irregularity.

The spatial algorithm also appears somewhat inefficient. Points in the tails of the wavefunction are relatively unimportant in the evolution of the system - field values near the mesh edges are not significantly changed in the random walk as may be seen from the wavefunction plots and the choice of the importance sampling field η . This suggests that a faster random walk might be generated by making correlated changes of all space points at one time slice.

An investigation is made of an alternative algorithm using a momentum space decomposition of the fields

$$\sigma(x,t) = \sum_{q=1}^{M-1} \sin(2q\pi x / L) \sigma_q(t) \quad x: -L/2 \rightarrow L/2 , \quad (9.1)$$

where the sine decomposition imposes zero boundary conditions on the σ fields at the ends of the mesh. The spatial discretization sets an upper limit for the frequency components q of $M-1=L/dx$. The Metropolis random walk is performed according to

$$\sigma_q^{new}(t) = \sigma_q^{old}(t) + \delta \eta_q \Delta\sigma , \quad (9.2)$$

with δ a random variable on $[-1,1]$ and $\Delta\sigma$ a factor which determines the overall size of changes in the field. η_q is an importance sampling field which weights frequency components rather than individual mesh points. Note that every space point at a given time slice is altered by a single change in σ_q . The Metropolis test is performed after all frequency components are changed at a given time slice - i.e., after the value of $\sigma_q(t_j)$ is changed for all q . This method is essentially the same as the previous AFMC algorithm, merely using a different importance sampling scheme. In actual calculations, a fast Fourier transform rather than a sine series decomposition is used. This results in faster computational times, with good accuracy as long as zero boundary conditions on the wavefunction and one-body potential are maintained.

It seems likely that only the low and intermediate frequency components of σ will contribute significantly to the evolution - higher frequency components primarily affect the falloff of the wavefunction tails. In order to determine if this is true, calculations are made with σ_q fixed ($\eta_q = 0$) for $q > N_q$. N_q is then increased until the energy remains the same within statistical errors. The exact functional form of the non-zero components of the importance sampling field η_q is discussed for the individual systems below.

A considerable gain in CPU time is possible working in momentum space by the elimination of the convolution integrals in the potential. The spatial convolution, performed by Gaussian elimination and backwards substitution (see Eq. (8.9)), takes up on the order of 50% of the routine time (and more in the case of more complicated interactions). For a potential with spatial dependence only upon relative coordinates, the convolution integral $W(\mathbf{x},t)$ and Metropolis exponent $(\sigma, \nu \sigma)$ can be

replaced by a simple product and sum involving Fourier transform components:

$$W(k, t) = v(k) \sigma(k, t)$$

$$(\sigma, v \sigma) = \sum_k^{M-1} \sigma^*(k, t) W(k, t) .$$

Internal variables are suppressed for simplicity. A further savings results - the extension of the spatial mesh to insure zero boundary conditions on $W(x)$ is no longer necessary. Since these extensions are on the order of the length scale of the attractive potential, roughly $(2a/dx) \times N$ mesh points can be eliminated. (N is the number of time steps in the calculation.) It should be noted that the potential is assumed to have a Fourier transform. However, this imposes no further limits on the applicability of this frequency importance sampling, since it seems unlikely that the algorithm would be an improvement for a potential not satisfying this condition (e.g., a hard core potential).

Though the space mesh can be entirely eliminated, for the purposes of this section, it is more convenient to perform only the importance sampling and the convolutions in momentum space. However, in a case involving two potentials of significantly different length scales, the use of momentum space provides a great increase in efficiency (see the discussion in Section 10 on systems with repulsive cores). The wavefunctions are still Slater determinants, but are expressed in terms of their Fourier components while the propagator is given by

$$U(T) = \int D[\sigma(k)] e^{\int dt \frac{1}{2} \sum_k \sigma^*(k, t) v(k) \sigma(k, t)} e^{-\int dt \sum_k \sigma^*(k, t) v(k) \rho(k, t)} \quad (9.3)$$

where $\rho(k)$ is the density operator and $D[\sigma(k)]$ is the measure of integration in momentum space.

Bosons. The two AFMC importance sampling algorithms are compared for the case of 10 bosons interacting with the exponential potential of the previous section. Table 5 lists the various parameters used. The mesh contains 64 space points with $\Delta x = 0.15$ fm and up to 180 time steps of size $\Delta t = 5.0 \times 10^{-25}$ s. All of the standard tests on the discretization are performed. The center-of-mass harmonic oscillator is chosen to have strength $\hbar\Omega = 10$ MeV and the trial function is taken to be a product of the single-particle wavefunctions $C_N e^{-\frac{1}{2}\beta^2 x^2}$, with β determined variationally to minimize the energy. Energies are calculated over 2000 trajectories after a relaxation of 1000 sweeps.

Results are shown as Figure 15 as a plot of $E(T)$, for two different importance sampling fields - the spatial sampling function

$$\eta(x) = |\sigma_{init}(x)|^2, \quad (9.4a)$$

and a momentum space field, reflecting the initial Fourier decomposition of the σ field

$$\eta_q = \sigma_q^{init} \quad q \leq N_q. \quad (9.4b)$$

Both cases yield the same ground state energy, with a total time for convergence on the order of 4.0×10^{-23} s. Note that the center-of-mass harmonic oscillator shifts the true ground state energy by 5 MeV. Correlation lengths are not significantly different for the two methods - statistical independence is assured by calculating the energy estimators only once every 40 sweeps.

Other than the considerable gain in CPU time from the elimination of the convolution integral, there is an improvement in efficiency for momentum importance sampling because only the 10 lowest frequency terms in the decomposition must be changed to obtain the results shown, i.e. $\eta_q = 0$ for $q > 10$. Hence, for a given Metropolis step, only 10 random

changes must be made as contrasted to 60 (the number of space mesh points) for the spatial importance sampling scheme. The limit on N_q implies that significant length scales are on the order of 1.0-2.0 fm - a reasonable result for an exponential potential of range 0.8 fm. Overall, the momentum space routines require roughly 50% of the CPU time of the spatial algorithm.

This example indicates the critical nature of importance sampling in establishing an efficient algorithm. A momentum space scheme, produces a significantly faster random walk, by changing Fourier frequency components rather than individual field values. However, a poor choice of the η_q field will negate this advantage by requiring a very long thermalization period and therefore failing to converge in a reasonable number of trajectories. It should be recalled from the previous section, that an importance sampling based on $W(x)$ resulted in extremely long correlation lengths and poor statistics for the delta function system. In general, the autocorrelation test eliminates the worst choices for the importance sampling field. However, it does not indicate the optimum choice of η , since it cannot distinguish between schemes changing the field at single points and those performing spatially correlated changes. The present AFMC method does not allow Metropolis steps involving time correlations.

Fermions. The case of 12 spin-isospin degenerate fermions with an exponential interaction, calculated in Section 8, is treated by various Fourier decomposition algorithms and the results are compared. Parameters are given in Table 6 for the spatial and two frequency importance sampling functions

$$\eta_q = |\sigma_q^{init}| \quad q < N_q \quad (9.5a)$$

and

$$\eta_q = 1.0 \quad q < N_q \quad , \quad (9.5b)$$

which has a faster falloff with q . Results for the weighting function

$$\eta_q = \frac{1}{q} \quad q \leq N_q \quad , \quad (9.5c)$$

are not shown, since they are similar to those obtained for $\eta_q = \sigma_q$. The mesh parameters, the trial wavefunction and the initial condition on the σ field are the same as in Section 8.

Energy results calculated over 2000 trajectories after a 1000 trajectory thermalization are shown in Figure 16. Note that the actual ground state is 5 MeV lower, after the contribution from the center-of-mass oscillator is removed. Only the ten lowest frequencies are used in the momentum space calculations ($N_q = 10$), implying that interparticle spacings on the order of 1.0-2.0 fm are typical. Convergence to the asymptotic energy occurs after a total time $T = 3.0 \times 10^{-23}$ s for spatial importance sampling and for the Fourier weighting field of Eq. (9.5b). This value of T for the optimal importance sampling functions, indicates that an energy gap on the order of $\Delta E = \hbar / \Delta t \approx 20$ MeV is being resolved. Importance sampling schemes with a bias towards the very lowest frequencies (Eqs. (9.5a) and (9.5c)) are not successful.

A typical autocorrelation plot is shown in Figure 17. The correlation lengths for the three choices of importance sampling show significant differences. The $\eta_q = 1$ function has $\tau_{corr} = 18$ trajectories, some 30% smaller than the spatial weighting method and 80% less than the $\eta_q = \sigma_q^{init}$ function. This implies that the importance sampling field of Eq. (9.5a) is a poor choice. In fact, it is apparent from the energy plot that thermalization is not achieved - not surprisingly, since a relaxation period of only 8 correlation lengths (1000 trajectories) is used. The energy values of Eq. (9.5) are consistently above those resulting from the

use of spatial importance sampling - only for many time steps are the correlations reduced sufficiently so that convergence is attained.

Plots of the wavefunction, σ field and one-body potential are shown in Figures 18-20. The wavefunctions are a slightly smoother variation of those obtained with spatial importance sampling (Figure 14); in fact, they are identical within statistical errors except for the arbitrary normalizations. The sigma fields remain erratic, though slightly smoother than before. The one-body potential shows some structure - three symmetrically situated potential wells which reflect the three orbital states of the fermions.

The saving of CPU time is again on the order of 50% for the momentum schemes, primarily from the elimination of the convolution integrals and the need to use only 10 frequency changes for each time interval. Part of the differences in efficiency is masked, since energies can actually be obtained with the same statistics for fewer trajectories in the frequency importance sampling scheme of Eq. (9.5a), due to the reduced correlation length.

§10. Treatment of repulsive potentials

Application of the AFMC algorithm to systems including repulsive potentials involves additional difficulties. For the evaluation of the energy integral, the inner product $(\sigma, \nu \sigma)$ in the Metropolis exponent must be negative definite or the integrals will not converge. This requirement is explicitly enforced for the delta function system by a suitable choice of the center-of-mass oscillator frequency. In the case of a finite range attractive potential, the negativity property can still be satisfied for a sufficiently weak oscillator potential and may be explicitly confirmed during the Monte-Carlo evaluation. However, for systems containing repulsive potentials, it may not be possible to satisfy the condition for any choice of Ω . This depends on the relative strengths and ranges of the attractive and repulsive components of the potential - for very weak repulsive cores a straightforward application of the algorithms of the previous sections is adequate. Unfortunately, to treat nuclear systems a way must be found to deal with interactions including strong repulsive cores.

Two methods are considered for dealing with such systems. Using the same formulation as before, an appropriate two-body interaction term can be added to the Hamiltonian to ensure that the eigenvalues of the resulting effective potential are negative definite. This additional potential can be constructed so that a known energy shift results. The second method involves a generalized formulation using complex fields. The extra degree of freedom provided by the imaginary part of the field allows the construction of the exponential factor $(\sigma, \nu \sigma)$ in such a way as to satisfy the negativity condition.

Additional potential method. Consider the Hamiltonian for a system with local instantaneous two-body interactions and explicit dependence

on "color" variables

$$\begin{aligned}
 H &= K + \frac{1}{2} \int dx dx' \sum_{\alpha\beta} \rho_\alpha(x) v_{\alpha\beta}(x, x') \rho_\beta(x') \\
 &= K + \frac{1}{2} \int dx dx' \sum_{\alpha\beta} a_\alpha^\dagger(x) a_\alpha(x) v_{\alpha\beta}(x-x') a_\beta^\dagger(x') a_\beta(x) .
 \end{aligned} \tag{10.1}$$

The sums over α and β range over all the internal degrees of freedom and K includes the potential self-energy term. The propagator is the coherent sum

$$U = \int D[\sigma_\alpha(x, t)] e^{\frac{1}{2} \sum_{\alpha\beta} \int dt (\sigma_\alpha, v_{\alpha\beta} \sigma_\beta)} U_\sigma , \tag{10.2}$$

with the inner product defined to be

$$(\sigma_\alpha, v_{\alpha\beta} \sigma_\beta) \equiv \int dx dx' \sigma_\alpha(x, t) v_{\alpha\beta}(x-x') \sigma_\beta(x', t) .$$

For an arbitrary potential, there is no guarantee that $(\sigma, v \sigma)$ is negative definite. However, consider the effect of an additional potential

$$V_{\alpha\beta}^{add}(x, x') = C \delta_{\alpha\beta} \delta(x-x') ,$$

where C is some constant. This potential contributes an extra term to the exponent in the Metropolis weight:

$$(\sigma, v \sigma)^{add} = C \int dx \sum_\alpha \sigma_\alpha^2(x) . \tag{10.3}$$

Since this has the sign of C , by choosing the strength of the potential to be sufficiently negative, the exponent can be forced to satisfy the sign condition.

Now, consider the effect on the energy. The potential V^{add} contributes an additional term to the Hamiltonian

$$\begin{aligned}
 H^{add} &= \frac{1}{2} \int \sum_{\alpha\beta} dx dx' a_\alpha^\dagger(x) a_\beta^\dagger(x') C \delta_{\alpha\beta} \delta(x-x') a_\beta(x') a_\alpha(x) \\
 &= \frac{1}{2} C \int \sum_\alpha dx a_\alpha^\dagger(x) a_\alpha^\dagger(x) a_\alpha(x) a_\alpha(x) .
 \end{aligned} \tag{10.4}$$

For fermions, this expression vanishes immediately since the $a_\alpha a_\alpha$ term vanishes by standard antisymmetric statistics. Thus, the added potential

yields a zero energy shift while allowing the enforcement of the exponent negativity condition. Bosons can be incorporated into the formalism by treating them as fermions with A internal degrees of freedom.

The evolution operator U_σ describes propagation under the single-particle hamiltonian

$$h_\sigma = K + \int dx \sum_\alpha C \sigma_\alpha(x) \rho_\alpha(x) + \int dx dx' \sum_\alpha \sigma_\alpha(x) v_{\alpha\beta}(x-x') \rho_\beta(x') \quad (10.5)$$

where the kinetic term is given by

$$K = \sum_\alpha \int a_\alpha^\dagger(x) \left[-\frac{\hbar^2}{2m} \nabla^2 - \frac{1}{2} v(0) \right] a_\alpha(x)$$

and the term in C is the contribution from the added potential. In actual calculations, a harmonic oscillator is also added to the system to confine the center-of-mass. This contributes a piece to both K and $v_{\alpha\beta}$.

In Eqs. (10.4)-(10.5), it is no longer possible to use the combined sigma field and density of Eq. (8.3) - the dependence of the additional potential on the internal variables results in products over α so that we can no longer perform the sums. Hence, fields and wavefunctions must be stored separately for each of the N_{deg} non-spatial degrees of freedom. The resulting AFMC calculations then consist of simultaneously evolving N_{deg} identical systems.

Static potential. A test case is chosen which has been solved using standard techniques in a study of meson-nucleon field theory [Se83]. For static heavy baryons, the scalar and vector meson interaction reduces to a sum of attractive and repulsive Yukawa potentials that reproduce the basic properties of the nucleon-nucleon force. In one-dimension, Yukawas become exponentials and the static potential is given by

$$v(x) = \frac{1}{2} \left[\frac{g_V^2}{m_V} e^{-m_V |x|} - \frac{g_S^2}{m_S} e^{-m_S |x|} \right] \quad (10.6)$$

$$= \frac{1}{2}(V_A e^{-|x|/a_A} + V_R e^{-|x|/a_R}) .$$

The parameters are set to provide a reasonable nucleon-nucleon potential with a repulsive core, $V(x=0) > 0$, and a typical nuclear core radius, x_c - defined by $V(x_c) = 0$ - which is taken to be 0.4 fm. The range of the potential is fixed by the meson masses - m_S is chosen to be the mass of the pion, $m_\pi = 140$ MeV, and $m_V = m_\omega = 783$ MeV, the mass of the omega.

The binding energy per particle for nuclear matter in the mean-field approximation is

$$\frac{E_{m.f.}}{A} = \frac{\pi^2 \rho^2}{6 M} + \frac{1}{2} \left[\frac{g_V^2}{m_V^2} - \frac{g_S^2}{m_S^2} \right] \rho , \quad (10.7)$$

where ρ is the density and M is the nucleon mass, 939 MeV. Note that the one-dimensional system saturates in the mean-field approximation as long as the volume integral of the potential

$$\int_{-\infty}^{\infty} dx v(x) = C$$

is attractive ($C < 0$). Motivated by three-dimensional nuclear matter, the binding energy per nucleon is fixed to be -16 MeV at saturation, ρ_0 , defined by

$$\left[\frac{\partial (E_{m.f.}/A)}{\partial \rho} \right]_{\rho_0} = 0 .$$

These considerations are sufficient to specify $g_S = 196$ MeV and $g_V = 890$ MeV, yielding potential parameters

$$\begin{aligned} V_A &= -137.283 \text{ MeV} & a_A &= 1.407 \text{ f} \\ V_R &= 506.002 \text{ MeV} & a_R &= 0.250 \text{ f} . \end{aligned} \quad (10.8)$$

Figure 21 shows a plot of this potential.

The potential is slightly unrealistic in setting the scalar meson mass to be that of the pion - in realistic calculations of the nucleon-nucleon

potential, the intermediate range attraction is dominated by two-pion exchange. Thus, the range is actually characterized by twice m_π , and phenomenological potentials are of considerably shorter range than that of Figure 21. A more realistic model is described in [Ne82a], consisting of a sum of a repulsive and attractive gaussian potentials with parameters defined to reproduce appropriate dimensionless ratios of realistic nuclear interactions.

AFMC model calculation. A test case involving four nondegenerate fermions is calculated. This is just about the smallest system that can be treated using the AFMC - four is very few particles for a mean-field formulation to be valid. Application of the AFMC method to a two particle system in the same potential does not succeed in converging to the ground state energy with good statistics, though it does set an upper bound. However, AFMC solutions for the potential of Eqs. (10.6) and (10.8) require a great deal of computational time and as a test case on a small machine, the four particle system seems sufficient.

Table 7 lists the parameters for the AFMC calculation. The calculation is performed using both spatial and Fourier decomposition importance sampling. The mesh consists of 150 points of spacing $\Delta x = 0.08$ fm. The time interval is $\Delta t = 0.001 \times 10^{-25}$ s and up to 60 time steps are used. All standard test on the mesh discretization are performed. The difference in the ranges of the attractive and repulsive potentials requires the mesh spacing to be roughly four times as dense as would be needed for the purely attractive case. Most of these points are wasted however - while close spacing is needed over the range of V_R , for mesh points in the exponential tail of V_A , a much larger spacing is sufficient to resolve details. To reduce the necessary computational time, either a variable

spaced mesh can be used or the formulation in momentum space can be set up (see Section 9).

A center-of-mass harmonic oscillator is again added to the Hamiltonian in order to confine the system to the mesh. The strength of the oscillator is chosen so that the zero-point motion is significantly smaller than the spatial mesh and yet large enough to be resolved by the mesh intervals; i.e., $\Delta x < r_{c.m.} < L/2$. The added potential V^{add} must be sufficiently strong to enforce the negativity condition on the Metropolis exponent $(\sigma, \nu \sigma)$ including the contribution from the center-of-mass oscillator. This is checked explicitly during the calculation. For the four particle system, the strength of the harmonic oscillator potential is taken to be $\hbar\Omega = 2$ MeV, corresponding to a range of 2.3 fm. The strength of the added potential (10.3) is then set at -200 MeV.

The choice of the trial function is motivated by the results for the purely attractive potential - i.e., Slater determinant wavefunctions built on harmonic oscillator basis states with a parameter determined variationally by minimization of the energy. Since fermions already exhibit antisymmetrization "repulsion", these wavefunctions should still be reasonable choices for the present potential. The initial condition on the σ field is again taken to be $\sigma_{init}(\mathbf{x}) = \sum_{i=1}^4 |\varphi_i(\mathbf{x})|^2$.

Importance sampling in both the spatial and momentum schemes is determined by the initial condition, $\eta = \sigma_{initial}$. Only the 15 lowest frequency components in the Fourier decomposition are changed during the random walk. Results are checked to be the same within statistical errors when more components are included. This indicates that the important length scales are on the order of 0.8-2.0 fm - a result that

seems physically understandable since the potential has this range (Figure 21). Higher components are resolving details much smaller than average inter-particle spacing.

Results. The results shown in Figure 22 are in agreement with the value obtained by [Se83], $E_0 = -64.7 \pm 0.7$ MeV, when the 1 MeV center-of-mass energy is taken into account. Both importance sampling schemes converge to the asymptotic energy in a time on the order of $T = 1.0 \times 10^{-22}$ s. However, the results from the spatial weighting process fluctuate considerably. The value of T suggests that an energy gap on the order of 10 MeV is being resolved - however this is only a rough estimate as there is no way of identifying the various excited states for this interaction.

The autocorrelation function for the momentum space routine is shown in Figure 23. There is a significant difference in correlation lengths for the two importance sampling methods - the spatial weighting scheme has τ_{corr} half again as large as for the η_q case. This is another indication that momentum importance sampling is more efficient. The correlation test also provides a check on how much the additional potential is affecting the evolution.

Plots of the wavefunction and one-body potential are shown in Figures 24-25. The wavefunction remains smooth, with the evolved functions showing a slightly greater repulsion. Normalizations are not meaningful, since constant energy shifts have again been introduced into the evolution hamiltonian h_σ . The one-body potential is a relatively smooth function showing several symmetrically placed barriers, separating potential wells where the particle density is concentrated - a physically reasonable result. The center-of-mass oscillator compresses the overall radius and

increases the density in the center.

The CPU time required for the momentum space routine is 12 hours on the Vax 11/750 with floating point accelerator and roughly twice that for spatial importance sampling. The major difficulty with extending this calculation to systems containing more particles is that the computer time goes as the number of particles - and hence spatial orbitals, even for systems with internal degrees of freedom. However, the convergence and statistics are expected to be better for such systems, as the mean-field picture becomes increasingly valid.

Complex field formulation. A different method for the treatment of repulsive potentials uses a formulation involving complex fields. The derivation of the expression for the many-body propagator can be performed formally as in Section 2 for the case where σ and ρ are complex variables. The resulting expression for the propagator is then

$$\begin{aligned} U(T) &= \int D[\sigma(x), \sigma^*(x)] e^{-\frac{1}{2} \int (\rho, \nu \rho)} \\ &= \int D[\sigma(x), \sigma^*(x)] e^{\frac{1}{2} \int (\sigma, \nu \sigma)} e^{-\int (\sigma, \nu \rho)} \end{aligned} \quad (10.9)$$

where the measure of integration contains both real and imaginary components of σ and the matrix products involve complex conjugates, i.e. the inner products are given by

$$(\sigma, \nu \sigma) \equiv \int dx dx' \sigma^*(x) \nu(x-x') \sigma(x') \quad (10.10)$$

$$(\rho, \nu \rho) \equiv \int dx dx' \rho^\dagger(x) \nu(x-x') \rho(x')$$

$$(\sigma, \nu \rho) \equiv \int dx dx' [\sigma^*(x) \nu(x-x') \rho(x') + \sigma(x) \nu(x-x') \rho^\dagger(x')]$$

In the above equations, "color" variables are suppressed for simplicity.

It is clear that for a real two-body potential depending only on relative coordinates (i.e. $\nu(x, x') = \nu(x', x)$), the Metropolis weight exponent

becomes

$$\begin{aligned} (\sigma, \nu \sigma) &= ([\sigma_R - i \sigma_I], \nu [\sigma_R + i \sigma_I]) \\ &= (\sigma_R, \nu \sigma_R) + (\sigma_I, \nu \sigma_I) \end{aligned}$$

as the two terms involving an inner product of the real part and the imaginary part of the sigma field vanish. In this case, the exponent is explicitly real and contains an extra degree of freedom which allows the negativity condition to be enforced.

However, since the fields are complex, the Slater determinant wavefunctions and overlap elements have a phase as well as a magnitude. The equation for the ground state energy E_0 must be rewritten so that a real Metropolis weight factor is obtained. This is done by noting that the energy itself must be real and therefore can be expressed by the ratio of the real parts of the integrals:

$$\begin{aligned} E_0 &= \lim_{T \rightarrow 0} \operatorname{Re} \frac{\int D[\sigma, \sigma^*] e^{\frac{1}{2} \int (\sigma, \nu \sigma)} \langle \Phi | U_\sigma | \Phi \rangle \frac{\langle \Phi | H U_\sigma | \Phi \rangle}{\langle \Phi | U_\sigma | \Phi \rangle}}{\int D[\sigma, \sigma^*] \langle \Phi | U_\sigma | \Phi \rangle} \quad (10.11) \\ &= \lim_{T \rightarrow 0} \frac{\int D[\sigma, \sigma^*] e^{\frac{1}{2} \int (\sigma, \nu \sigma)} \operatorname{Re} \left[\langle \Phi | U_\sigma | \Phi \rangle \frac{\langle \Phi | H U_\sigma | \Phi \rangle}{\langle \Phi | U_\sigma | \Phi \rangle} \right]}{\int D[\sigma, \sigma^*] \operatorname{Re} \langle \Phi | U_\sigma | \Phi \rangle} \\ &= \lim_{T \rightarrow 0} \frac{\int D[\sigma, \sigma^*] e^{\frac{1}{2} \int (\sigma, \nu \sigma)} \left[|\langle \Phi | U_\sigma | \Phi \rangle| \frac{\operatorname{Re} \langle \Phi | H U_\sigma | \Phi \rangle}{|\langle \Phi | U_\sigma | \Phi \rangle|} \right]}{\int D[\sigma, \sigma^*] |\langle \Phi | U_\sigma | \Phi \rangle| \frac{\operatorname{Re} \langle \Phi | U_\sigma | \Phi \rangle}{|\langle \Phi | U_\sigma | \Phi \rangle|}}. \end{aligned}$$

The resulting equation expresses the ground state energy as a ratio of the average of two quantities - the energy estimator $\frac{\langle \Phi | H U_\sigma | \Phi \rangle}{\langle \Phi | U_\sigma | \Phi \rangle}$ and the signature estimator $\frac{\langle \Phi | U_\sigma | \Phi \rangle}{|\langle \Phi | U_\sigma | \Phi \rangle|}$.

This algorithm has been tried for both the spatial and the Fourier

decomposition importance sampling schemes. The results have not been good - while the approximate energies have been obtained, the statistics are poor. This is due to cancellations in the denominator integral. Apparently, in order to use this scheme, a cleverer importance sampling scheme for biasing the random walk is necessary.

§11. Conclusion

The auxiliary field formalism provides a method for determining the exact ground state energies of many-body systems. In principle, using the numerical techniques developed in this thesis, AFMC solutions can be obtained for a variety of interactions. In practice, of course, there are limits imposed by the amount of computer time required. Also, it should be noted that the use of the AFMC is restricted to systems for which a mean-field picture is reasonable; otherwise, the underlying HS transformation is not valid. In particular, systems of two particles do not yield good results when treated by the algorithm.

The AFMC has been tested on several boson and fermion systems in one-dimension, involving both attractive and repulsive potentials. While the formalism is identical in both cases, numerically, an antisymmetrization procedure is used for fermions in order to maintain proper statistics (Section 8). In cases where results are known from other techniques, whether exact solutions or Monte-Carlo values, comparisons of the ground state energies show good agreement (Sections 7 and 10). These results are an encouraging demonstration that the AFMC algorithm provides correct results for a number of many-body systems.

A principal advantage of the AFMC method is its proper treatment of fermions. The HS representation of the propagator allows the system to be described by a set of single-particle wavefunctions for which antisymmetrization can be enforced exactly - a property not shared by the GFMC and DMC algorithms. However, whether or not the AFMC will be able to resolve ground state energies to give better results than the other Monte-Carlo methods for systems of physical interest remains an open question.

A good choice for the initial conditions is necessary to obtain convergence to the ground state for a reasonable amount of computational effort. As noted earlier, the AFMC method becomes more efficient as the trial state Φ approaches the true ground state. Unfortunately, there are no precise criteria for an optimal choice of either the trial wavefunction or the initial sigma field. Note that the simplest possible choice, the SPA solution, does not take into account the particle statistics - yielding Hartree rather than Hartree-Fock energies for fermions. However, SPA results as well as physically likely wavefunction solutions provided reasonable choices of Φ for the models calculated in Sections 7-10.

From the results for the various systems treated, it is also clear that as in other Monte-Carlo methods for many-body ground states, importance sampling is critical to obtaining efficient convergence and good statistics. A poor choice of the weighting function η causes extremely long correlation and thermalization lengths, making calculations impractical. A choice for η based on the initial conditions has been found to be generally adequate, though not necessarily optimal. The trick in the AFMC is to build into the method as much as possible of the physics without biasing the results by limiting the degrees of freedom of the system. In fact, the full power of the method is shown when as many symmetries as possible are broken.

The proper incorporation of fermion statistics in the AFMC is paid for by the need to specify wavefunctions and fields involving many values rather than a single coordinate for each particle. If the wavefunction is defined on a spatial mesh, the number of lattice points becomes prohibitive. This is especially true in several dimensions where meshes become extremely large, unless there is symmetry so that various spatial degrees

of freedom can be integrated out (i.e., axial or radial symmetry). Potentials with repulsive cores add to the problem, since they require a very fine mesh spacing to resolve the short length scale of that part of the potential. However, the momentum space AFMC algorithm appears to circumvent this problem, at least for regular potentials with Fourier transforms. It eliminates the need for a spatial lattice and appears to reduce the number of Metropolis steps required for the evolution of the wavefunction. The method is also more efficient since the momentum space random walk scheme involves only the lowest frequency components. This provides some hope that more complicated systems can be treated with the AFMC.

The treatment of other systems is fairly straightforward. Preliminary investigation of the $1/r$ potential indicates that calculations are only feasible using the momentum space algorithm, due to the nature of the convolution integral. A similar statement applies to infinite systems such as nuclear matter, where periodic boundary conditions are enforced. As an aside, it should be noted that many-body forces can be treated in the AFMC formalism. Successive application of the following schematic formulas for reducing even and odd powers of \hat{p}

$$\exp(-\int \hat{p}^{2n}) = \int D[\varphi] \exp(\int \varphi^{2n}) \exp(-2\int \varphi^n \hat{p}^n) \quad (11.1a)$$

$$\begin{aligned} \exp(-\int \hat{p}^{2n+1}) &= \exp(-\frac{1}{2}\int [\hat{p}^n + \hat{p}^{n+1}]^2) \exp(\frac{1}{2}\int \hat{p}^{2n}) \\ &\quad \exp(\frac{1}{2}\int \hat{p}^{2(n+1)}) \end{aligned} \quad (11.1b)$$

$$\begin{aligned} &= \int D[\chi] \exp(\frac{1}{2}\int \chi^2) \exp(-\int [\hat{p}^n + \hat{p}^{n+1}]\chi) \\ &\quad \exp(\frac{1}{2}\int \hat{p}^{2n}) \exp(\frac{1}{2}\int \hat{p}^{2(n+1)}) \end{aligned}$$

ultimately leads to an expression linear in \hat{p} which may be incorporated into the AFMC propagator.

Certain limitations restrict the kind of expectation values for which the AFMC method can provide adequate results. The ground state energy is given by an integral over a product of a function $E(\sigma)$ times a probability distribution $P(\sigma)$

$$\int D[\sigma] P(\sigma) E(\sigma) = \lim_{N \rightarrow \infty} \sum_{i=1}^N E(\sigma_i) \quad (11.2)$$

where the σ are distributed according to $P[\sigma]$. Though generally true, in practice, this formula is only useful when the variance is small or equivalently when the integrand is at least predominantly of one sign. This means that only imaginary-time calculations are possible in order to eliminate cancelling phases in the evolution operator. Further, the exponential weighting of eigenstates implies that only low-lying states may be calculated.

The formulation of Eq. (2.1) using a trial wavefunction leads to good energy and density values but makes the calculation of other observables difficult - often requiring the introduction of new approximations. Operators O which are constants of the motion are an exception, of course, since they can be calculated using the same random walk as in the energy determination and the eigenvalue estimator $\langle \Phi | O U | \Phi \rangle / \langle \Phi | U | \Phi \rangle$. A typical method for the evaluation of other ground state expectation values makes use of the trace - i.e. for a one-body operator

$$\begin{aligned} \langle \Psi | O | \Psi \rangle &= \lim_{T \rightarrow \infty} \frac{\sum_{\alpha} \langle \alpha | O | \alpha \rangle e^{-E_{\alpha} T}}{\sum_{\alpha} e^{-E_{\alpha} T}} \\ &= \lim_{T \rightarrow \infty} \frac{\text{Tr } O e^{-HT}}{\text{Tr } e^{-HT}} . \end{aligned} \quad (11.3)$$

Though formally straightforward, the sum over all basis states α becomes difficult when working with wavefunctions.

The many-body wavefunction is taken to be a Slater determinant of single-particle states (or a simple product for bosons), since the HS representation of the propagator is a product of one-body operators. This restricts the AFMC algorithm to the evaluation of expectation values of few-body operators which involve only a few single-particle wavefunctions. In the AFMC calculations described, the Crank-Nicholson approximation for the evolution operator $U(T)$ has been used. Another possible choice for $U(T)$ is a Taylor series expansion through the first few terms, which has proved accurate in TDHF calculations [F178]. Unfortunately, a practical algorithm using a general many-body wavefunction and propagator has not been developed. However, in the static case, the use of Slater determinants can be justified on the grounds that particles do not interact with each other directly because of the Pauli principle, but only indirectly through the wall of the self-consistent field.

For potentials with a very strong repulsive core, a determinantal form for the wavefunction is not a good approximation to the exact eigenstate. Unfortunately, such strong, short range interactions are needed in nuclear potentials and become even more important in several dimensions; the kinetic energy alone can cause saturation in one-dimension but not in three. The repulsive potential tested for the AFMC was not hard-core (Section 10). Dealing with the short range correlations required by stronger repulsive cores may not be possible in the AFMC algorithm, except by replacement with some sort of an effective interaction (e.g., a Skyrme potential).

While apparently not necessary for the systems treated thus far, for

more complicated systems it may be useful to incorporate second order and RPA corrections in choosing the initial and importance sampling fields. Whether this results in faster computational times will be system dependent - a balance between quicker convergence to the ground state and the extra effort in performing the random walk. The Metropolis weight factor can be written as $e^{S[\sigma]}$ with

$$S[\sigma] = (\sigma, v \sigma) - \ln \langle \Phi | U | \Phi \rangle \quad (11.4)$$

$$\approx S[\sigma_0] + S_1 + (\sigma - \sigma_0) M (\sigma - \sigma_0) + \dots ,$$

where σ_0 is the mean-field approximation solution, S_1 the linear term, which vanishes by definition of the SPA, and the last term gives the quadratic corrections:

$$\frac{\delta S}{\delta \sigma_i \delta \sigma_j} = \delta_{t_i t_j} v(x_i - x_j) - \left[\frac{\langle \Phi | U v \rho U v \rho U | \Phi \rangle}{\langle \Phi | U | \Phi \rangle} - \frac{\langle \Phi | U v \rho U | \Phi \rangle^2}{\langle \Phi | U | \Phi \rangle^2} \right] .$$

By diagonalization, the quadratic term is incorporated into the Metropolis exponent by writing

$$e^{\sum_{\lambda} \omega_{\lambda} \sigma_{\lambda}^2} e^{S[\sigma_{\lambda}] - \sum_{\lambda} \omega_{\lambda} \sigma_{\lambda}^2} ,$$

where the σ_{λ} are used as the new field variables. This allows correlated changes in space and time, although the present evolution routines restrict this to space correlations only. The method is similar to that used for Ising models near the critical points, in which blocks of spins are changed.

Recently, progress has been made in developing functional integral techniques for nuclear physics using a variety of representations of the evolution operator [Ko82a, Ne82a], including the many particle Feynman path integral

$$\int d(x_1, \dots, x_A) e^{\Delta t \sum_i \left[\frac{1}{2} m \left(\frac{x_{i+1} - x_i}{\Delta t} \right)^2 - v(x_i) \right]} , \quad (11.5)$$

sums involving overcomplete sets of states and the auxiliary field formulation. Each offers a different possibility for SPA and Monte-Carlo solutions. In the Feynman path integral, the number of stochastic variables equals the number of particles. Both the other two forms allow explicit enforcement of fermion statistics by using fields defined on a mesh and hence require considerably more variables than particles - both to resolve details on the order of inter-particle spaces and to generate the exponential tails of the wavefunctions. This makes their application in many dimensions numerically difficult. However, the AFMC formulation in momentum space appears to provide a considerable easing of this situation. The AFMC also possesses another significant and perhaps crucial advantage - it is the only form that allows the integral to be cast into a form involving predominantly non-negative terms in several dimensions (see equation (11.2)). For the Feynman path integral of Eq. (11.5), the sign of the integrand is path dependent in more than one-dimension due to the antisymmetric nature of particle interchange.

Comparison of exact ground state and mean-field solutions is a rich testing ground for approximation methods presently utilized in many-body physics. Questions concerning the validity of the SPA approximation and the appropriate choices for the effective interaction in the mean-field equations can be investigated. Three-dimensional systems have more freedom than their one-dimensional counterparts, including phase transitions and the breakdown of mean-field theory near critical points. However, the scale of computations means that the treatment of realistic potentials will be extremely time consuming. For multidimensional systems, the AFMC approach lies at the limit of presently available computer facilities. The development of more powerful stochastic techniques for

many-fermion problems therefore remains a major conceptual challenge in this field.

References

- [Ab70] M. Abramowitz and I. Stegun, Handbook of Mathematical Functions (National Bureau of Standards, 1970)
- [Al81a] Y. Alhassid, B. Muller and S. E. Koonin, Phys. Rev. C **23**, 487 (1981)
- [Al81b] Y. Alhassid and S. E. Koonin, Phys. Rev. C **23**, 1590 (1981)
- [Al83] Y. Alhassid and S. E. Koonin, Caltech preprint, submitted to Ann. Phys. (1983)
- [An75] J. B. Anderson, J. Chem. Phys. **63**, 1499 (1975); **73**, 3897 (1980), **74**, 6307 (1981)
- [Ar82] D. M. Arnow, M. H. Kalos, M. A. Lee and K. E. Schmidt, J. Chem. Phys **77**, 5562 (1982)
- [Av83] Y. Avishai and J. Richert, Phys. Rev. Lett. **50**, 1175 (1983)
- [Bi79] K. Binder, Introduction: Theory and Technical Aspects of Monte-Carlo Simulations in *Monte-Carlo Methods in Statistical Physics*, K. Binder, ed. (Springer-Verlag, N.Y., 1979), p1
- [Bl80] J. P. Blaiziot and H. Orland, Univ. of Ill. preprint (1980)
- [Bl81] R. Blankenbecler, R. Sugar and D. Scalapino, Phys. Rev. **D24**, 2278 (1981)
- [Bo76] P. Bonche, S. E. Koonin and J. W. Negele, Phys Rev **C13**, 1226 (1976)
- [Br66] D. Brink, in Proceedings of the International School of Physics, *Enrico Fermi Course XXXVI* (1966)
- [Ca75] F. Calogero and A. Degasperis, Phys. Rev. **A11**, 269 (1975)

- [Ce79] D. Ceperley and M. H. Kalos, *Quantum Many-Body Physics in Monte-Carlo Methods in Statistical Physics*, K. Binder, ed. (Springer-Verlag, N.Y., 1979) p149 and references cited therein
- [Ce80] D. M. Ceperley and B. Alder, *Phys. Rev. Lett.* **45**, 566 (1980)
- [Ce81] D. M. Ceperley and B. Alder, *Physica B&C* **107**, 875 (1981)
- [Ce83] D. M. Ceperley, *J.Comp Phys.* **51**, 404 (1983)
- [Da75] R. F. Dashen, B. Hasslacher and A. Neveu, *Phys Rev.* **D12**, 2443 (1975)
- [De74] A. De-Shalit and H. Feshbach, *Theoretical Nuclear Physics* (John Wiley and Sons, Inc., New York, 1974), p.768
- [Fe65] R. P. Feynman and A. R. Hibbs, *Quantum Mechanics and Path Integrals* (McGraw-Hill, New York, 1965)
- [Fe71] A. Fetter and J. Walecka, *Quantum Theory of Many-Particle Systems* (McGraw Hill, New York, 1971); R.D.Mattuck, *A Guide to Feynman Diagrams in Many-Body Problems* (McGraw-Hill, New York, 1971)
- [Fl78] H. Flocard, S. E. Koonin and M. Weiss, *Phys. Rev.* **C17**, 1682 (1978)
- [Fu81] F. Fucito, G. Marinari, G. Parisi, and C. Rebbi, *Nucl. Phys.* **B180**, 369 (1981)
- [Hi82] J. E. Hirsch, R. L. Sugar, D. J. Scalapino and R. Blankenbecker, *Phys. Rev. B* **26**, 5035 (1982)
- [Hi83] J. E. Hirsch, *Phys. Rev. B* **28**, 4059 (1983)

- [Hu59] J. Hubbard, Phys. Lett. **3**, 77 (1959)
- [Ka74] M. H. Kalos, D. Levesque and L. Verlet, Phys. Rev. A **9**, 2178 (1974)
- [Ka81] M. H. Kalos, M. A. Lee, P. A. Whitlock and G. V. Chester, Phys. Rev. B **24**, 115 (1981)
- [Ke76] A. K. Kerman and S. E. Koonin, Ann. Phys. **100**, 332 (1976)
- [Ke81] A. K. Kerman and S. Levit, Phys. Rev. C **24**, 1029 (1981)
- [Ke83] A. K. Kerman and T. Troudet, Caltech preprint, submitted Ann. of Physics. (1983)
- [Kog82] J. Kogut et. al., Phys Rev. Lett. **48**, 1140 (1982) and references cited therein
- [Ko77] S. E. Koonin, K. T. R. Davies, V. Maruhn-Rezwani, H. Feldmeir, S. J. Krieger and J. W. Negele, Phys. Rev. C **15**, 1359 (1977)
- [Ko82a] S. E. Koonin in *Nuclear Theory 1981*, G. Bertsch, ed., Proceedings of the Nuclear Theory Summer Workshop, Santa Barbara, California, 1981 (World Scientific, Singapore (1982)
- [Ko82b] S. E. Koonin, G. Sugiyama and H. Friedrich, in *Time-Dependent Hartree-Fock and Beyond*, K. Goeke and P. G. Reinhard, ed. (Springer-Verlag, N.Y., 1982) p 214
- [Le80a] S. Levit, Phys Rev **C21**, 1594 (1980)
- [Le80b] S. Levit, J. W. Negele and Z. Paltiel, Phys. Rev. **C21**, 1603 (1980)
- [Le80c] S. Levit, J. W. Negele and Z. Paltiel, Phys Rev. **C22**, 1979 (1980)
- [Li76] P. C. Lichtner and J. J. Griffin, Phys. Rev. Lett. **37**, 1521 (1976)
- [Mc64] J. B. McGuire, J. Math. Phys., **5**, 622 (1964)

- [Mc65] J. B. McGuire, J. Math. Phys., **6**, 432 (1965)
- [Me53] N. Metropolis, A. W. Rosenbluth, M. N. Rosenbluth, A. M. Teller and E. Teller, J. Chem. Phys. **21**, 1087 (1953)
- [Mu78] B. Muhlshlegel, *Path Integrals and the Applications in Quantum Statistics and Solid State Physics*, ed. G. J. Papudopoulos and J. T. Devereese (Plenum, N.Y., 1978), Vol. 34
- [Ne78] J. W. Negele, S. E. Koonin, N. Muller, J. R. Nix and A. J. Sierk, Phys. Rev. C **17**, 1098 (1978)
- [Ne82a] J. W. Negele in *Time-Dependent Hartree-Fock and Beyond*, K. Goeke and P. G. Reinhard, ed. (Springer-Verlag, N.Y., 1982) p 198
- [Ne82b] J. W. Negele, Rev. of Mod. Phys. **54**(4), (October, 1982)
- [Ra75] R. Rajarman, Phys Rep. **21C**, 227 (1975)
- [Re79] H. Reinhardt, Nucl. Phys. A **331**, 353 (1979)
- [Re80] H. Reinhardt, Nucl. Phys. A **346**, 1 (1980)
- [Re82] P. J. Reynolds, D. M. Ceperley, B. J. Alder and W. A. Lester, J. Chem. Phys. **77**, 5593 (1982)
- [Ri80] P. Ring and P. Shuck, *The Nuclear Many-Body Problem*, (Springer-Verlag, N.Y., 1980)
- [Sc81] D. Scalapino and R. Sugar, Phys. Rev. B **24**, 4295 (1981)
- [Se83] B. Serot, S. E. Koonin and J. W. Negele, Phys. Rev. C **28**, 1679 (1983)
- [St57] R. D. Stratonovitch, Doklady Akad. Nauk. SSSR **115**, 1907 (1957) translated in Soviet Phys. Doklady **2**, 416 (1958)

- [Su84] G. Sugiyama and S.E.Koonin, submitted
- [Tr83a] T. Troudet and S. E. Koonin, Phys. Rev. C **28**, 1465 (1983)
- [Tr83b] T. Troudet and S. E. Koonin, Phys. Rev. C **28**, 2171 (1983)
- [Va62] R. Varga, *Matrix-Iterative Analysis* (Prentice-Hall, Englewood Cliffs, 1962), p195
- [Wh79] P. A. Whitlock, M. H. Kalos, G. V. Chester and D. M. Ceperley, Phys. Rev. B **19**, 5598 (1978)
- [Wh83] P. A. Whitlock and M. H. Kalos, *Monte-Carlo Methods* (Wiley Interscience, N.Y., 1983)
- [Yo76] B. Yoon and J. W. Negele, Phys. Rev. **A16**, 1451 (1976)
- [Za81] J. G. Zabolitsky and M. H. Kalos, Nucl. Phys. **A356**, 114 (1981)

Figures and Tables

Table 1. Energy contributions for the delta function potential corresponding to the Goldstone diagrams in Figure 1. C is the number of closed loops, I the number of interactions. The order of the energy contribution is A^{C-I+2} .

Diagram	C	I	Order	Energy
SPA	2	1	A^3	} $-A^2(A-1)V_0^2/24$
n=1	1	1	A^2	
n=2	2	2	A^2	$-0.9956A(A-1)V_0^2/24$
RPA	C	C	A^2	remaining A^2 energy contribution

Table 3. Parameters for A spin-isospin degenerate fermions, exponential potential interaction. The mesh is defined by $N \Delta t \times (M-1) \Delta x$, the harmonic oscillator by the frequency Ω with length $r_{c.m.}$, and the random walk by the step size $\Delta\sigma$ yielding an acceptance ratio of R_{acc} . Energies are calculated every τ_{corr} trajectories from trajectory ν_i to ν_f . The trial wavefunction is specified to be either the harmonic oscillator (g) or the delta function (c) basis with parameter $b = 1/\beta$.

A	4	4	4	8	8	12	12
$\Delta t (\times 10^{-25} s)$	20.0	40.0	40.0	2.5	5.0	2.5	5.0
N	50	70	70	140	100	160	100
Δx (fm)	0.25	0.25	0.25	0.20	0.20	0.20	0.20
M	40	40	40	50	50	70	70
$\hbar\Omega$ (Mev)	10	10	10	10	10	10	10
$r_{c.m.}$ (fm)	1.0	1.0	1.0	0.72	0.72	0.59	0.59
Trial wavefunction	g	g	c	g	g	g	g
b (fm)	1.4	1.4	0.9	1.4	1.4	1.6	1.6
$\Delta\sigma$	8.0	6.0	5.5	14.0	11.0	12.0	8.0
R_{acc}	0.50	0.50	0.50	0.55	0.55	0.51	0.50
τ_{corr} (trajectories)	25	25	25	25	25	25	20
ν_i (trajectories)	1000	1000	1000	1000	1000	1000	1000
ν_f (trajectories)	6000	6000	6000	6000	3000	3000	3000

Table 4. Variational energies for A particles, exponential potential interaction. E_A refers to the energy of A particles for the Hermite-Gaussian (HG) or the Hartree delta function potential (HD) trial wavefunction with length parameter $b=1/\beta$. The harmonic oscillator is not included in the variational determination of β .

A	Trial wavefunction	b (fm)	E_4 (MeV)	E_8 (MeV)	E_{12} (MeV)	Harmonic Oscillator (MeV)
4	HG	1.4	-36.4	-	-	0.8
4	HD	0.9	-35.8	-	-	-
8	HG	1.3	-36.3	-98.3	-	1.5
12	HG	1.6	-36.2	-98.3	-168.5	3.1

Table 5. Parameters for $A=10$ bosons, exponential potential interaction. The mesh is defined by $N\Delta t \times (M-1)\Delta x$, the harmonic oscillator by the frequency Ω with length $\tau_{c.m.}$, and the random walk by the step size $\Delta\sigma$ yielding an acceptance ratio of R_{acc} . Energies are calculated every τ_{corr} trajectories from trajectory ν_i to ν_f . The harmonic oscillator trial function parameter is $b=1/\beta$. The importance sampling schemes used are indicated, with only the lowest N_q frequencies involved in the random walk.

	Spatial importance sampling	Momentum importance sampling $\eta_q \approx \eta_q^{initial}$
Δt ($\times 10^{-25}$ s)	5.0	5.0
N	160	140
Δx (fm)	0.15	0.15
M	64	64
$\hbar\Omega$ (MeV)	10.0	10.0
$r_{c.m.}$ (fm)	0.65	0.65
b (fm)	1.5	1.5
N_q	all space points changed	10
$\Delta\sigma$	8.5	27.0
R_{acc}	0.53	0.56
τ_{corr} (trajectories)	40	40
ν_i (trajectories)	1000	1000
ν_f (trajectories)	3000	3000

Table 6. Parameters for $A=12$ spin-isospin degenerate fermions, exponential potential interaction. The mesh is defined by $N \Delta t \times (M-1) \Delta x$, the harmonic oscillator by the frequency Ω with length $\tau_{c.m.}$, and the random walk by the step size $\Delta\sigma$ yielding an acceptance ratio of R_{acc} . Energies are calculated every τ_{corr} trajectories from trajectory ν_i to ν_f . The harmonic oscillator trial function parameter is $b=1/\beta$. The importance sampling schemes used are indicated, with only the lowest N_q frequencies involved in the random walk.

	Spatial importance sampling	Momentum importance sampling $\eta_q \approx \sigma_q^{int}$	Momentum importance sampling $\eta_q \approx 1$
$\Delta t (\times 10^{-25} s)$	2.5	2.5	2.5
N	160	100	120
Δx (fm)	0.20	0.22	0.22
M	70	64	64
$\hbar\Omega$ (MeV)	10.0	10.0	10.0
$r_{c.m.}$ (fm)	0.59	0.59	0.59
b (fm)	1.6	1.6	1.6
N_q	all space points changed	10	10
$\Delta\sigma$	12.0	32.0	16.0
R_{acc}	0.51	0.52	0.52
τ_{corr} (trajectories)	25	125	18
ν_i (trajectories)	1000	1000	1000
ν_f (trajectories)	3000	3000	3000

Table 7. Parameters for $A=4$ fermions, attractive and repulsive exponential potential interaction. The mesh is defined by $N \Delta t \times (M-1) \Delta x$, the harmonic oscillator by the frequency Ω with length $r_{c.m.}$, and the random walk by the step size $\Delta\sigma$ yielding an acceptance ratio of R_{acc} . Energies are calculated every τ_{corr} trajectories from trajectory ν_i to ν_f . The harmonic oscillator trial function parameter is $b=1/\beta$. The importance sampling schemes used are indicated, with only the lowest N_q frequencies involved in the random walk. V_{add} is the strength of the additional potential required by the negativity condition on the Metropolis exponent.

	Spatial importance sampling	Momentum importance sampling $\eta_q \approx \sigma_{init}$
$\Delta t (\times 10^{-24} \text{s})$	1.0	1.0
N	100	100
Δx (fm)	0.08	0.09
M	150	128
$\hbar\Omega$ (MeV)	2.0	2.0
$r_{c.m.}$ (fm)	2.3	2.3
b (fm)	1.3	1.3
N_q	-	15
$\Delta\sigma$	3.5	3.0
R_{acc}	0.54	0.52
τ_{corr} (trajectories)	45	30
ν_i (trajectories)	1000	1000
ν_f (trajectories)	3000	3000
V_{add} (MeV)	-200	-200

Figure 1. The Goldstone diagram expansion for the energy of the delta function potential system. Table 1 gives the order and values of the energy contributions from each diagram.

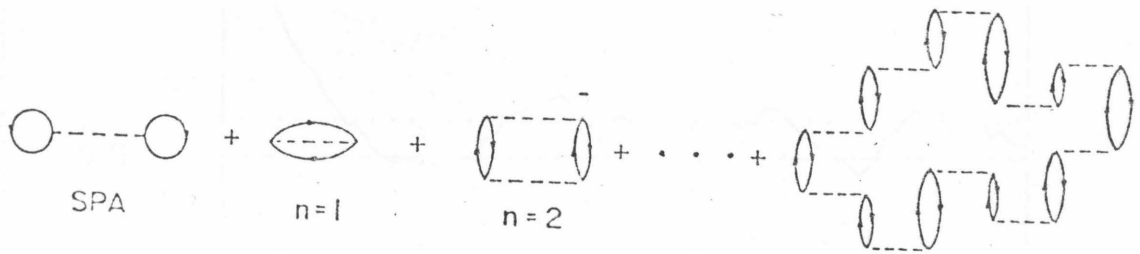


Figure 2. The energy autocorrelation function (6.6) versus trajectory number for a system of 10 bosons interacting via the delta function potential. The correlation length is defined to be the number of trajectories at which the function drops to less than 0.1. Parameters are given in Table 2.

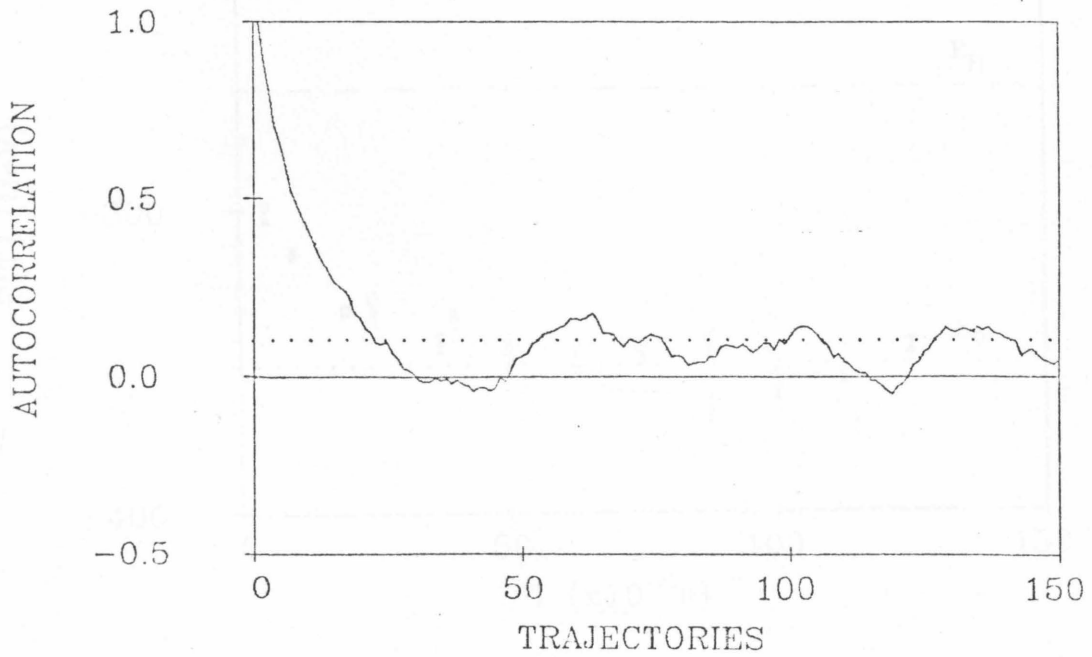


Figure 3. $E(T)$ for 6 bosons, delta function interaction. $E_H = -259.19$ is the Hartree energy and $E_0 = -350.36$ the exact ground state energy, including the center-of-mass harmonic oscillator. Two size time steps are used: $\tau = 1.0 \times 10^{-25}$ s and $\Delta = 2.5 \times 10^{-25}$ s. Parameters are given in Table 2.

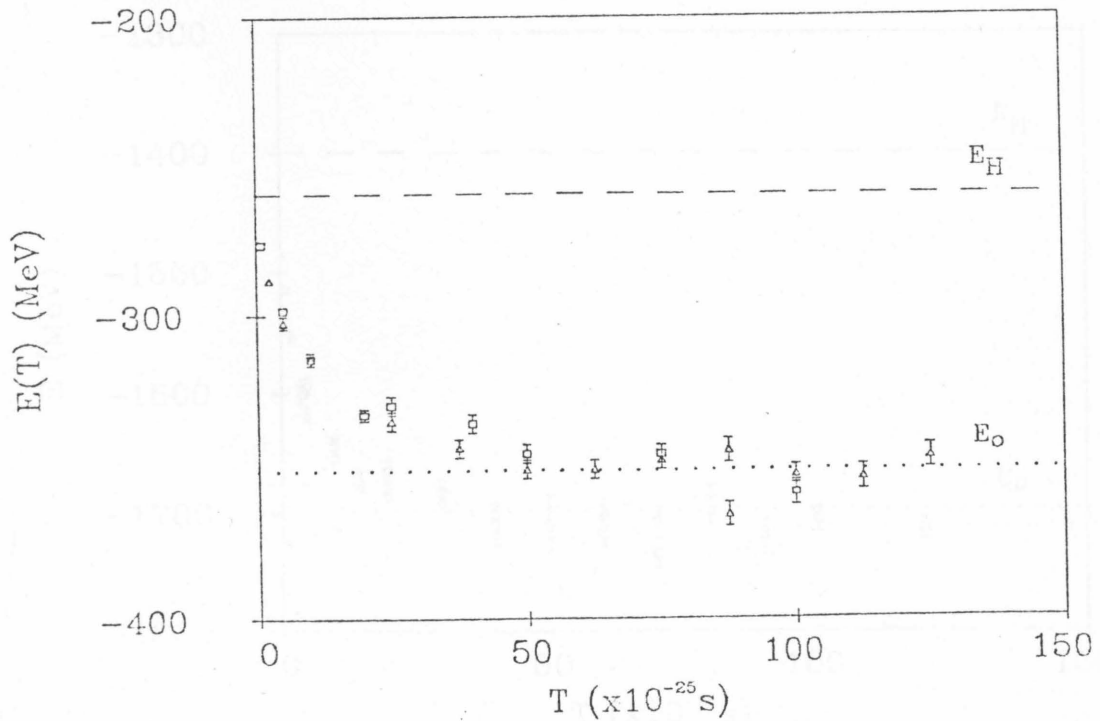


Figure 4. $E(T)$ for 10 bosons, delta function interaction. $E_H = -1399.61$ is the Hartree energy and $E_0 = -1698.14$ the exact ground state energy, including the center-of-mass harmonic oscillator. Two size time steps are used: $\tau = 1.0 \times 10^{-25}$ s and $\Delta = 0.5 \times 10^{-25}$ s. Parameters are given in Table 2.

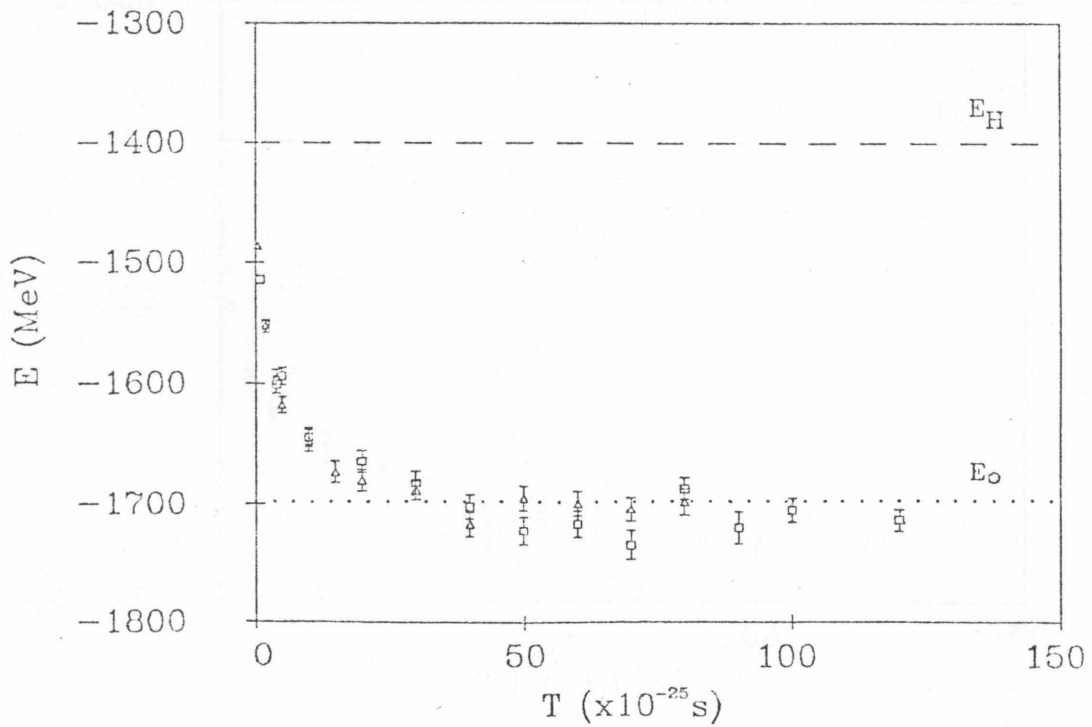


Figure 5. $E(T)$ for a 20 bosons, delta function interaction. $E_H = -12475.6$ is the Hartree energy and $E_o = -13776.3$ the exact ground state energy, including the center-of-mass harmonic oscillator. Two size time steps are used: $\tau = 1.0 \times 10^{-26}$ s and $\Delta = 0.5 \times 10^{-26}$ s. Parameters are given in Table 2.

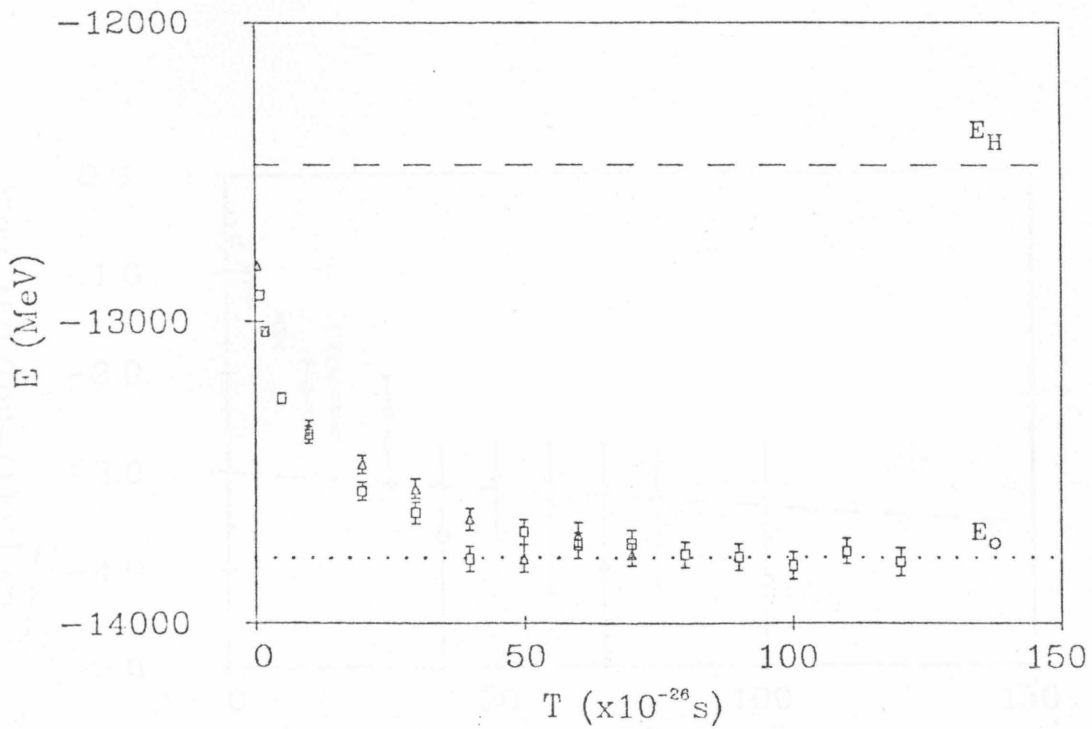


Figure 6. Plot of $\ln[E(T)-E_0/E_H-E_0]$ for 10 bosons, delta function interaction. Two size time steps are used: $\square = 1.0 \times 10^{-25} \text{s}$ and $\Delta = 0.5 \times 10^{-25} \text{s}$. The dotted line shows the relaxation due to the energy gap between the ground and the first excited state. The second relaxation due to the center-of-mass oscillator, is indicated by the dashed line. Parameters are given in Table 2.

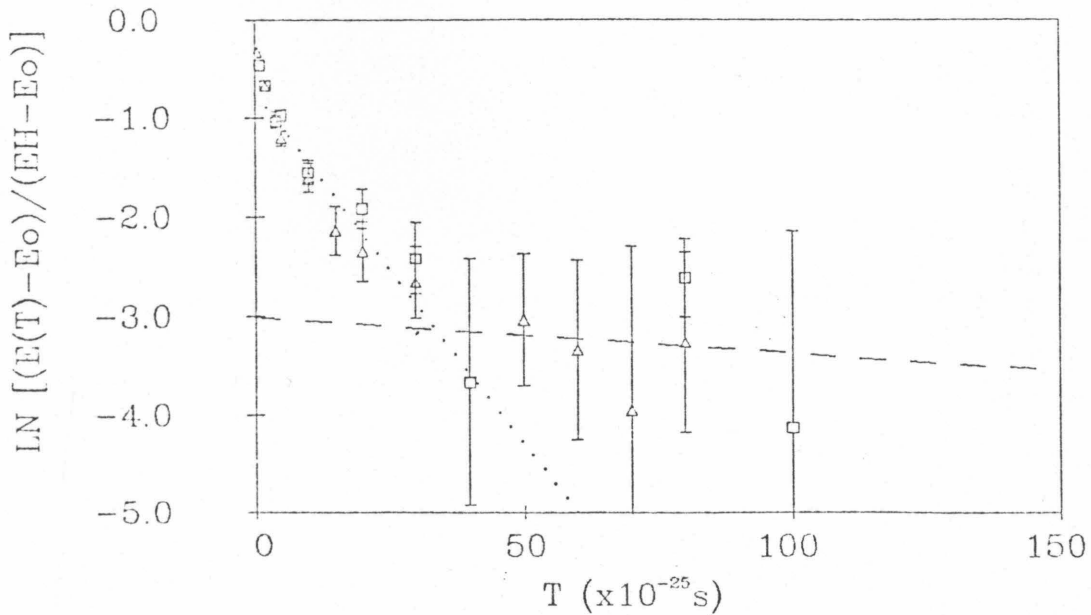


Figure 7. The wavefunction for 10 bosons interacting via the delta function potential is shown for the time step size $\Delta t = 0.5 \times 10^{-25}$ s after 0 (trial wavefunction), 20, 40, 60, 80, and 100 evolution steps. The results are averaged over trajectories 1000-2000, computed every 25 trajectories. Parameters are given in Table 2. For clarity, the wavefunctions at later time slices are shifted up and to the right as indicated by the zeroing base line for each.

Figure 8. Sigma field for the delta function potential. The σ field for 10 bosons is shown for the size $\Delta t = 0.5 \times 10^{-25}$ s after 0 (trial σ field), 20, 40, 60, 80, 100 evolution steps. The results are averaged over trajectories 1000-2000, computed every 25 trajectories. Parameters are given in Table 2. For clarity, the fields at later time slices are shifted up and to the right as indicated by the zeroing base line for each.

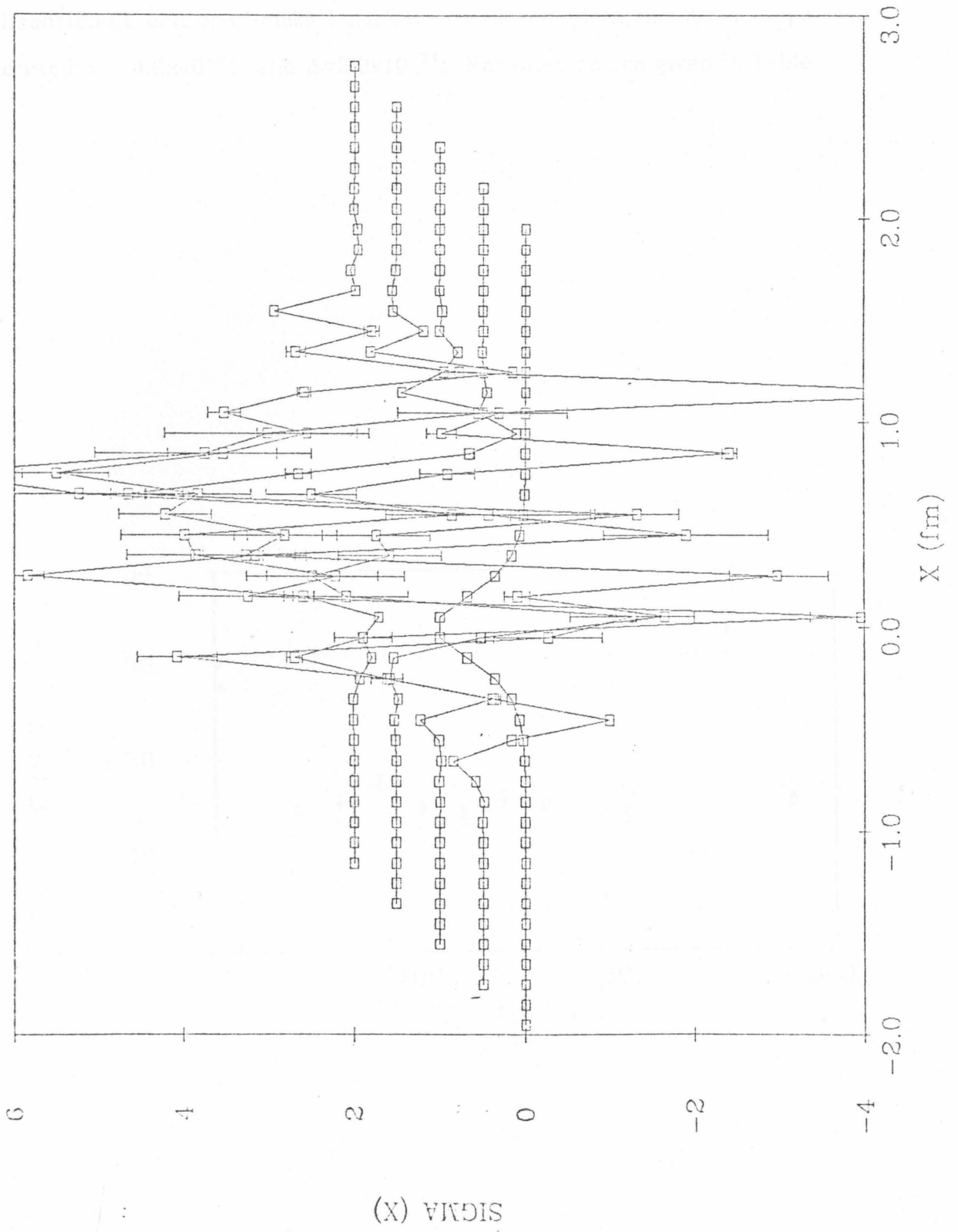


Figure 9. $E(T)$ for 4 spin-isospin degenerate fermions, exponential potential interaction. $E_{var} = -35.8 MeV$ is the variational energy plus non-selfconsistent center-of-mass harmonic oscillator. Two size time steps are used: $\sigma = 4.0 \times 10^{-24} s$ and $\Delta = 2.0 \times 10^{-24} s$. Parameters are given in Table 3.

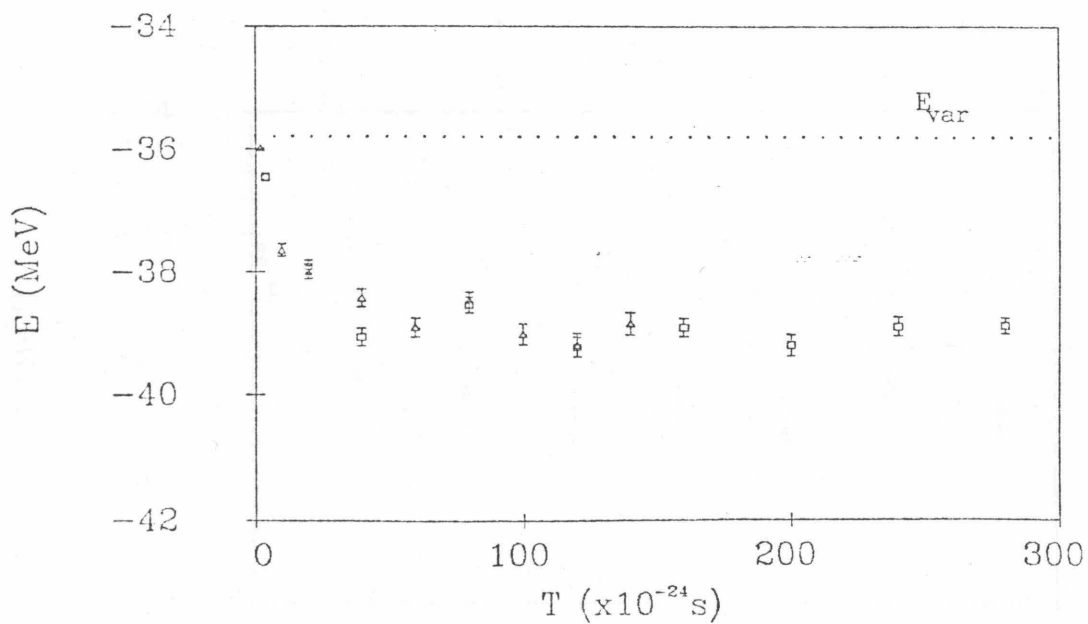


Figure 10. $E(T)$ for 4 spin-isospin degenerate fermions, exponential potential interaction. $E_{var} = -35.8 \text{ MeV}$ is the variational energy plus non-selfconsistent center-of-mass harmonic oscillator. Two different initial conditions are used: \square = harmonic oscillator basis and Δ = delta function basis with the size of the time step $4.0 \times 10^{-24} \text{ s}$ in both cases. Parameters are given in Table 3.

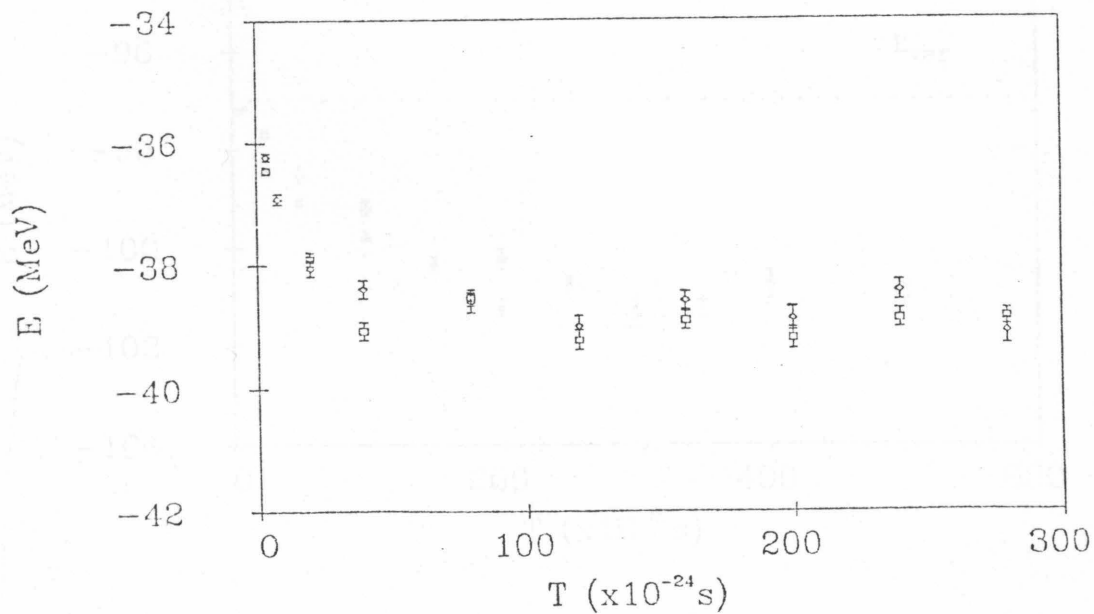


Figure 11. $E(T)$ for 8 spin-isospin degenerate fermions, exponential potential interaction. $E_{var} = -96.5 \text{ MeV}$ is the variational energy plus non-selfconsistent center-of-mass harmonic oscillator. Two size time steps are used: $\sigma = 5.0 \times 10^{-25} \text{ s}$ and $\Delta = 2.5 \times 10^{-25} \text{ s}$. Parameters are given in Table 3.

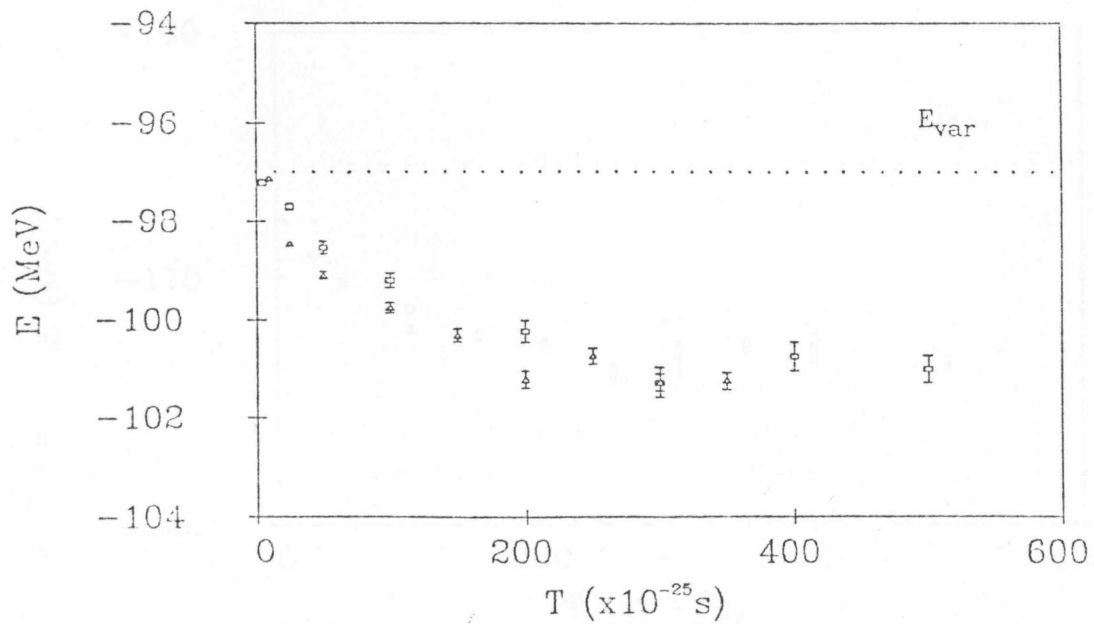


Figure 12. $E(T)$ for 12 spin-isospin degenerate fermions, exponential potential interaction. $E_{var} = -164.4 MeV$ is the variational energy plus non-selfconsistent center-of-mass harmonic oscillator. Two size time steps are used: $\tau = 2.5 \times 10^{-25} s$ and $\Delta = 5.0 \times 10^{-25} s$. Parameters are given in Table 3.

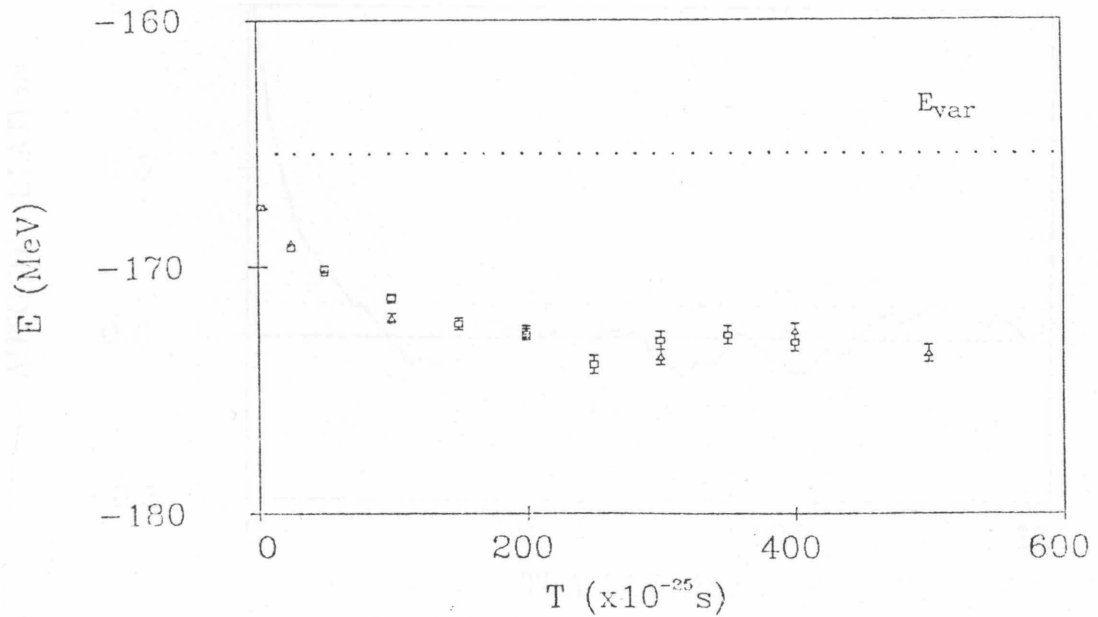


Figure 13. Typical autocorrelation function for 12 spin-isospin degenerate fermions, exponential potential interaction. This example is for 30 time steps of size 5.0×10^{-25} s. The correlation length is defined to be the number of trajectories at which the function drops to less than .1. Parameters are given in Table 3.

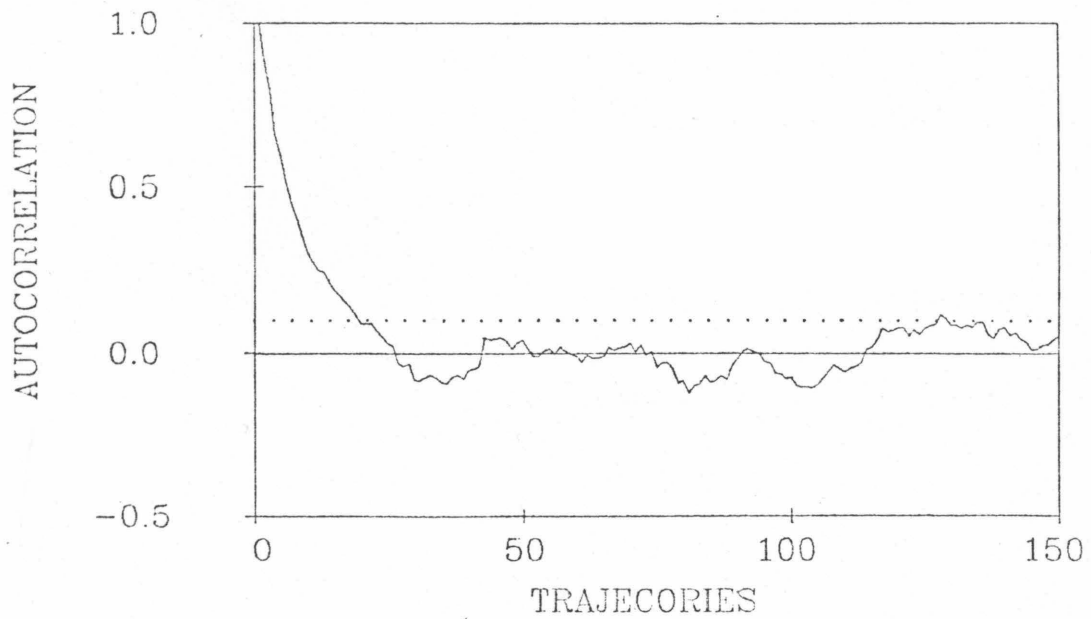
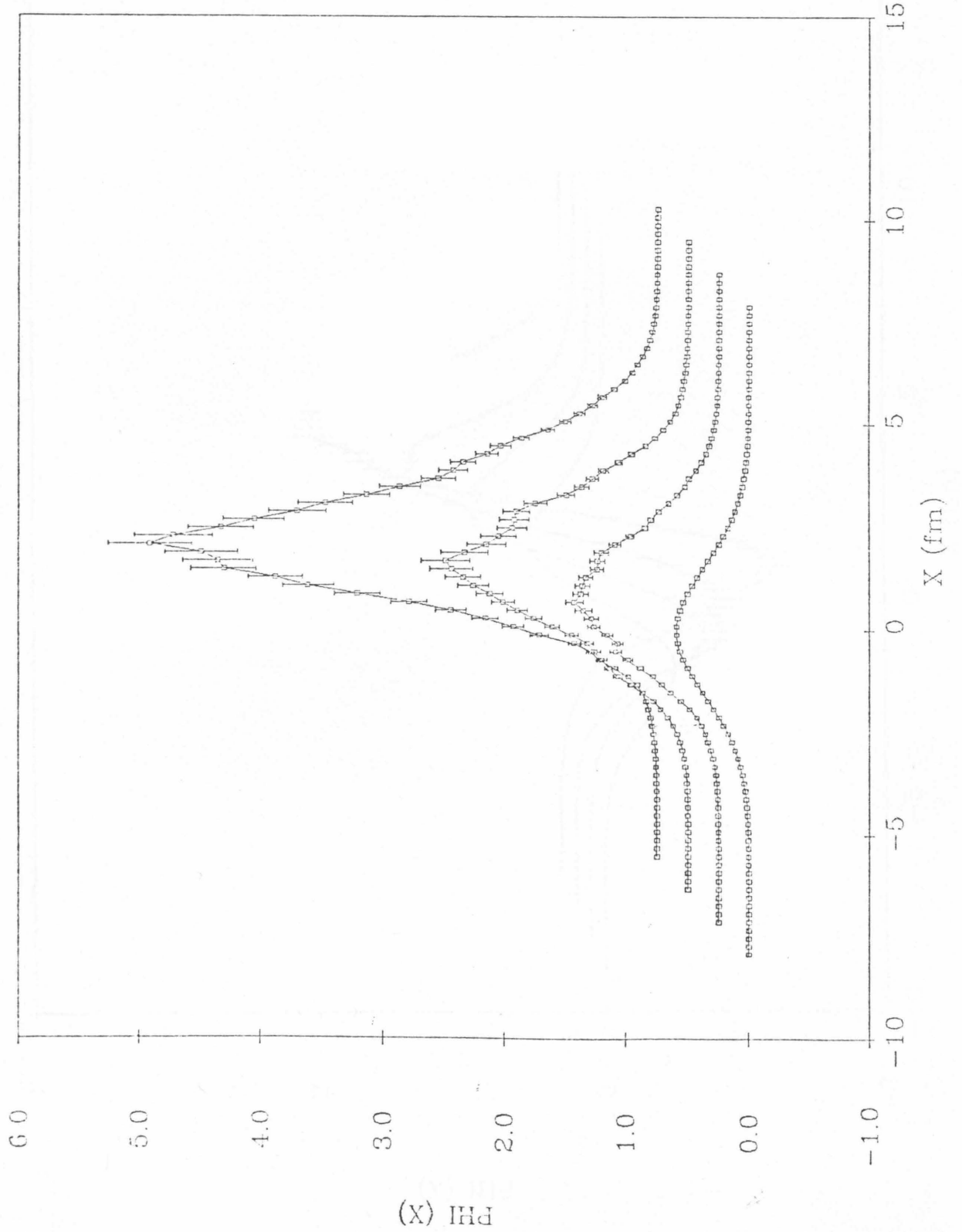
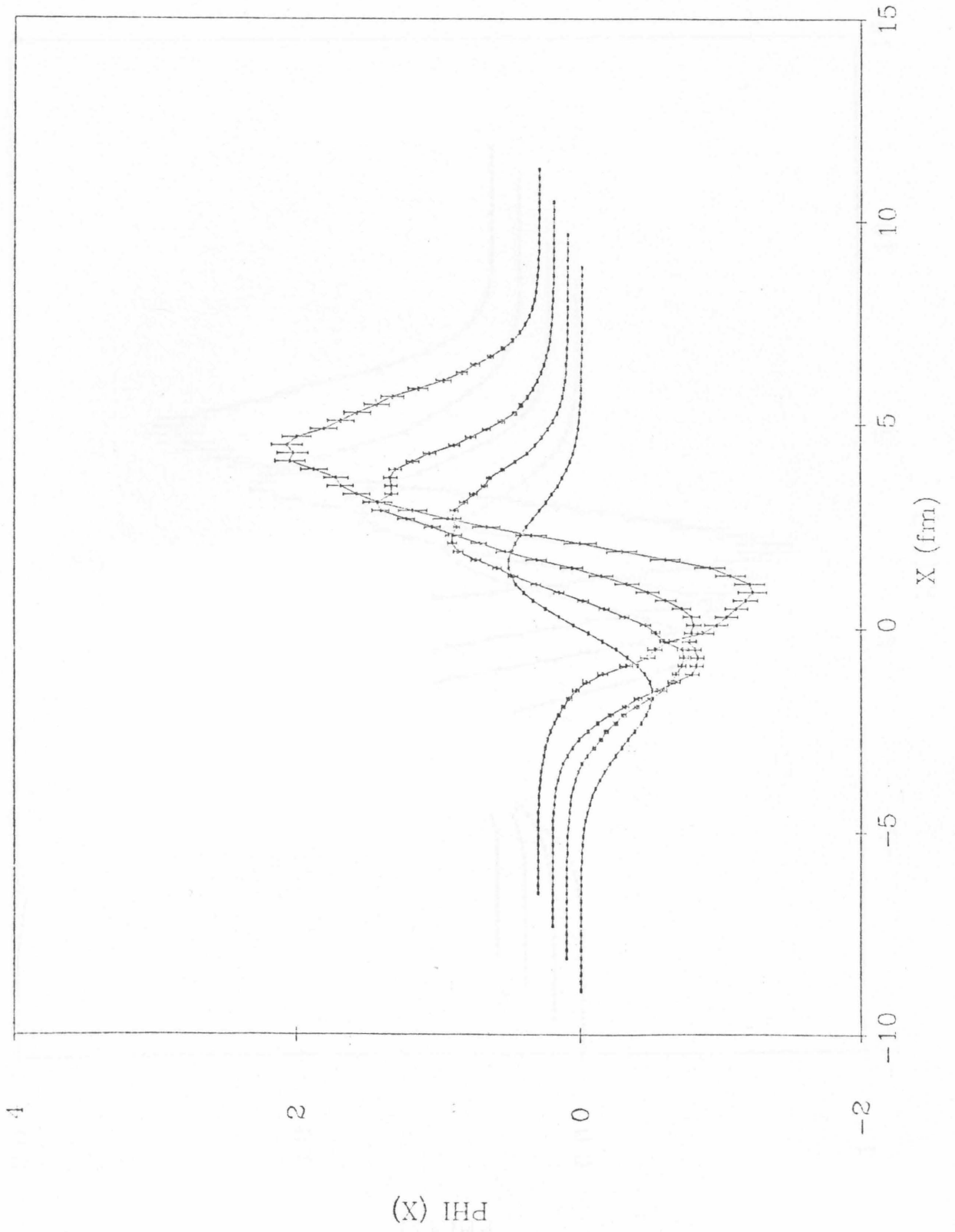


Figure 14. The three orbital wavefunctions for 12 spin-isospin degenerate fermions interacting via an exponential potential are shown for the size $\Delta t = 2.5 \times 10^{-25} \text{s}$ after 0 (trial wavefunction), 40, 80, and 120 evolution steps. The results are averaged over trajectories 1000-2000, computed every 25 trajectories. Parameters are given in Table 3. For clarity, the wavefunctions at later time slices are shifted up and to the right as indicated by the zeroing base line for each.





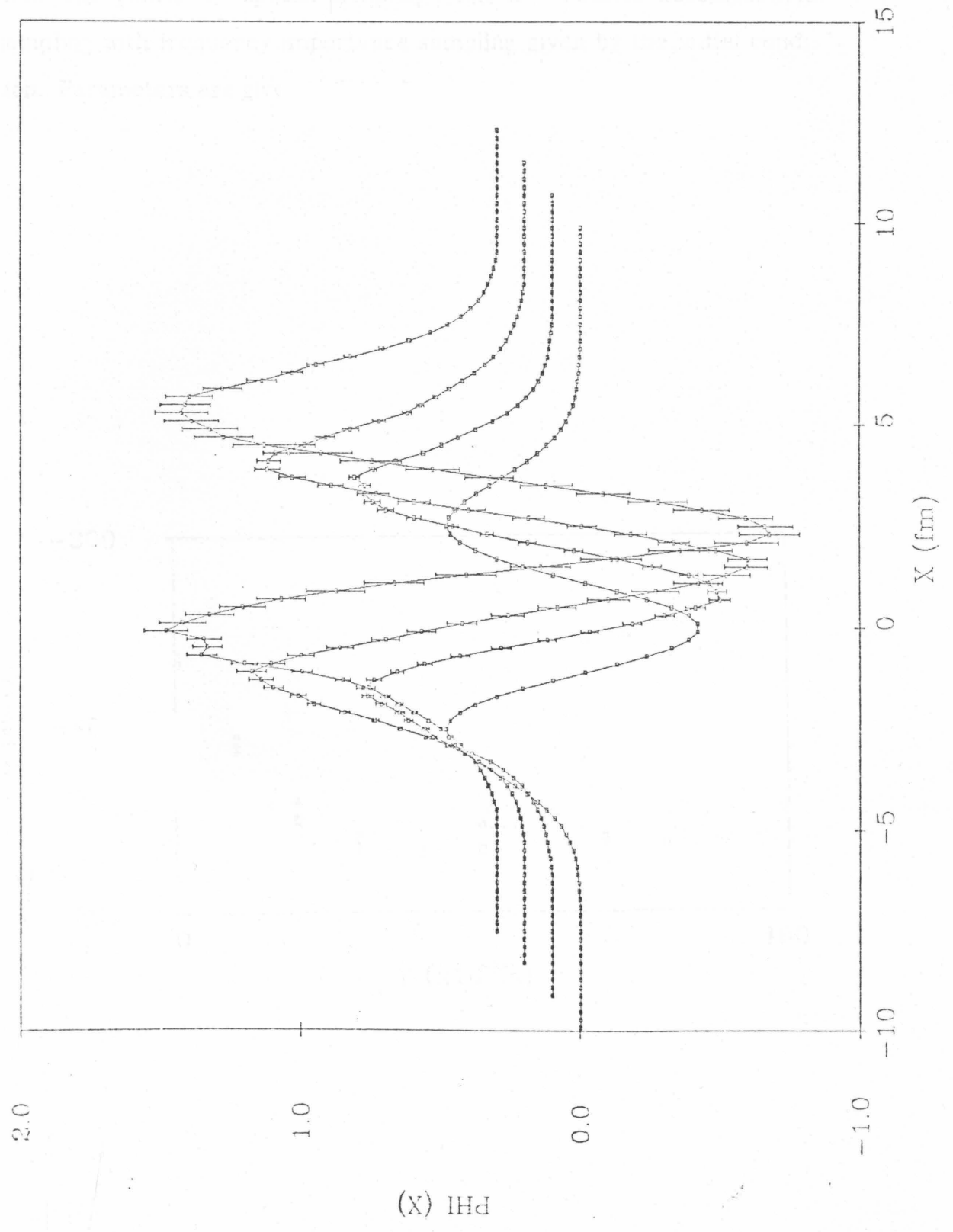


Figure 15. Comparison of $E(T)$ for spatial and momentum space importance sampling for a system of 10 bosons, exponential potential interaction. The points \square = spatial sampling while Δ = Fourier decomposition sampling with frequency importance sampling given by the initial condition. Parameters are given in Table 5.

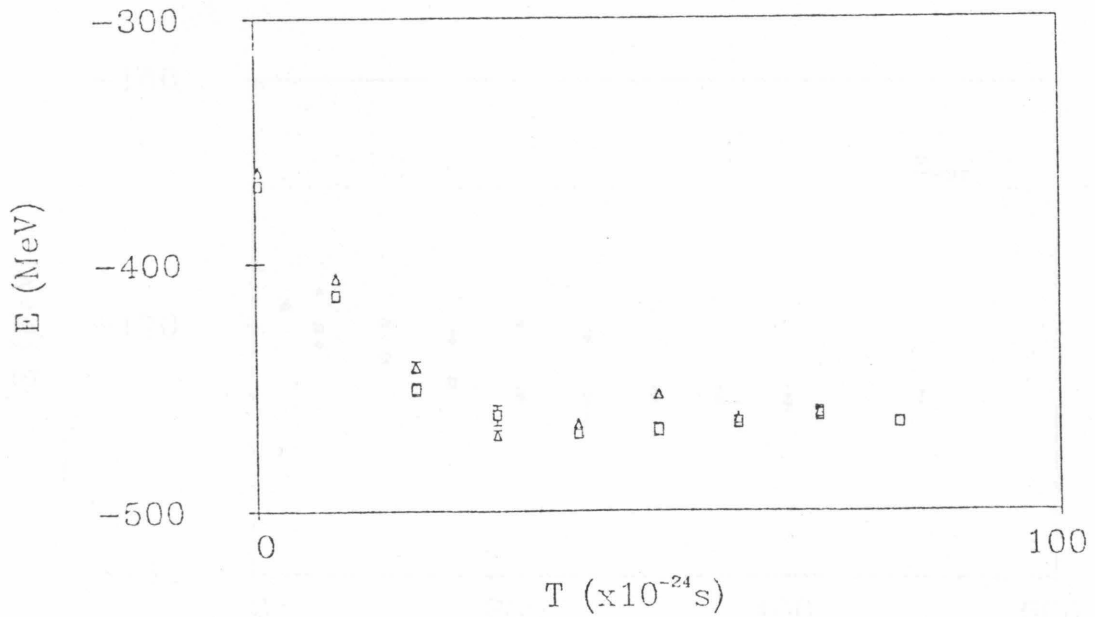


Figure 16. $E(T)$ for 12 spin-isospin degenerate fermions exponential potential interaction. The \square points are identical to Figure 12, and the Δ and the diamond points show Fourier decomposition sampling with $1/q$ and uniform frequency importance sampling respectively. All three use a time step of 2.5×10^{-25} s. Parameters are given in Table 6.

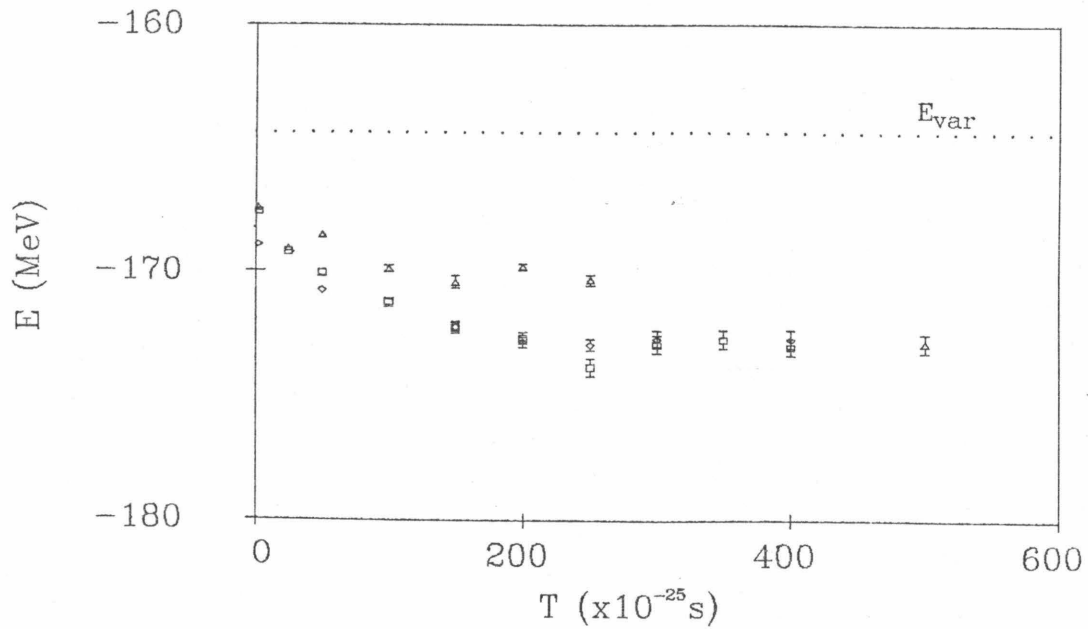


Figure 17. Energy autocorrelation function for 12 spin-isospin degenerate fermions interacting via an exponential potential using Fourier decomposition sampling with uniform frequency importance sampling. This plot is for 30 time steps of size 2.5×10^{-25} s. The correlation length is defined to be the number of trajectories at which the function drops to less than 0.1. Parameters are given in Table 6.

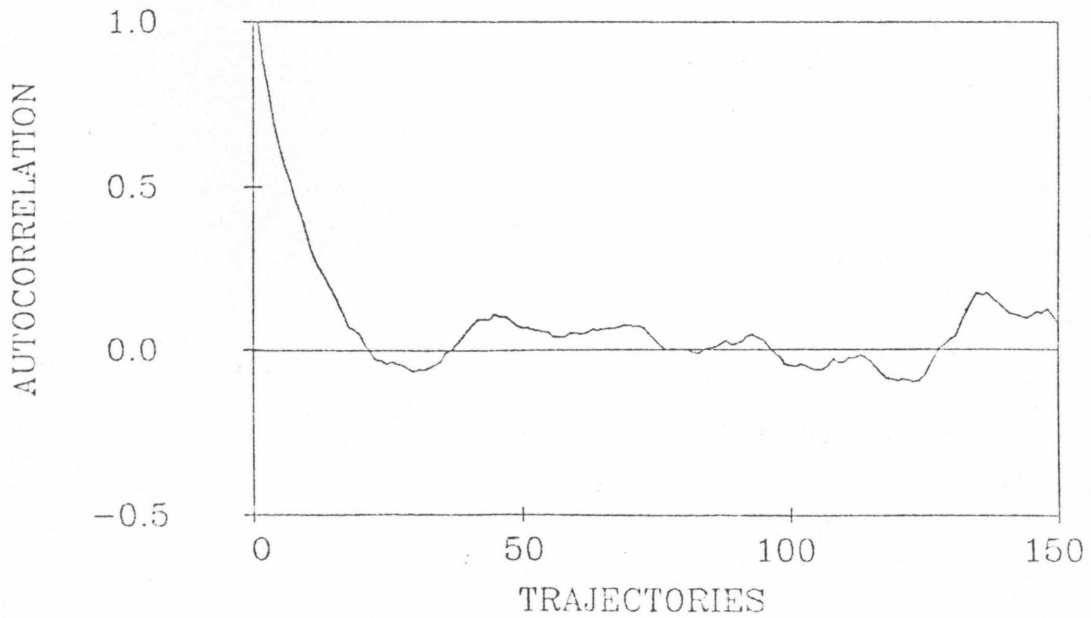
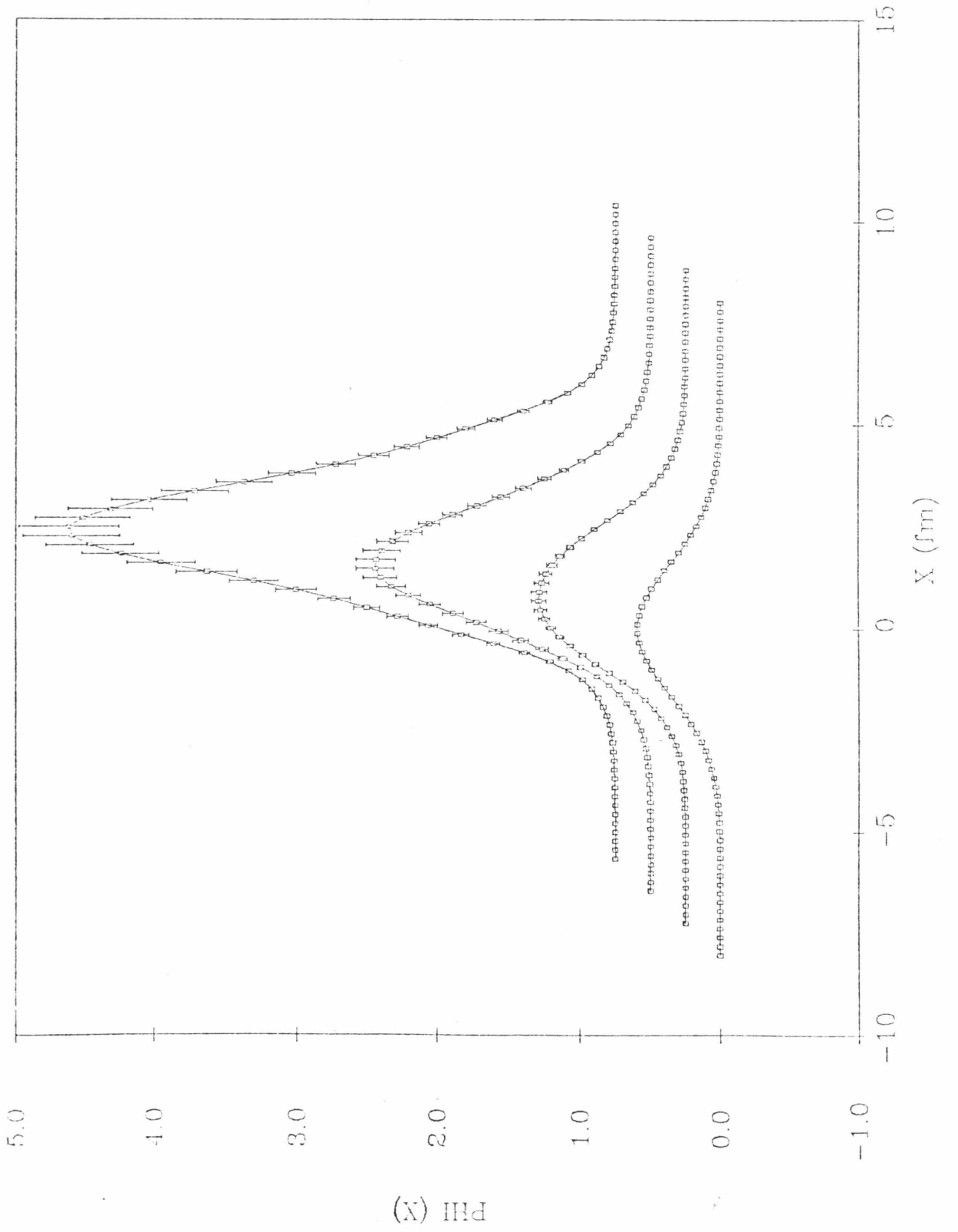


Figure 18. The three orbital wavefunctions for 12 spin-isospin degenerate fermions interacting via exponential potential are shown for $\Delta t = 2.5 \times 10^{-25}$ s after 0 (trial wavefunction), 40, 80, and 120 evolution steps. The results are averaged over trajectories 1000-2000, computed every 25 trajectories. In this case the changes in the sigma field are performed with Fourier decomposition importance sampling with uniform weighting. Parameters are given in Table 6. For clarity, the wavefunctions at later time slices are shifted up and to the right as indicated by the zeroing base line for each.



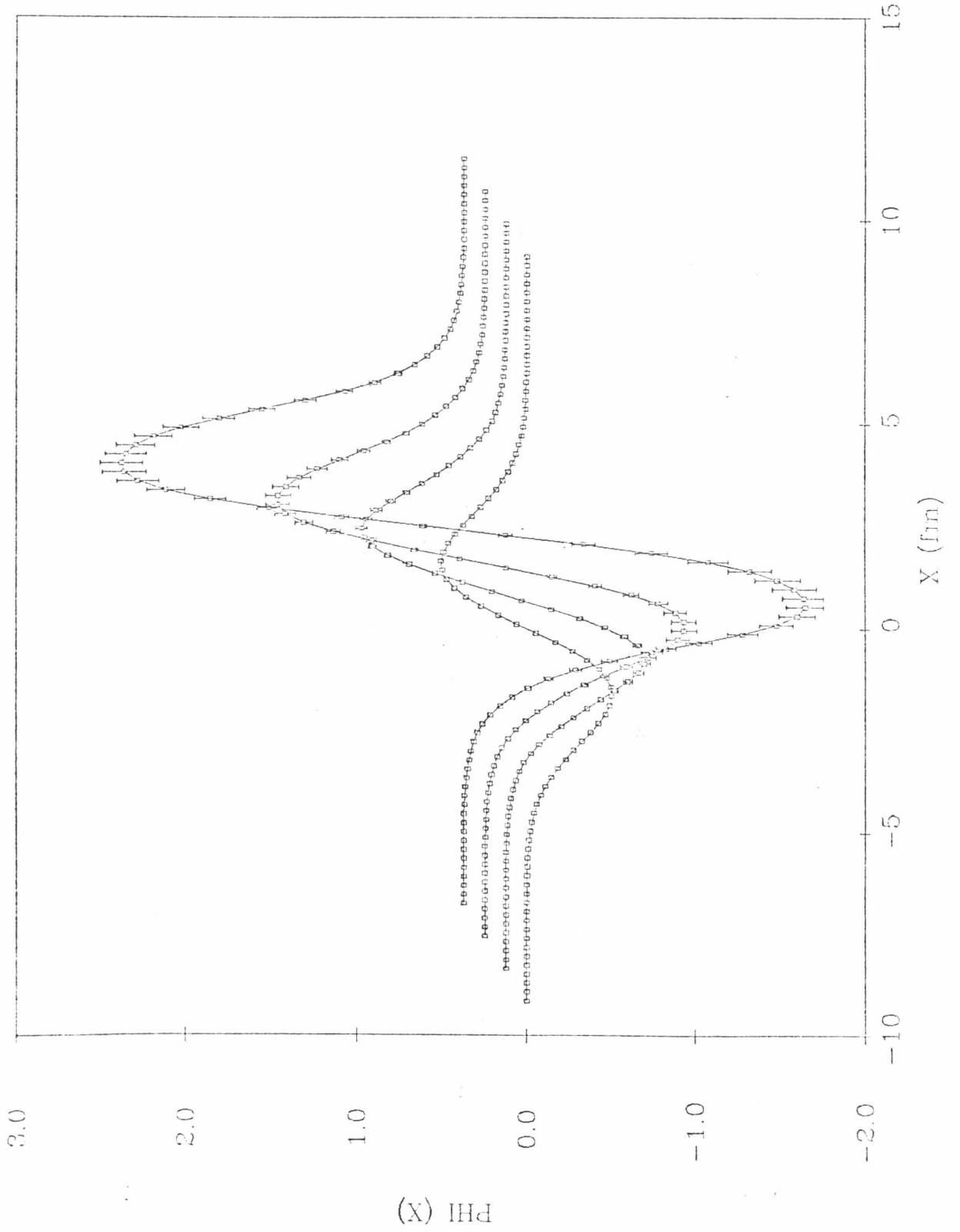
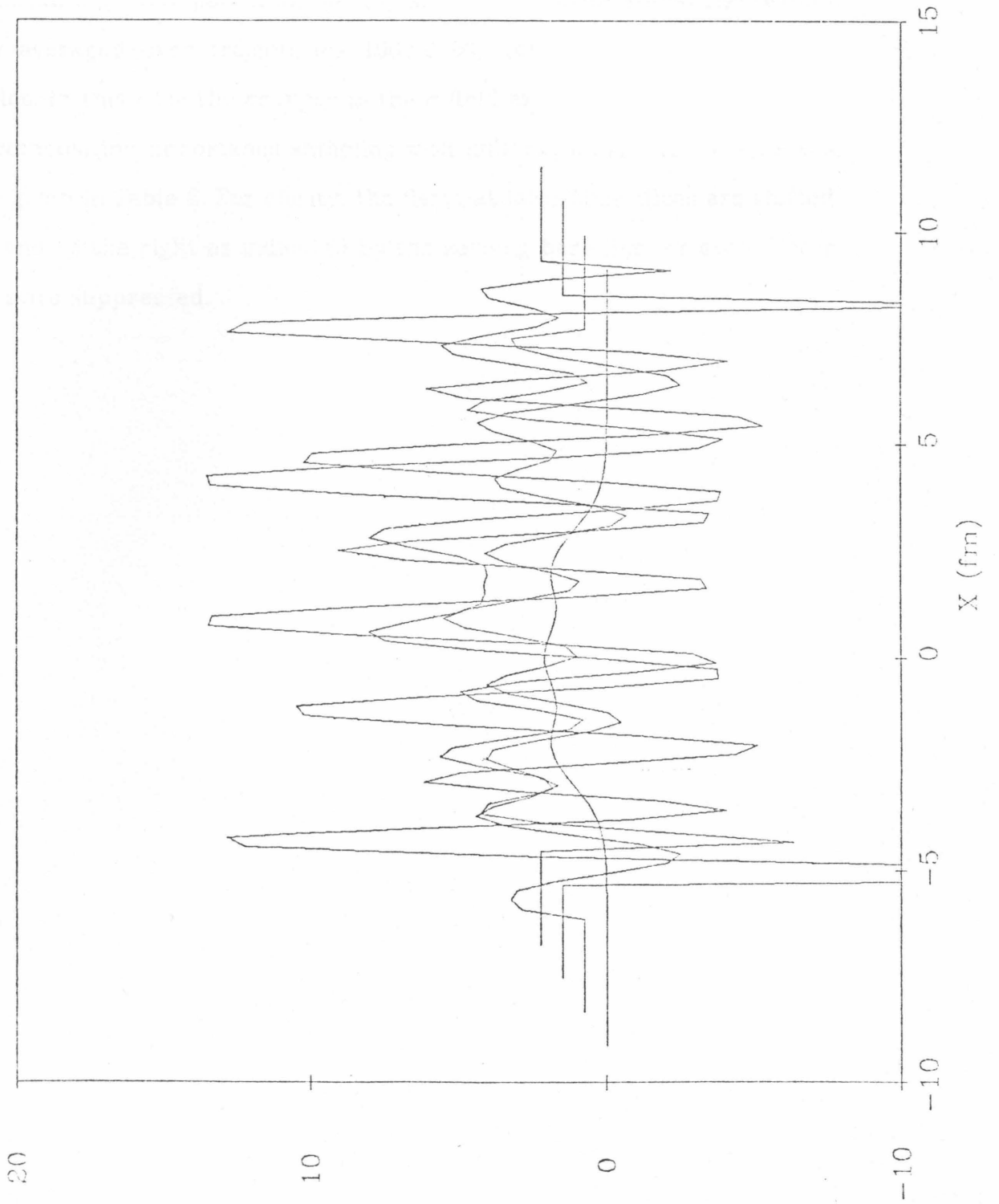


Figure 19. The combined σ field for 12 spin-isospin degenerate fermions interacting via an exponential potential is shown for the size $\Delta t = 2.5 \times 10^{-25}$ s after 0 (trial sigma field), 40, 80, and 120 evolution steps. The results are averaged over trajectories 1000-2000, computed every 25 trajectories. In this case, the changes in the sigma field are performed with Fourier decomposition importance sampling with uniform weighting. Parameters are given in Table 6. For clarity, the fields at later time slices are shifted up and to the right as indicated by the zeroing base line for each. Error bars are suppressed.



(X) SIGMA

Figure 20. The one-body potential for 12 spin-isospin degenerate fermions interacting via an exponential potential is shown for $\Delta t = 2.5 \times 10^{-25}$ s after 0 (initial one-body potential), 40, 80, and 120 evolution steps. The results are averaged over trajectories 1000-2000, computed every 25 trajectories. In this case the changes in the σ field are performed with Fourier decomposition importance sampling with uniform weighting. Parameters are given in Table 6. For clarity, the fields at later time slices are shifted up and to the right as indicated by the zeroing base line for each. Error bars are suppressed.

Figure 21. The static nuclear potential of 1_0n (1_0n + 1_0n)

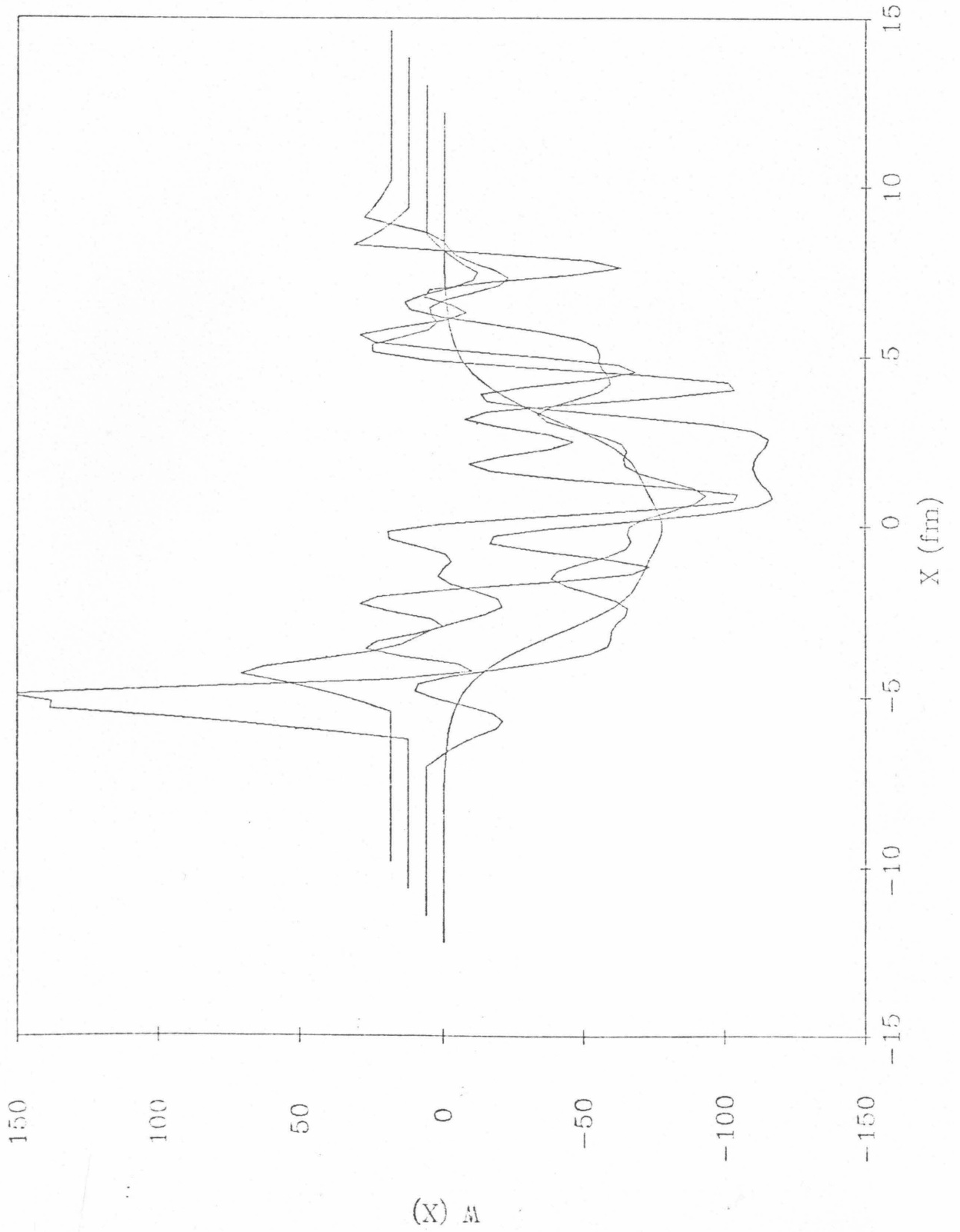


Figure 21. The static nuclear potential of Eqs. (10.6)-(10.8).

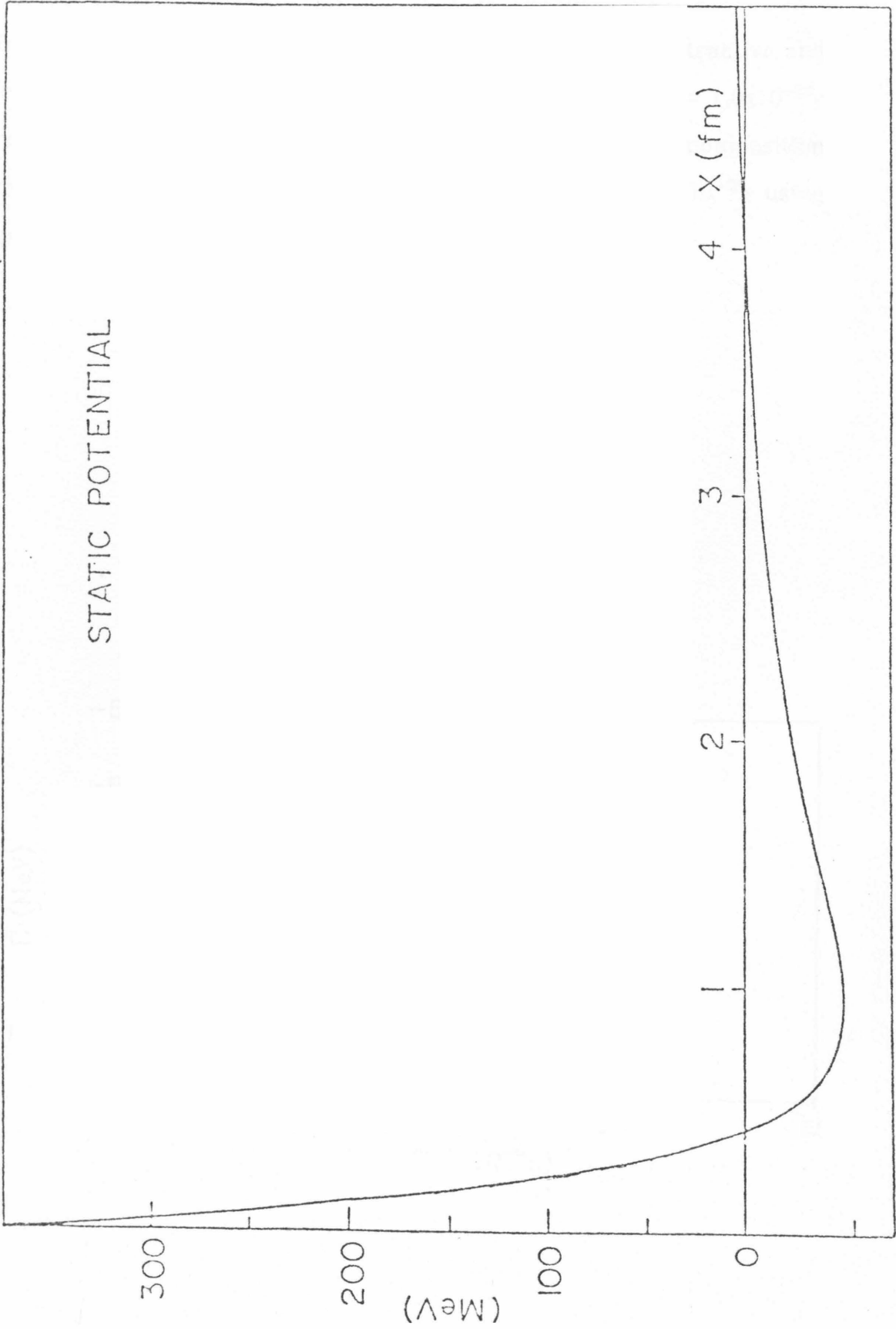


Figure 22. $E(T)$ for 4 fermions interacting via a combined attractive and repulsive exponential potential. The time step sizes are $\tau = 1.0 \times 10^{-26} \text{s}$ with the changes in the σ field performed using Fourier decomposition importance sampling given by the initial condition and $\Delta = 2.5 \times 10^{-26} \text{s}$ using spatial sampling. Parameters are given in Table 7.

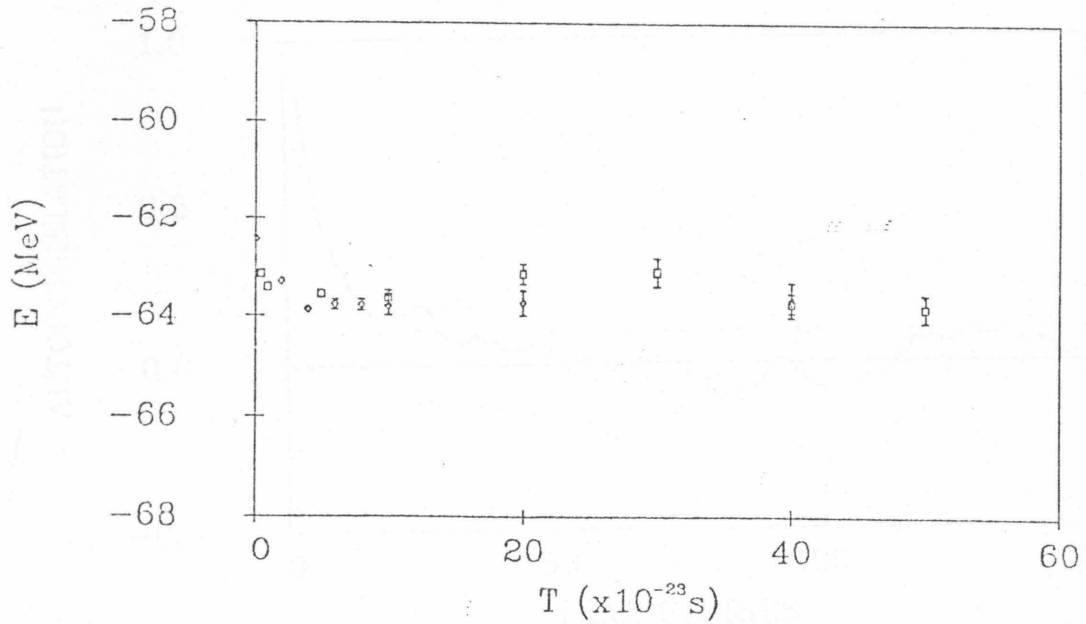


Figure 23. Energy autocorrelation function for 4 fermions interacting via a combined attractive and repulsive exponential potential with Fourier decomposition importance sampling using the initial condition. This plot is for 30 time steps of size 2.5×10^{-25} s. The correlation length is defined to be the number of trajectories at which the function drops to less than 0.1. Parameters are given in Table 7.

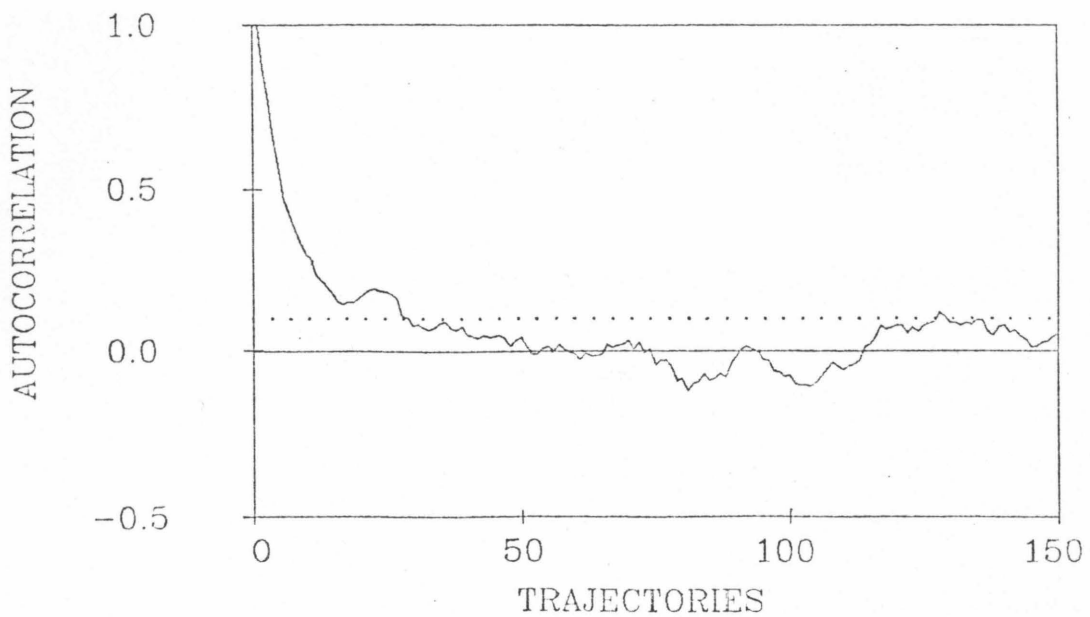
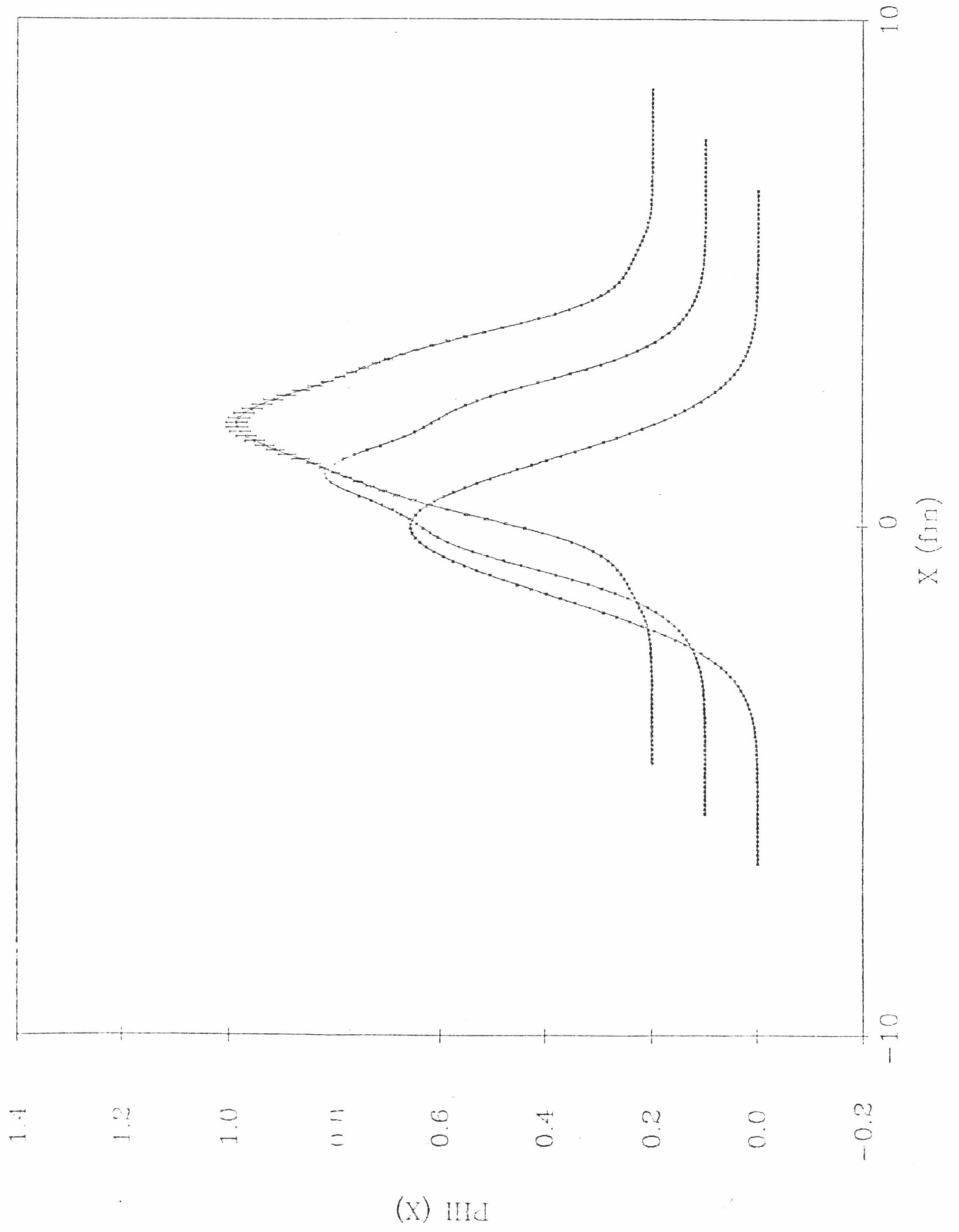
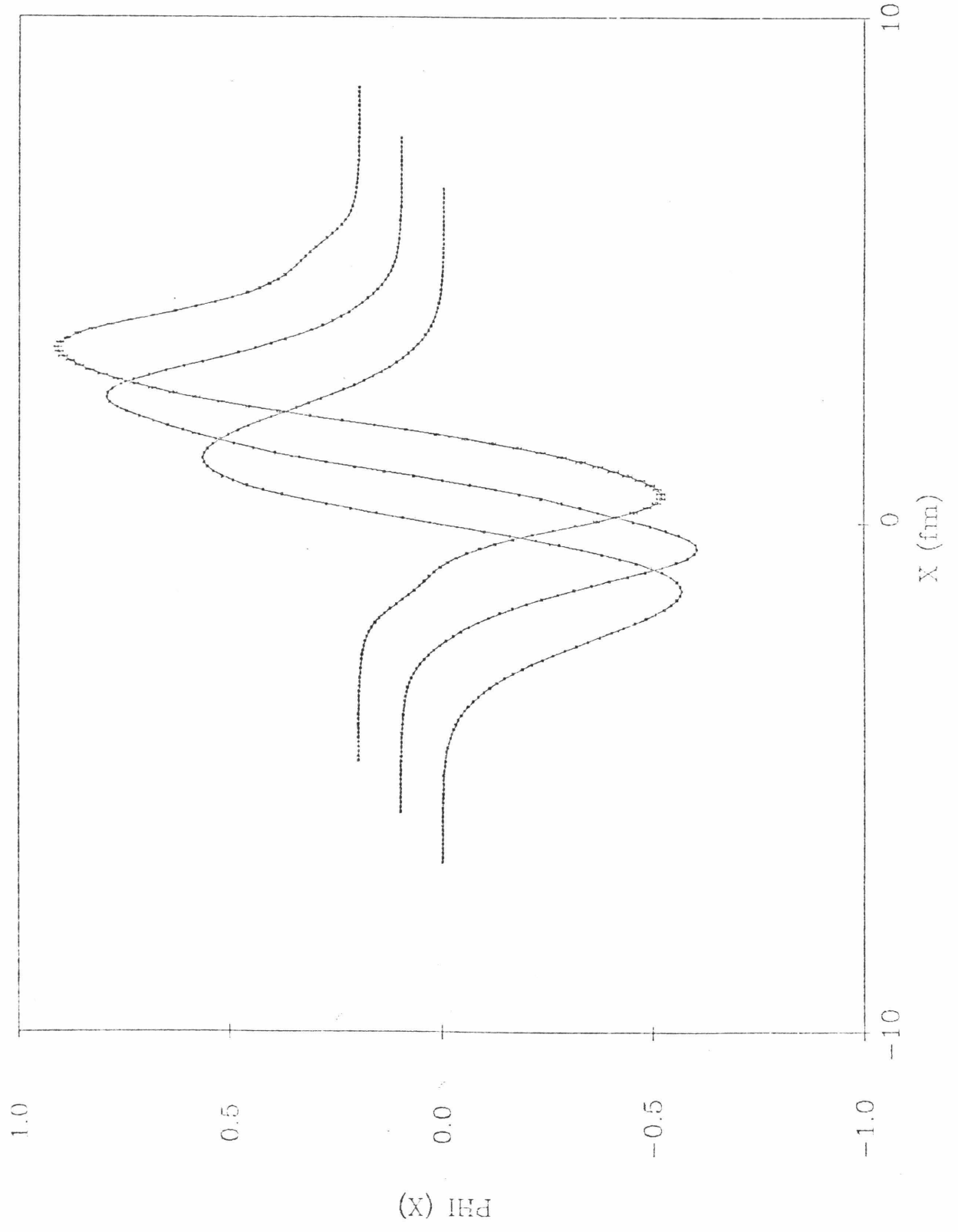
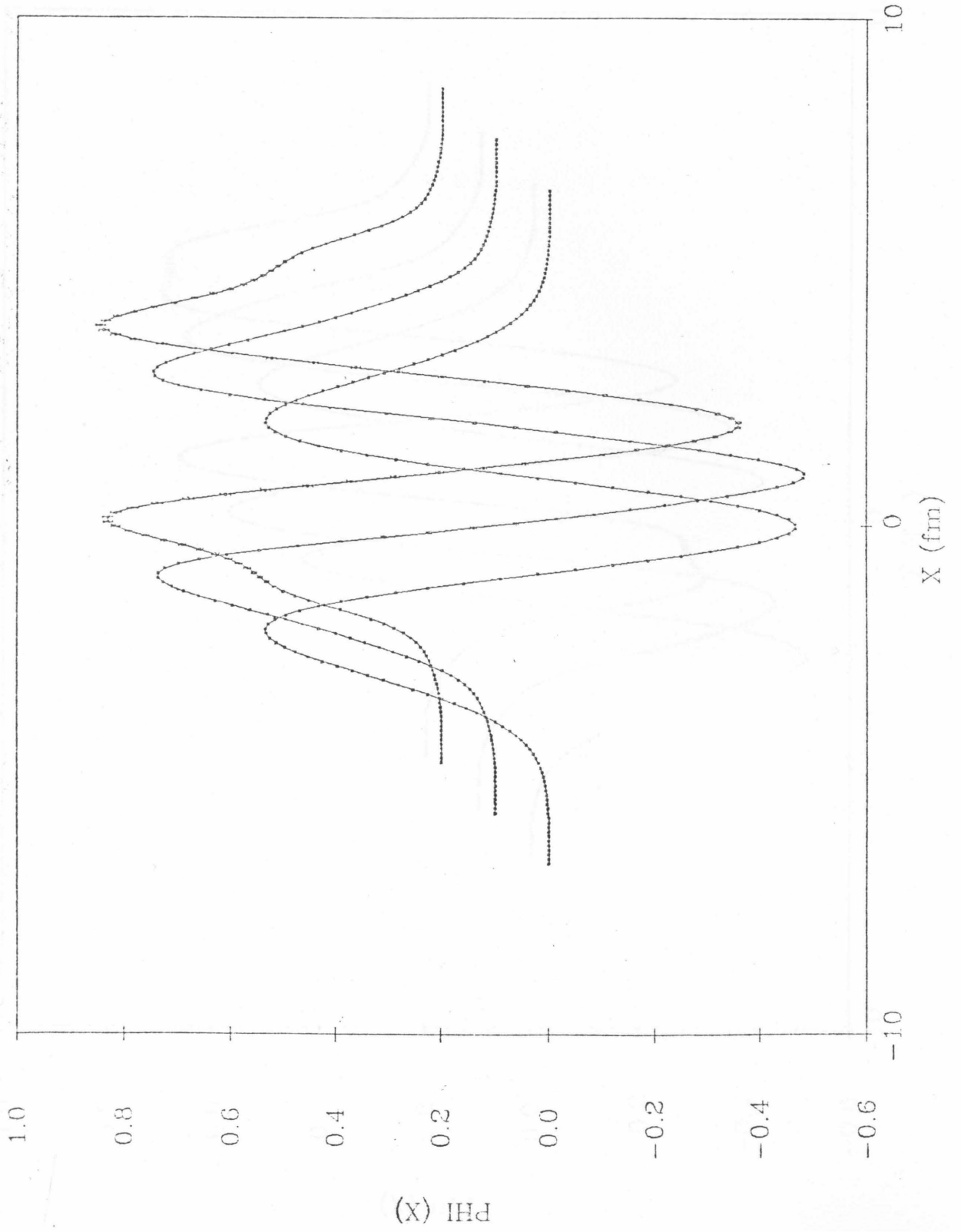


Figure 24. The four orbital wavefunctions for 4 fermions interacting via a combined attractive and repulsive exponential potential are shown for $\Delta t = 1.0 \times 10^{-24}$ s after 0 (trial wavefunction), 10 and 20 evolution steps. The results are averaged over trajectories 1000-2000, computed every 30 trajectories. The changes in the σ field are performed with Fourier decomposition importance sampling given by the initial condition. Parameters are given in Table 7. For clarity, the wavefunctions at later time slices are shifted up and to the right as indicated by the zeroing base line for each.







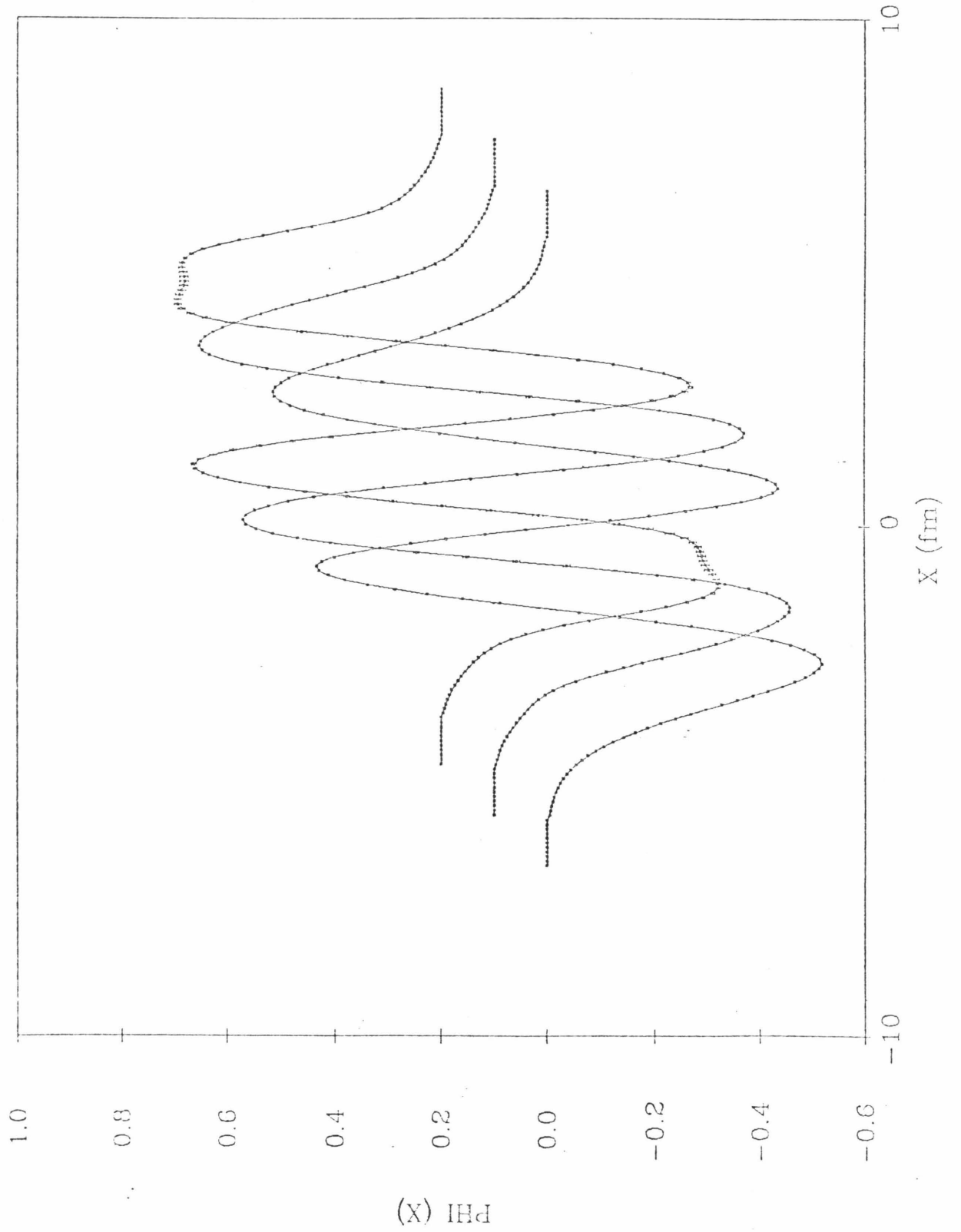


Figure 25. The one-body potential $W(x)$ for 4 fermions interacting via a sum of an attractive and repulsive exponential potential is shown for the size $\Delta t = 1.0 \times 10^{-24}$ s after 20 evolution steps. The results are averaged over trajectories 1000-2000, computed every 30 trajectories. In this case, the changes in the σ field are performed with Fourier decomposition importance sampling given by the initial condition. Parameters are given in Table 7. For clarity, the fields at later time slices are shifted up and to the right as indicated by the zeroing base line for each.

